Maize endosperm texture characterisation using the Rapid Visco Analyser (RVA), X-ray micro-computed tomography (μCT) and micro-near infrared (microNIR) spectroscopy

by

Anina Guelpa

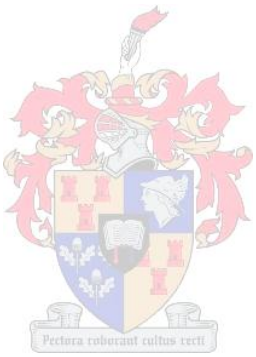

Dissertation presented for the degree of
Doctor of Philosophy (Food Science) in the
Faculty of AgriSciences at
Stellenbosch University

Supervisor: Prof Marena Manley
Co-supervisor: Prof Paul Geladi
Co-supervisor: Dr Anton du Plessis

March 2015

DECLARATION

By submitting this dissertation electronically, I declare that the entirety of the work contained therein is my own, original work, that I am the sole author thereof (save to the extent explicitly otherwise stated), that reproduction and publication thereof by Stellenbosch University will not infringe any third party rights and that I have not previously in its entirety or in part submitted it for obtaining any qualification.

Anina Guelpa
March 2015

Acknowledgements

My journey back into the world of academics after 10 years in the industry has been unpredictable to say the least. During this time some people and institutions have been consistent in their support and guidance, allowing me to take the next step in my career with confidence.

I would like to express sincere gratitude to the following people and institutions for their professional contributions to my studies:

- my supervisor, Prof Manley for the opportunity to further my studies in Food Science, being patient when it took me some time to get used to the world of academics again and her professional guidance;
- my co-supervisor, Prof Geladi for his expert NIR hyperspectral imaging advice and for introducing me to the world of chemometrics;
- my co-supervisor, Dr Du Plessis, for reviewing my work and providing feedback;
- a sincere thank you to Prof Kidd who spent many hours analysing my data and giving great advice;
- the staff of CAF including Stephan le Roux, Olwethu Majodina, Jarlen Beukes and Stacy-Lee Lewis for X-ray µCT assistance and analysis;
- Ayanda Myende, who played an important role in ensuring that the RVA analysis of my samples got done in time;
- Umbio AB (Umeå, Sweden) for the use of their Umbio Inspector SWIR pushbroom hyperspectral imaging system and BÜCHI Labortechnik GmbH (Flawil, Switzerland) for the use of their BÜCHI NIRFlex N-500 Fourier transform near-infrared (FTNIR) spectrophotometer;
- Sasko, a division of Pioneer Foods (Pty) Ltd (Paarl, South Africa), for the use of their research and development facilities supplying analytical reference results (Essential Foods) as well as donation of the Rapid Visco Analyser and Perten Laboratory Mill; and
- Anchen Lombard for assisting with travel arrangements and other financial aspects. Without your support and meticulous way of staying on top of things with great humour, my journey would probably have been much longer.

I am also sincerely grateful for the financial assistance I have received from various institutions during my three years of study. To this end I would like to acknowledge the contributions of:

- Maize Trust for a study bursary
- FoodBev
- Harry Crossley
- Stellenbosch University merit bursary

This work is based upon research supported by the National Research Foundation (grant specific unique reference numbers (UID) 76641, 70863 and 83974).

On a personal level I have been blessed with a wonderful family who always have my best interests at heart. I am grateful to my parents for their continuous interest in my progress and believing in my abilities. To my mother, the hours spent looking after my family when I couldn't was a wonderful gift and great blessing to us all.

To my sons, I am truly blessed to have such great boys, who, at a young age already understand the meaning of support, whether it is helping with breakfast or dinner or just making sure that it is quiet around the house for me to concentrate.

To my husband Wickus, thank your for sharing this journey with me. Your continuous interest and sometimes challenging critique is sincerely appreciated. Your assistance with household tasks, looking after the boys and surviving my overseas trips made this all possible. LVJ

Abstract

Maize kernels consists of two types of endosperm, a harder vitreous endosperm and a softer floury endosperm, and the ratio of the vitreous and floury endosperm present mainly determines the hardness of the kernel. Maize (*Zea mays* L.) is a staple food in many countries, including South Africa, and is industrially processed into maize meal using dry-milling. For optimal yield and higher quality products, hard kernels are favoured by the milling industry. Despite many maize hardness methods available, a standardised method is still lacking, furthermore, no dedicated maize milling quality method exists.

Using an industrial guideline (chop percentage), a sample set of different maize hybrids was ranked based on milling performance. Unsupervised inspection (using principal component analysis (PCA) and Spearman's rank correlation coefficients) identified seven conventional methods (hectoliter mass (HLM), hundred kernel mass (HKM), protein content, particle size index (PSI c/f), percentage vitreous endosperm (%VE) as determined using near infrared (NIR) hyperspectral imaging (HSI) and NIR absorbance at 2230 nm (NIR @ 2230 nm)) as being important descriptors of maize milling quality. Additionally, Rapid Visco Analyser (RVA) viscograms were used for building prediction models, using locally weighted partial least squares (LW-PLS). Hardness properties were predicted in the same order or better than the laboratory error of the reference method, irrespective of RVA profile being used.

Classification of hard and soft maize hybrids was achieved, based on density measurements as determined using an X-ray micro-computed tomography (µCT) density calibration constructed from polymers with known densities. Receiver operating classification (ROC) curve threshold values of 1.48 g.cm^{-3}, 1.67 g.cm^{-3} and 1.30 g.cm^{-3} were determined for the entire kernel (EKD), vitreous (VED) and floury endosperm densities (FED), respectively at a maximum of 100% sensitivity and specificity.

Classification based on milling quality of maize hybrids, using X-ray µCT derived density and volume measurements obtained from low resolution (80 µm) µCT scans, were achieved with good classification accuracies. For EKD and vitreous-to-floury endosperm ratio (V:F) measurements, 93% and 92% accurate classifications were respectively obtained, using ROC curve. Furthermore, it was established that milling quality could not be described without the inclusion of density measurements (using PCA and Spearman's rank correlation coefficients).

X-ray µCT derived density measurements (EKD) were used as reference values to build NIR spectroscopy prediction models. NIR spectra were acquired using a miniature NIR spectrophotometer, i.e. a microNIR with a wavelength range of 908 – 1680 nm. Prediction statistics for EKD for the larger sample set (where each kernel was scanned both germ-up and germ-down) was: R^2_V = 0.60, RMSEP = 0.03 g.cm^{-3}, RPD = 1.67 and for the smaller sample set (where each kernel was scanned only germ-down): R^2_V = 0.32, RMSEP = 0.03 g.cm^{-3}, RPD = 1.67. The results

from the larger sample set indicated that reasonable predictions can be made at the fast NIR scan rate that would be suitable for breeders as a rough screening method.

Uittreksel

Mieliepitte bestaan uit twee tipes endosperm, ‘n harder glasagtige endosperm en ‘n sagter melerige endosperm, en die verhouding waarin die twee tipes endosperm aangetref word, bepaal hoofsaaklik die hardheid van die pit. Mielies (*Zea mays* L.) is ‘n stapelvoedsel in baie lande, insluitende Suid-Afrika, en word industrieël geprosesseer na mieliemeel deur van droë-vermaling gebruik te maak. Vir optimale produksie en beter kwaliteit produkte, word harde pitte deur die meule verkies. Ongeag die beskikbaarheid van verskeie mielie hardheid metodes, ontbreek ‘n gestandardiseerde metode nog, en verder bestaan ‘n metode om mielies se maalprestasie te bepaal ook nie.

‘n Monsterstel, bestaande uit verskillende mieliebasters, is op grond van maalprestasie ingedeel deur van ‘n industriële riglyn (chop persentasie) gebruik te maak. Inspeksie sonder toesig (deur gebruik te maak van hoofkomponentanalise (HKA) en Spearman’s rangkorrelasiekoëffisiënte) het sewe onkonvensionele metodes (hektoliter massa, honderd pit massa, protein inhoud, partikel grootte indeks, persentasie glasagtige endosperm soos bepaal deur gebruik te maak van naby-infrarooi (NIR) hiperspektrale beelding en NIR absorbansie by 2230 nm) identifiseer as belangrike beskrywers van maalprestasie. Daarbenewens, is Rapid Visco Analyser (RVA) viskogramme gebruik om voorspellingsmodelle te bou deur gebruik te maak van plaaslik geweegte gedeeltelike kleinstekwadrate (PG-GKK) wat hardheidseienskappe kon voorspel met laer, of in dieselfde orde, laboratorium foute van die verwysingsmetodes, ongeag die gebruik van verskillende RVA profiele.

Klassifikasie tussen harde en sagte mieliebasters was moontlik, gebasseer op digtheidsmetings soos bepaal met ‘n X-staal mikro-berekende tomografie (µBT) digtheids kalibrasie gebou vanaf polimere met bekende digthede. Ontvanger bedryf kenmerkende (OBK) kurwe drempelwaardes van 1.48 g.cm^{-3}, 1.67 g.cm^{-3} en 1.30 g.cm^{-3} is bepaal vir hele pit, glasagtige en melerige endosperm digthede, onderskeidelik, teen ‘n maksimum van 100% sensitiwiteit en spesifisiteit.

Klassifikasie van die mieliebasters, gebasseer op maalprestasie en deur gebruik te maak van X-straal µBT afgeleide digtheid en volume metings soos verkry teen lae resolusie (80 µm) skanderings, was moontlik met goeie klassifikasie akkuraatheid. Vir heel pit digtheid en glasagtig-tot-melerige endosperm verhouding metings is 93% en 92% akkurate klassifikasies verkry wanneer OBK kurwes gebruik is. Verder is dit vasgestel (deur gebruik te maak van HKA en Spearman’s rangkorrelasiekoëffisiënte) dat digtheidsmetings ingesluit moet word vir ‘n volledige beskrywing van maalprestasie.

X-straal µBT afgeleide digtheid metings is gebruik as verwysings waardes om NIR spektroskopie voorspellings modelle te bou. NIR spektra is verkry deur van ‘n miniatuur NIR spektrofotometer, naamlik ‘n microNIR, bebruik te maak vanaf 908 – 1680 nm. Voorspellings statestiek vir die groter monsterstel (waar elke pit beide kiem-bo en kiem-onder geskandeer is)

was vir HPD: R^2_V = 0.60, RMSEP = 0.03 g.cm^{-3}, RPD = 1.67 en vir die kleiner monsterstel (waar elke pit was slegs kiem-onder geskandeer is) vir HPD: R^2_V = 0.32, RMSEP = 0.03 g.cm^{-3}, RPD = 1.67. Die resultate van die groter monsterstel het aangedui dat redelike voorspellings moontlik is, teen die vinnige NIR skaderings tempo wat as rowwe vertoningsmetode geskik sal wees vir telers.

Table of contents

List of Figures

List of Tables

List of Abbreviations

%cavity:	Percentage cavity
%chop:	Percentage chop
%FE:	Percentage floury endosperm
%porosity:	Percentage porosity
%VE:	Percentage vitreous endosperm
µCT:	Micro-computed tomography
2-D:	Two dimensional
3-D:	Three dimensional
ANOVA:	Analysis of variance
c/f:	Coarse-over-fine ratio
CAF:	Central Analytical Facility
CAT:	Computerised axial tomography
CT:	Computed tomography
dH_2O:	Distilled water
E:	Residual
EKD:	Entire kernel density
EKV:	Entire kernel volume
FED:	Floury endosperm density
FEV:	Floury endosperm volume
FTNIR:	Fourier transform near infrared
G x E:	Genotype by environment interaction
HDPE:	High density polyethylene
HKM:	Hundred kernel mass
HLM:	Hectoliter mass
HSI:	Hyperspectral imaging
ICC:	Interclass correlation coefficients
LV:	Latent variable
LVF:	Linear variable filter
LW:	Locally weighted
LW-PLS2:	Locally weighted partial least squares
MI:	Milling index
MIA:	Multivariate image analysis
MSC:	Multiplicative scatter correction
N.S.:	Non-significant
NIR:	Near infrared
NIR @ 2230 nm:	Near infrared spectroscopy (hardness index)

PC:	Principal component
PCA:	Principal component analysis
PET:	Polyethylene terephthalate
PLS:	Partial least squares
PP:	Polypropylene
PSI:	Particle size index
PTFE:	Polytetrafluoroethylene
R^2_C:	Coefficient of determination for calibration
R^2_V:	Coefficient of determination for validation
RMSECV:	Root mean square error of cross-validation
RMSEP:	Root mean square error of prediction
ROC:	Receiver operating characteristic
ROI:	Region-of-interest
RVA:	Rapid Visco Analyser
SAGL:	Southern African Grain Laboratory
SD:	Standard deviation
SE:	Standard error
SEL:	Standard error of laboratory
SEM:	Scanning electron microscopy
SNV:	Standard normal variate
T:	Score vector
TADD:	Tangential abrasive dehulling device
UHMW PE:	Ultra-high molecular weight polyethylene
V:	Loadings vector
V:F:	Vitreous-to-floury endosperm ratio
VED:	Vitreous endosperm density
VEV:	Vitreous endosperm volume

Chapter 1

Introduction

Kernel hardness is the main physical parameter that determines the end-use of maize *(Zea mays* L.) (Gaytán-Martínez *et al.*, 2006). Eighty percent of a maize kernel consists of two types of endosperm, i.e. a harder vitreous endosperm, and a softer floury endosperm (Watson, 1987). The ratio of the vitreous to floury endosperm present determines the hardness of the kernel (Robutti *et al.*, 1974). Hardness is mainly a genetic trait (Johnson & Russell, 1982), although environmental influences (Hamilton *et al.*, 1951) and external factors such as postharvest handling (Peplinski *et al.*, 1989) will also affect this property. Maize processors, i.e. the dry-milling industry, favour hard maize as hard kernels produce greater yield, as well as higher quality meals and grits, than soft maize (Lee *et al.*, 2007).

Numerous methods have been used for the last 60 years to determine maize hardness (Fox & Manley, 2009). These methods include measuring resistance to grinding and abrasion (Lee *et al.*, 2007); yield of grits (Wu, 1992); starch gelatinisation properties (Almeida-Dominguez *et al.*, 1997); as well as the determination of particle size index (PSI) (Pomeranz *et al.*, 1984; Wu, 1992). The use of near infrared (NIR) spectroscopy has also been widely investigated (Pomeranz *et al.*, 1984; Robutti, 1995; Eyherabide *et al.*, 1996). Other methods include hand dissection, which determines the ratio of vitreous to floury endosperm, and machine vision technology for non-destructive classification of maize kernels (Erasmus, 2003). Quality properties such as protein, starch, fat and fiber contents (Blandino *et al.*, 2010) and protein (zein) composition (Dombrink-Kurtzman & Bietz, 1993; Robutti *et al.*, 1997) have also been used to characterise kernel hardness. Density measurements were performed by means of a floating test (Blandino *et al.*, 2010; Blandino *et al.*, 2012) or gas pycnometry (Siska & Hurburgh, 1995).

Regardless of all the hardness methods that are available, no standardised method exists (Fox & Manley, 2009; Blandino *et al.*, 2010). Although maize hardness and milling quality are correlated, the mechanism or relationship between these two properties is not clearly defined. Currently, the most appropriate method for testing maize milling quality seems to be the actual milling process, simulated on pilot plant scale.

The Rapid Visco Analyser (RVA) is a viscometric tool that has been shown to quantify maize hardness differences between maize hybrids (Yamin *et al.*, 1999; Seetharaman *et al.*, 2001; Ji *et al.*, 2003; Sandhu & Singh, 2007). This is based on hard maize producing mainly coarse particles when being milled, whereas soft maize produces smaller particles (Almeida-Dominguez *et al.*, 1997), therefore resulting in different rates of hydration and gelatinisation. For each of the measurements, viscosity (cP), temperature (°C), speed (rpm) and the heat-cool ratio are recorded. The resulting curve, a viscogram, can be subjected to multivariate data analysis techniques to simultaneously predict multiple measurements (Visser, 2011).

NIR spectroscopy is one of a few non-destructive methods and is prominent among major analytical technologies, as it is a fast and low-cost method with broad application possibilities (McClure, 2004; Manley, 2014). NIR analysis has been successfully used for bulk maize characterisation for a number of measurements, i.e. oil, protein, starch and moisture contents (Osborne *et al.*, 1993). As reviewed by Fox and Manley (2009), NIR spectroscopy has been used to predict bulk kernel hardness traits for more than 20 years. However, the prediction of single-kernel traits are not as widely studied due to the difficulty of collecting reliable and representative spectra from a heterogeneous sample. Spectral changes are observed as a kernel's orientation towards the spectrometer and optics changes (Janni *et al.*, 2008; Fox & Manley, 2014). Different approaches have been studied to overcome these limitations (Armstrong, 2006; Spielbauer *et al.*, 2009).

In addition to NIR spectroscopy that only conveys average chemical (or physical) information of a sample, NIR hyperspectral imaging (HSI) facilitates the visualisation of the distribution of the chemical components in a sample (Manley, 2014). Predictions of heterogeneous samples will thus benefit from this technology. Successful maize hardness predictions, using NIR HSI, were achieved recently (Manley *et al.*, 2009; Williams *et al.*, 2009; McGoverin & Manley, 2012).

Micro-computed tomography (µCT) uses the differences in X-ray attenuation arising principally from differences in density and atomic composition within the material (Chawanji *et al.*, 2012; Zhu *et al.*, 2012; Cnudde & Boone, 2013). For a particular material (at a specific energy) the X-ray attenuation is approximately proportional to the material's density (Sinka *et al.*, 2004). The main advantage of the X-ray µCT technique is the ability to perform non-destructive and non-invasive capturing of high resolution three dimensional (3-D) detail, as recently illustrated on maize kernels (Gustin *et al.*, 2013).

The aim of this study was to estimate maize hardness and maize milling quality and consequently characterise maize endosperm texture, using RVA, X-ray µCT and MicroNIR spectroscopy, combined with statistical and multivariate data analysis. Specific objectives were to:

- determine the usefulness of RVA viscograms as milling quality descriptors;
- construct an X-ray µCT density calibration to non-destructively estimate kernel hardness from calculated density, percentage porosity and percentage cavity measurements of the entire maize kernel as well as that of selected ROIs (vitreous and floury endosperm);
- perform milling quality classification of maize kernels, based on X-ray µCT derived densities and volumes (entire kernel, vitreous and floury endosperm); and
- investigate the possibility of predicting whole kernel density, fast and non-destructively, using single-kernel MicroNIR reflectance spectroscopy.

References

Almeida-Dominguez, H.D., Suhendro, E.L. & Rooney, L.W. (1997). Factors affecting Rapid Visco-Analyser curves for the determination of maize kernel hardness. *Journal of Cereal Science*, **25**, 93-102.

Armstrong, P. (2006). Rapid single-kernel NIR measurement of grain and oil-seed attributes. *Applied Engineering in Agriculture*, **22**, 767.

Blandino, M., Mancini, M.C., Peila, A., Rolle, L., Vanara, F. & Reyneri, A. (2010). Determination of maize kernel hardness: comparison of different laboratory tests to predict dry milling performance. *Journal of the Science of Food and Agriculture*, **90**, 1870-1878.

Blandino, M., Sacco, D. & Reyneri, A. (2012). Prediction of the dry milling performance of maize hybrids through hardness associated properties. *Journal of the Science of Food and Agriculture*, **93**, 1356-1364.

Chawanji, A.S., Baldwin, A.J., Brisson, G. & Webster, E. (2012). Use of X-ray micro tomography to study the microstructure of loose-packed and compacted milk powders. *Journal of Microscopy*, **248**, 49-57.

Cnudde, V. & Boone, M.N. (2013). High-resolution X-ray computed tomography in geosciences: A review of the current technology and applications. *Earth-Science Reviews*, **123**, 1-17.

Dombrink-Kurtzman, M.A. & Bietz, J.A. (1993). Zein composition in hard and soft endosperm of maize. *American Association of Cereal Chemists*, **70**, 105-108.

Erasmus, C. (2003). Maize kernel translucency measurement by image analysis and its relationship to vitreousness and dry milling performance. PhD Thesis. University of Pretoria, Pretoria, South Africa.

Eyherabide, G.H., Robutti, J.L. & Borras, F.S. (1996). Effect of near-infrared transmission-based selection on maize hardness and the composition of zeins. *Cereal Chemistry*, **73**, 775-778.

Fox, G. & Manley, M. (2009). Hardness methods for testing maize kernels. *Journal of Agricultural and Food Chemistry*, **57**, 5647-5657.

Fox, G. & Manley, M. (2014). Applications of single kernel conventional and hyperspectral imaging near infrared spectroscopy in cereals. *Journal of the Science of Food and Agriculture*, **94**, 174-179.

Gaytán-Martínez, M., Figueroa-Cárdenas, J., Reyes-Vega, M., Rincón-Sánchez, F. & Morales-Sánchez, E. (2006). Microstructure of starch granule related to kernel hardness in corn. *Revista Fitotecnia Mexicana*, **29**, 135-139.

Gustin, J.L., Jackson, S., Williams, C., Patel, A., Armstrong, P.R., Peter, G.F. & Settles, A.M. (2013). Analysis of maize (*Zea mays*) kernel density and volume using micro-computed tomography and single-kernel near infrared spectroscopy. *Journal of Agricultural and Food Chemistry*, **61**, 10872-10880.

Hamilton, T., Hamilton, B.C., Johnson, B.C. & Mitchell, H. (1951). The dependence of the physical and chemical composition of the corn kernel on soil fertility and cropping system. *Cereal Chemistry*, **28**, 163-176.

Janni, J., Weinstock, B.A., Hagen, L. & Wright, S. (2008). Novel near-infrared sampling apparatus for single kernel analysis of oil content in maize. *Applied spectroscopy*, **62**, 423-426.

Ji, Y., Wong, K., Hasjim, J., Pollak, L.M., Duvick, S., Jane, J. & White, P.J. (2003). Structure and function of starch from advanced generations of new corn lines. *Carbohydrate Polymers*, **54**, 305-319.

Johnson, D.Q. & Russell, W.A. (1982). Genetic variability and relationships of physical grain-quality traits in the BSSS population of maize. *Crop Science*, **22**, 805-809.

Lee, K.M., Herrman, T.J., Rooney, L.W., Jackson, D.S., Lingenfelser, J., Rausch, K.D., McKinney, J., Iiams, C., Byrum, L., Hurburgh, J.C.R., Johnson, L.A. & Fox, S.R. (2007). Corroborative study on maize quality, dry-milling and wet-milling properties of selected maize hybrids. *Journal of Agricultural and Food Chemistry*, **55**, 10751-10763.

Manley, M. (2014). Near-infrared spectroscopy and hyperspectral imaging: non-destructive analysis of biological materials. *Chemical Society Reviews*, **43**, 8200-8214.

Manley, M., Williams, P., Nilsson, D. & Geladi, P. (2009). Near infrared hyperspectral imaging for the evaluation of endosperm texture in whole yellow maize (*Zea mays* L.) kernels. *Journal of Agricultural and Food Chemistry*, **57**, 8761-8769.

McClure, W.F. (2004). Review: 204 years of near infrared technology: 1800–2003. *Journal of Near Infrared Spectroscopy*, **11**, 487-518.

McGoverin, C. & Manley, M. (2012). Classification of maize kernel hardness using near infrared hyperspectral imaging. *Journal of Near Infrared Spectroscopy*, **20**, 529-535.

Osborne, B.G., Fearn, T. & Hindle, P.H. (1993). *Practical NIR Spectroscopy with Applications in Food and Beverage Analysis.* Harlow, UK: Longman Scientific and Technical.

Peplinski, A.J., Paulsen, M.R., Anderson, R.A. & Kwolek, W.F. (1989). Physical, chemical, and dry-milling characteristics of corn hybrids from various genotypes. *Cereal Chemisty*, **66**, 117-120.

Pomeranz, Y., Martin, C.R., Traylor, D.D. & Lai, F.S. (1984). Corn hardness determination. *Cereal Chemistry*, **61**, 147-150.

Robutti, J.L. (1995). Maize kernel hardness estimation in breeding by near-infrared transmission analysis. *Cereal Chemistry*, **72**, 632-636.

Robutti, J.L., Borras, F.S. & Eyherabide, G.H. (1997). Zein compositions of mechanically separated coarse and fine portions of maize kernels. *Cereal Chemistry*, **74**, 75-78.

Robutti, J.L., Hoseney, R.C. & Wassom, C.E. (1974). Modified opaque-2 corn endosperms. ll. Structure viewed with a scanning electron microscope. *American Association of Cereal Chemists*, **51**, 173-180.

Sandhu, K.S. & Singh, N. (2007). Some properties of corn starches II: Physicochemical, gelatinization, retrogradation, pasting and gel textural properties. *Food Chemistry*, **101**, 1499-1507.

Seetharaman, K., Tziotis, A., Borras, F., White, P.J., Ferrer, M. & Robutti, J. (2001). Thermal and functional characterization of starch from Argentinean Corn1. *Cereal Chemistry*, **78**, 379-386.

Sinka, I.C., Burch, S.F., Tweed, J.H. & Cunningham, J.C. (2004). Measurement of density variations in tablets using X-ray computed tomography. *International Journal of Pharmaceutics*, **271**, 215-224.

Siska, J. & Hurburgh, C.R. (1995). Corn density measurement by near-infrared transmittance. *Transactions of the ASAE*, **38**, 1821-1824.

Spielbauer, G., Armstrong, P., Baier, J.W., Allen, W.B., Richardson, K., Shen, B. & Settles, A.M. (2009). High-throughput near-infrared reflectance spectroscopy for predicting quantitative and qualitative composition phenotypes of individual maize kernels. *Cereal Chemistry*, **86**, 556-564.

Visser, M.J. (2011). Evaluation of malted barley with different degrees of fermentability using the Rapid Visco Analyser (RVA). MSc Thesis. Stellenbosch: University of Stellenbosch, South Africa,

Watson, S.A. (1987). Structure and Composition. In: *Corn Chemistry and Technology* (edited by S.A. Watson & P.E. Ramstad). Pp. 53-82. St. Paul, Minnesota, USA: American Association of Cereal Chemists, Inc.

Williams, P., Geladi, P., Fox, G. & Manley, M. (2009). Maize kernel hardness classification by near infrared (NIR) hyperspectral imaging and multivariate data analysis. *Analytica Chimica Acta*, **653**, 121-130.

Wu, Y.V. (1992). Corn hardness as related to yield and particle size of fractions from a micro hammer-cutter mill. *Cereal Chemistry*, **69**, 343-347.

Yamin, F., Lee, M., Pollak, L. & White, P. (1999). Thermal properties of starch in corn variants isolated after chemical mutagenesis of inbred line B73 1. *Cereal Chemistry*, **76**, 175-181.

Zhu, L.J., Dogan, H., Gajula, H., Gu, M.H., Liu, Q.Q. & Shi, Y.C. (2012). Study of kernel structure of high-amylose and wild-type rice by X-ray microtomography and SEM. *Journal of Cereal Science*, **55**, 1-5.

Chapter 2

Literature Review

Introduction

Kernel hardness is an important quality feature of maize (*Zea mays* L.) and has been thoroughly studied in the pursuit of understanding this characteristic better. An attempt of providing a snap shot of the existing body of knowledge on the topic of maize hardness is presented in the literature review chapter in a format where factors that influence maize hardness are discussed, followed by the factors that are affected by maize hardness. The proportion in which the different endosperm types are present in maize, as well as environmental and postharvest influences, are seen as the factors that determine maize hardness. On the other hand, maize hardness affects storage and handling, as well as the milling process. A comparison of the different hardness methods are given, with discussion based on the different approaches, i.e. resistance to breakage, chemical analysis, physical analysis, indirect tests, less common methods, direct and time consuming methods, as well as micro-milling and a multivariate approach. X-ray micro-computed tomography is discussed as a relatively new analytical tool in cereal science. Lastly, statistical methods, both univariate and more advanced multivariate data analysis techniques, are addressed.

Factors that affect maize hardness

Maize hardness is determined and/or influenced by the compositional, morphological and environmental factors associated with the respective kernels. The effects these factors have on maize kernel hardness are addressed in this section.

Endosperm types

Maize kernels consist of, amongst others, two types of endosperm: i.e. vitreous and floury endosperm. It is the ratio in which these endosperm types are present that determines whether a kernel is hard or soft (Watson, 1987; Paiva *et al.*, 1991; Delcour & Hoseney, 2010). The biggest part of a maize kernel (80 – 84%) comprises of these endosperm cells, which can either be of the harder vitreous type or the softer floury type. The harder and more translucent endosperm is situated to the outside of the kernel and the softer and mealy textured endosperm is found in the center of the kernel (Fig. 2.1) (Wolf *et al.*, 1952; Watson, 1987; Lee *et al.*, 2006; Delcour & Hoseney, 2010).

The vitreous endosperm is tightly compacted and kept together with a thick continuous protein matrix (Fig. 2.2a). The vitreous endosperm cells are also polygonal shaped and there are few or no air spaces present (Fig. 2.2a), therefore appearing translucent when emitted with light (Gaytán-Martínez *et al.*, 2006; Lee *et al.*, 2006). In the soft endosperm (Fig. 2.2b) starch granules are spherical and covered with a protein matrix that is thinner than that of the vitreous endosperm and

that shrinks easily, consequently no longer completely covering the starch granules (Gaytán-Martínez *et al.*, 2006; Delcour & Hoseney, 2010). The floury endosperm is thus not as tightly packed as the vitreous endosperm (Delcour & Hoseney, 2010). Due to the small air pockets around the starch granules, the light is reflected and the endosperm appears opaque.

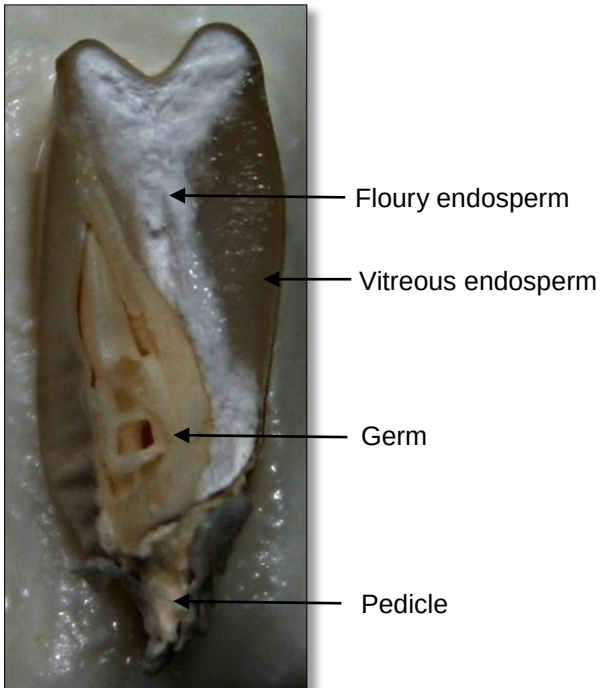

Figure 2.1. A longitudinal digital image (Canon EOS 300D digital camera, fitted with a Canon 30 – 80 mm lens) of a maize kernel, depicting the internal structure of the maize kernel, i.e. floury and vitreous endosperm, germ and pedicle.

Watson (1987) proposed that the ratio of the endosperm types present, were genetically inherited with that of the vitreous endosperm linked to the zein composition and the floury endosperm in turn produced by recessive genes. The zein composition refer to protein bodies that function as the storage protein (prolamin proteins) (Fig. 2.2c) (Delcour & Hoseney, 2010). Four classes of zein bodies have been identified: alpha (α), beta (β), gamma (γ), and delta (δ) (Lending & Larkins, 1989). It is generally agreed that there is a relationship between vitreous and floury endosperm and the proportion of zein types present in each (Paiva *et al.*, 1991; Dombrink-Kurtzman & Bietz, 1993; Eyherabide *et al.*, 1996; Mestres & Matencio, 1996; Robutti *et al.*, 1997; Chandrashekar & Mazhar, 1999; Lee *et al.*, 2006). It is thus apparent that maize kernels will develop with a specific ratio of vitreous and floury endosperm depending on the genetic code of that hybrid of maize (Erasmus, 2003).

Recently, it has been reported by Manley *et al*. (2009) that a third type of endosperm exists that differs from the vitreous and floury endosperm in terms of chemical composition and physical properties. O'Kennedy referred to this endosperm as the transition phase (O'Kennedy, 2011) and it might be similar to the region referred to as "the junction" by Dombrink-Kurtzman (1994).

(a)

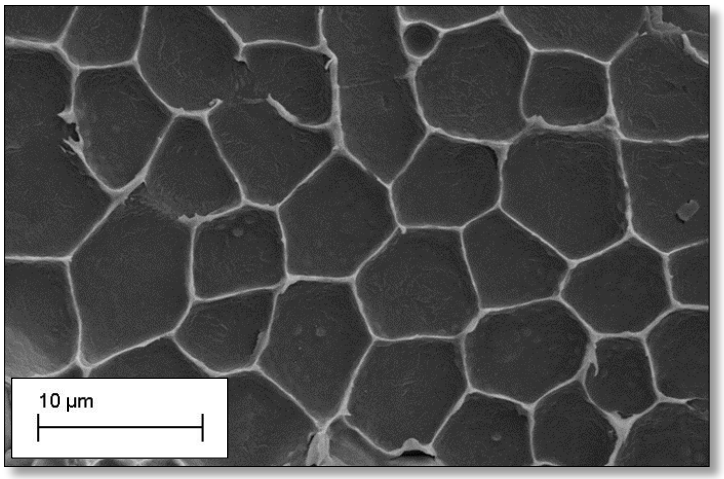

(b)

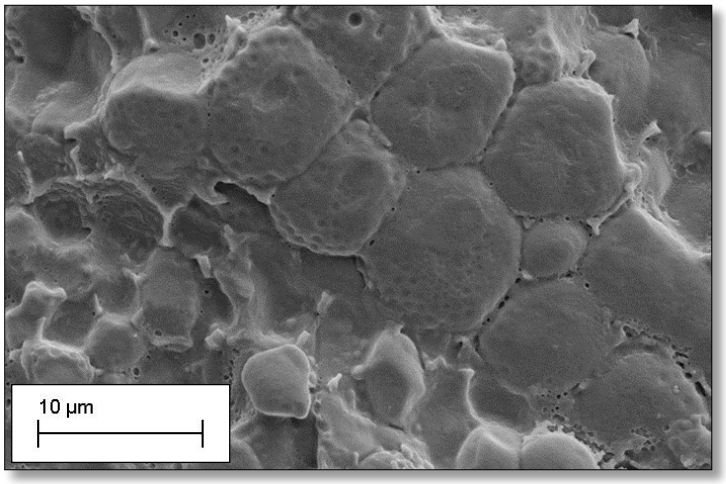

(c)

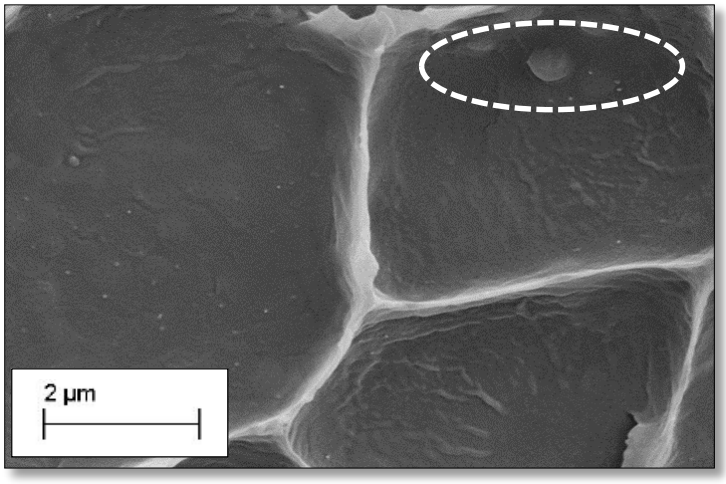

Figure 2.2. Scanning electron microscopy (SEM) micrographs (LEO1430 VP, Zeiss, Germany) (4500X) of (a) tightly packed polygonal shaped starch granules from vitreous endosperm covered in a thick protein matrix, (b) loosely packed irregularly shaped starch granules from floury endosperm covered with a thin protein matrix and (c) protein (zein) bodies (inside dashed oval) visible.

Kernel morphology

Apart from the endosperm, a maize kernel also consists of a hull and a germ (Wolf *et al.*, 1952). The hull (or bran) includes the pericarp and the seed coat (testa) and is roughly equivalent to 5 - 6% of the weight of the kernel (Wolf *et al.*, 1952; Delcour & Hoseney, 2010). The seed coat lies inside the pericarp and covers the entire kernel except the base (or tip cap or pedicle), which is covered by the hilar layer (Wolf *et al.*, 1952). The germ (embryo) is embedded in the lower portion of the endosperm and comprises about 10 – 14% of the weight of the kernel (Wolf *et al.*, 1952; Watson, 1987). The scutellum functions as a nutritive organ for the embryo (Watson, 1987) and the plumule will form the vegetative part of the plant.

Where the endosperm is comprised mainly of starch and protein, the germ does not have starch; it is high in oil, protein, soluble sugars and hormones (Serna-Saldivar, 2010). All cells of the germ and scutellum are potentially metabolically active upon hydration (Watson, 1987). Refer to Figure 2.3 for a schematic representation of the morphology of a maize kernel. Note that the vitreous endosperm is presented as horny endosperm in this figure.

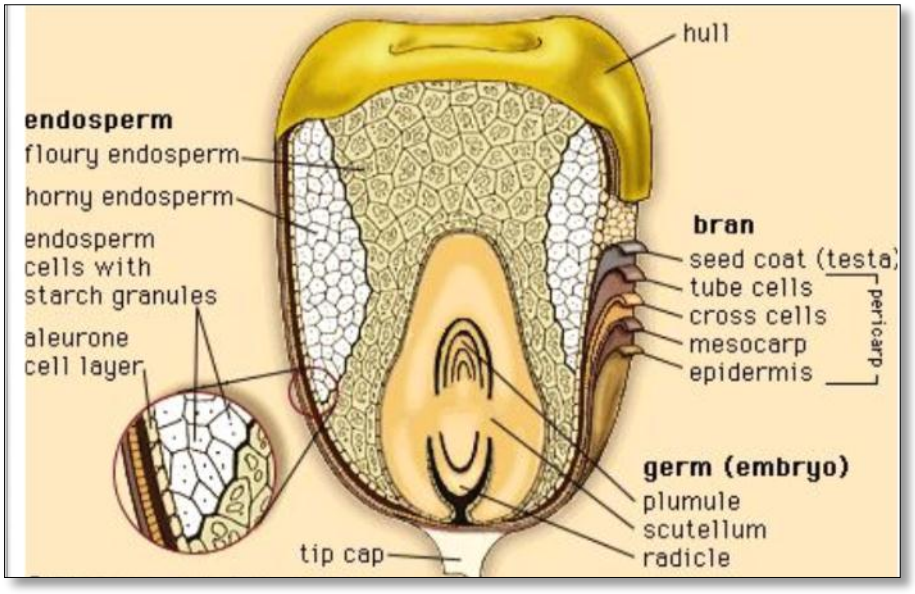

Figure 2.3. Schematic representation (Anon., 1996) of the layers and structures of a maize kernel.

The classes of maize (flint, flour, dent, sweet and pop) differ according to the physical shape of the kernels, as well as the structures of the individual components, and thus have an effect on maize hardness (Fox & Manley, 2009). Although flint and dent maize kernels are both intermediate with respect to their vitreous to floury endosperm ratio of about 2:1 (Wolf *et al.*, 1952), dent maize is generally softer than flint maize (flint kernels are long and flat, whereas dent kernels, are short and flat) (Fig. 2.4) (Fox & Manley, 2009). Pop maize kernels are round and short with a large portion of vitreous endosperm, and flour maize has predominantly floury endosperm. South African white maize falls within the dent maize class (dent maize is a derivative of flint-flour crosses) (Watson, 1987).

Figure 2.4. Front white cob is that of flint maize with the characteristic long and flat kernels, whereas the two maize cobs at the back of the picture are dent maize with short and flat kernels.

Environmental and postharvest factors

Even though maize hardness is mainly a genetic trait, another factor that has an effect on maize hardness, is the environment in which the crop is grown (Fox & Manley, 2009). This takes the soil nutrient profile into account, as well as the available moisture and environmental conditions prior to and during grain filling (Fox & Manley, 2009). It has been proven that nitrogen fertilisers greatly impact the final protein content of maize, and thus increase the vitreousness and hardness (Duarte *et al.*, 2005). Lee *et al*. (2012) conducted a genotype by environment interaction (G x E) study where they included environmental effects, correlations among quality parameters and genetic effects at the same time as they examined maize breeding crosses. They concluded that the correlations among the kernel quality traits were influenced both by hybrid type and environment. Another G x E study has been done by Robutti *et al.* (2000) on Argentinian hybrids. They had access to the Pergamino Maize Germplasm Bank where samples of more than 2500 localities were stored, as collected since the 1960's throughout Argentina. Correlating the kernel hardness to starch content was of great importance to their study and an inverse association between hardness and starch was indicated. They recognised other, more subtle, factors than the obvious factors such as thermal and storage history, and moisture content, to also affect kernel hardness (Robutti *et al.*, 2000).

Along with environmental factors, the manner in which the maize has been handled after harvesting can also influence the hardness thereof. Factors such as storage conditions, microbial infestation and germination are of importance (Peplinski *et al.*, 1989). A study by Peplinski *et al*.

(1989) reflected that the temperature used to dry (air temperatures from 25 to 60°C) maize kernels, greatly influenced the hardness thereof (seen by the increase in stress-cracked kernels and breakage susceptibility).

Factors affected by maize hardness

Currently, the factors that influence maize hardness have been discussed. It is just as important to understand how parameters, such as storage, handling and transport, as well as milling, can be affected by maize hardness. It should be clear from this section that the dry-milling industry would benefit from the inclusion of hardness parameters into the grading regulations. This would ensure the segregation (separate storage) of maize differing in hardness and would potentially assist the milling industry with respect to end product quality and milling performance.

Storage, handling and transportation

When looking at storage performance of maize, the harder kernels tend to store better than the softer kernels. This is also the case for handling and transportation, probably due to the limited breakage susceptibility as little or no stress cracks are present in hard maize compared to soft maize (Dorsey-Redding & Johnson, 1991; Lee *et al.*, 2007). Often maize is handled many times from harvest to end user, especially when exported, and the preferred maize is those resistant to breakage during handling as it results in better quality upon arrival at the destination (Mestres *et al.*, 1991; Wu, 1992; Lee *et al.*, 2006). Storage time is reduced with increased cracked kernels as these are more prone to increased moisture uptake and insect and mold infestation, and therefore reduced quality (Fox & Manley, 2009). The loss of economic value due to lower grading and less compensation is also a very important factor to consider as maize is not only a food and feed commodity, but also an export commodity (Peplinski *et al.*, 1989).

Wet-milling

The United States of America's main use of maize is for the production of ethanol and it entails the fermentation of the maize that is extracted during the wet-milling process (Hespell, 1998; Voca *et al.*, 2009). The hybrids planted for this purpose differ greatly from the South African hybrids as maize used for bio-fuel production contains large portions of floury endosperm and not significant amounts of vitreous endosperm. By-products from this process include protein (gluten meal), oil, germ meal, maize fiber (hulls or bran) and steep liquor (Hespell, 1998). Softer kernels perform better (Lee *et al.*, 2007) as they require less steeping and gives better starch-protein separation (Wu, 1992). The production of bio-fuel from maize is not yet widely practiced in South Africa.

Dry-milling

Maize meal is the main product of the dry-milling process. This process entails the removal of the germ and pericarp from the maize kernels during a de-germing process (Serna-Saldivar, 2010).

With the addition of water (conditioning step) the germ and pericarp is softened and easily removed (Serna-Saldivar, 2010). The endosperm that is obtained, is subjected to grinding and sieving (Watson, 1987). A series of mills with different roller gaps results in fractions with different particle sizes (Serna-Saldivar, 2010). Based on particle size, the isolated endosperm is reduced by sifting into predetermined classes (Watson, 1987). In dry-milling, a high yield of pure endosperm grits are desirable (Chiremba *et al.*, 2011).

There are 18 grades of maize products for sale in South Africa (Anon., 2008): i.e. fine maize bran, fine crushed maize, sifted maize meal, sifted crushed maize, coarse maize bran, mixed maize meal, maize rice, maize grits, maize flour, maize germ meal, No. 1 straightrun maize, No. 2 straightrun maize, unsifted crushed maize, unsifted maize meal, unspecified maize product, special maize meal, super maize meal and maize samp. To be graded special or super maize meal, the fineness by mass must fall within the following parameters: for super at least 90% shall pass through a 1.4 mm sieve and less than 90% shall pass through a 300 µm sieve; for special at least 90% shall pass through a 1.4 mm sieve (Anon., 2008). This results in super maize meal having a particle size distribution of 0.3 – 0.65 mm and for special maize meal 0.17 – 0.3 mm (Erasmus, 2003). The grit size of maize meal influences the porridge stickiness and texture (Bello *et al.*, 1995).

Maize hardness determinations: a comparison of different test methods

In an attempt to measure maize hardness, many diverse test methods have been established. Some of the methods test resistance to breakage, others test the chemical or physical composition of the kernels. Different hardness methods are mentioned and compared in this section.

Resistance to breakage

There are two types of mechanical breakage tests: the type that uses the impact of a moving blade (**Stein breakage tester**); and the other type that uses centrifugal impaction of individual kernels against a stationary surface (**Wisconsin breakage tester** (Paulsen & Hill, 1985; Mestres *et al.*, 1991). Hard kernels have lower breakage susceptibility than soft kernels (Paulsen & Hill, 1985). Not surprising, breakage susceptibility has been found to be strongly correlated (R^2 = 0.99) to stress crack percentage (Paulsen & Hill, 1985). This is in accordance to the study of Peplinski *et al*. (1989) where elevated drying temperatures resulted in an increase in stress-cracked kernels and subsequent breakage susceptibility.

Chemical analysis

Chemical analyses that are associated with maize hardness, are the determination of **dry matter** (residue weight after heating), **ash content** (residue weight after incineration) and **lipid** and **nitrogen content** (Mestres *et al.*, 1991). The analysis of **protein** (as the variation in zein-classes cause variation in hardness (Robutti *et al.*, 1997) **starch, moisture** and **fiber** are also associated

with maize hardness (Blandino *et al.*, 2010). Correlations that seem to be agreed upon between Blandino *et al*. (2010) and Mestres *et al.* (1991) are those between vitreousness and ash content, as well as density. Contradictory results are regularly found between kernel hardness and protein content. Mestres *et al.* (1991) found these factors to correlate, whereas Delcour & Hoseney (2010) agreed with Paulsen and Hill (1985) that hardness and protein content did not correlate. Robutti *et al*. (2000) found no significant correlation between protein content and kernel hardness. The inconsistency of results with respect to the association between hardness and protein, suggests that protein methods differ greatly and that specific types of proteins should be tested, individually.

Phenolic acids were quantified in maize bran, using high performance liquid chromatographic and mass spectrometric techniques, and it was shown that harder maize hybrids had more phenolic acids than softer maize hybrids (Chiremba *et al.*, 2012). The process of chemical bonding, through cross linking of compounds within plant cell walls, can be explained as the mechanism by which phenolic acids may influence maize hardness (Chiremba *et al.*, 2012). Furthermore, this study suggested that a correlation existed between phenolic acid content and the TADD method, which expressed kernel physical properties (Chiremba *et al.*, 2012). Due to the negative correlation, it was implied that hybrids with low phenolic acid content would break more easily than hybrids with a higher phenolic acid content (Chiremba *et al.*, 2012).

Physical analysis

Test weight, thousand kernel weight and **sphericity** calculated from measurements of three dimensions (length, width and depth) and kernel **density** are examples of physical traits of maize kernels, influencing maize hardness (Lee *et al.*, 2006; Blandino *et al.*, 2010). Abrasiveness is another similar method, measured using the **tangential abrasive dehulling device (TADD)** (Wehling *et al.*, 1996) where the remaining material is weighed after a set time of abrasion. This method results in a TADD index % that reveals kernel hardness. Lee *et al.* (2006) also used the TADD method when they assessed biochemical properties of maize and found it to have strong association with amylose content ($r = 0.89$, $P < 0.01$). Chiremba *et al*. (2012) did not only indicate phenolic acid content as an indicator of maize hardness, but also showed that the ferulic acid content was strongly correlated with TADD hardness ($r = -0.78$, $P < 0.001$).

Paulsen and Hill (1985) differentiated between incoming maize quality factors and dry-milling quality factors. For the incoming maize quality factors they made use of physical tests i.e. test weight and percentage floaters (density measurements). As both these factors are indicators of density, the results showed, not surprisingly, significant ($P < 0.05$) correlation ($r = 0.99$) between floating test results and test weight. This is in agreement with the conclusion drawn by Kirleis and Stroshine (1990) that a combination of test weight and kernel density are the best predictors of milling quality. Most density related studies used **pycnometry** as a measure of density (Wu, 1992; Lee *et al.*, 2006), but the **floating test** is also well used (Paulsen & Hill, 1985; Gaytán-Martínez *et al.*, 2006; Blandino *et al.*, 2010), as well as displacing a volume of water (Gaytán-Martínez *et al.*,

2006). The study by Gaytán-Martínez *et al*. (2006) indicated that both density measurements significantly ($P < 0.05$) correlated with hardness (r = -0.74 for the floating test and r = 0.69 for water displacement). Blandino *et al*. (2010) modified the floating test to obtain density results in the form of an area beneath a precipitation curve. This research group found the floating test to be significantly ($P < 0.05$) related to physical kernel characteristics observed by methods such as test weight (r = -0.89), the coarse over fine ratio (r = -0.93) and the Stenvert test (r = -0.70). But according to them, the test weight method is the simplest estimator of maize hardness and should be the first parameter to consider when determining maize hardness (Blandino *et al.*, 2010).

When interpreting density results, it should be noted that cracks and fissures can be present in kernels, mainly due to dehydration, which in turn lowers kernel density. Wu (1992) cautions that density results must be reported in combination with breakage susceptibility results.

Gaytán-Martínez *et al.* (2006) strongly expressed their viewpoint that physical traits, such as density, starch granules size and crystallinity are as important descriptors of maize hardness as that of the chemical composition of the maize. In their study, granule size and crystallinity were measured with scanning electron microscopy and an X-ray diffractometer, respectively. They found a positive correlation (r = 0.69) between hardness and density, as well as starch granule size and endosperm (r = 0.44), which contributed towards the description of the microstructure of the endosperm (Gaytán-Martínez *et al.*, 2006)

The **particle size index (PSI)** is a method that involves milling and sieving and although it is often used as a hardness method, Wu (1992) warns that the relatively high oil content present in maize may cause agglomeration which will conceal differences in particle size. For Blandino *et al.* (2010) the coarse-over-fine ratio (c/f), derived from the respective fractions obtained using this method, was the best descriptor of maize milling ability when using a sieve size of 2 mm. This c/f correlated better with milling quality than the floating test, test weight, the Stenvert test, sphericity and texture analysis, probably due to the clear evaluation of the vitreous (hard) and floury (soft) fractions (Blandino *et al.*, 2010).

Indirect tests

Near infrared spectroscopy

Near infrared **(NIR)** reflectance and transmittance spectroscopy are examples of indirect testing methods of maize hardness. These spectroscopic methods are non-destructive and can be calibrated against an unlimited choice of reference methods. The use of Fourier transform near infrared (FTNIR) spectroscopy has shown increased spectral reproducibility and wavelength precision and is thus a preferred technology in many types of analyses (Rotar *et al.*, 2009). In combination with chemometric techniques the analysis of materials can be achieved, without time-consuming practices such as sample preparation.

In past studies, NIR transmittance spectra were obtained from **whole** maize kernels (wavelengths between 850 and 1050 nm) and after data analysis only the absorbance values at

860 nm were used to measure kernel hardness, as this wavelength depicted particle size differences (Robutti *et al.*, 2000; Lee *et al.*, 2006). In other studies, a wider wavelength range was used (1000 to 2500 nm) to obtain reflectance spectra of whole kernels. A study by Orman & Schumann (1991) predicted protein, oil and starch content, whereas a study by Berardo *et al*. (2005) predicted kernel rot and mycotoxin infected kernels. With respect to **milled** samples, two wavelengths are of interest (1680 and 2230 nm) as they do not carry any chemical information and reflectance varies only with regards to particle size difference Downey *et al*. (1986).

Besides spectral absorbance differences found when scanning intact (whole) kernels versus ground samples, the scanning of **bulk** (multiple) maize samples are found to be less complicated compared to that of **single** maize kernels. Single kernel applications are far less common than that of bulk calibrations. This is due to the non-uniformity found within maize kernels as a result of the relatively large portion of germ present (Spielbauer *et al.*, 2009). Some researchers collect spectra from only the germ-down side of a kernel (Baye *et al.*, 2006), while others overcome the obstacle by developing sampling systems, such as that by Janni *et al.* (2008) that uses an airstream to tumble the individual kernels during spectral acquisition. In doing so, an average reflectance spectrum is obtained over the whole kernel surface. Armstrong (2006) and Baye *et al.* (2006) developed systems that collected the spectra as the kernels fell through glass tubes. Other single kernel applications include that of Pearson *et al.* (2001) and Dowell *et al.* (2006) where a probe was attached to the respective spectrophotometers. In the study by Pearson *et al.* (2001), aflatoxin concentration was predicted for single kernels with a 95% classification accuracy as containing either high (> 100 ppb) or low (< 10 ppb) levels of aflatoxin. Whereas, in the study by Dowell *et al.* (2006), fumonisin was detected on single maize kernels showing spectroscopy to be a useful tool for screening samples for online detection.

A new portable instrument, namely the **microNIR** (JDSU Corporation, Santa Rosa, CA, USA) has recently been introduced as a qualitative and quantitative analytical tool when applied to pharmaceuticals by Alcala *et al.* (2014). This device differs from conventional NIR spectrophotometers in that it is small (weight of only 60 g), hand-held and fitted with a linear variable filter (LVF) technology as monochromator (O'Brien *et al.*, 2012; Alcalà *et al.*, 2014). This instrument can be used in reflectance as well as transmission mode and can be applied for single kernel applications.

Near infrared hyperspectral imaging

A hyperspectral imaging system integrates conventional imaging and spectroscopy to produce a three-dimensional (spatial and spectral) hypercube from an object (Schweizer & Moura, 2001; Grahn & Geladi, 2007). Hyperspectral imaging is also called chemical or spectroscopic imaging or mapping, and is thus a technique that generates a spatial map of spectral variation (Sun, 2010). As explained by Burger (2006), spectral prediction or processing results can be mapped back to a

spatial location thereby demonstrating a major advantage (spatial information) of this spectroscopic technique.

As a single hyperspectral image with 256 x 320 pixels and 128 wavelength channels contains over ten million data values, simple multivariate statistical analysis are inadequate and need to be enhanced and adapted for these large data sets. These chemometric techniques will be discussed in a later section of this chapter.

Near infrared hyperspectral imaging (NIR-HSI) has been used to distinguish between individual maize kernels differing in hardness (Manley *et al.*, 2009; Williams *et al.*, 2009). It was also shown that NIR HSI could be used to classify maize kernels into hardness classes without the need for hardness reference data (McGoverin & Manley, 2012).

Other indirect tests

As studied by Pomeranz *et al.* (1985), **reporting the grinding time of maize** could also be a good method to estimate maize hardness. Another method described by Pomeranz *et al*. (1985) is that of the **Stenvert test**. This method is based on the measurement of the power consumption utilised during the milling process and the results are expressed as total milling energy and milling time (Blandino *et al.*, 2010). Li *et al*. (1996) also used the Stenvert test to derive hardness properties and found sound correlations with the vitreous to floury endosperm ratio. Principal component analysis revealed that milling energy and resistance time were the most effective parameters to asses grain hardness, and both these variables also correlated strongly with the vitreous to floury endosperm ratio (Li *et al.*, 1996).

Less common methods

Compression and **pearling** (Tran *et al.*, 1981) are two less common methods used to determine maize hardness. The first method involves **textural** properties and will be discussed shortly with reference to a study by Gaytan-Martinez *et al*. (2006) whereas the latter refers to a study where a barley pearler and a disk grinding mill was modified to record torque and energy during pearling and grinding (Tran *et al.*, 1981). Pearling resistance (torque) measures the resistance of a train to pearl and hard kernels ultimately result in higher resistance than soft kernels (Tran *et al.*, 1981). The relevance of this study was shown by the changes observed in hardness along with moisture content in maize kernels (Tran *et al.*, 1981). In the study by Gaytan-Martinez *et al*. (2006) they established a relationship between microstructural properties of maize kernels and physical variables (i.e. density), because they interpreted maize hardness more as a textural property. These researchers used a texture analyser to puncture maize kernels at their vitreous endosperm region to a depth of 2 mm. Blandino *et al*. (2010) also recognised the use of a puncture test as a method that has the potential for measuring single maize kernels' hardness.

Almeida-Dominguez *et al.* (1997) estimated maize hardness based on the viscosity of ground maize samples, using the **Rapid Visco Analyser (RVA)**. Using this viscometric procedure the thermal and rheological properties of a milled grain sample are provided, which in turn provide valuable information about the functionality thereof (Narváez-González *et al.*, 2006). RVA detects the changes in viscosity (pasting properties) of starches i.e. the viscosity developed during hydration and subsequent gelatinisation of starch granules during heating and stirring in excess water (Almeida-Dominguez *et al.*, 1997). Other researchers (Yamin *et al.*, 1999; Seetharaman *et al.*, 2001; Ji *et al.*, 2003; Sandhu & Singh, 2007) also observed differences in pasting properties between different maize hybrids, although they did not specifically link the results to maize hardness, but rather to starch and functional properties. The rationale behind hardness discrimination, using RVA, is as follows:

- hard maize has mainly coarse particles when milled, and soft maize smaller particles (Almeida-Dominguez *et al.*, 1997);
- coarse particles have slower water diffusion, limited swelling of the starch granules and slow viscosity development (Sahai *et al.*, 2001; Narváez-González *et al.*, 2006);
- smaller particles have bigger surface areas that result in better and more rapid hydration, thus better gelatinisation and higher viscosity (Almeida-Dominguez *et al.*, 1997);
- hard kernels show a more prominent protein-to-starch adhesion effect compared to soft kernels and require more time to gelatinise (Almeida-Dominguez *et al.*, 1997); and
- the protein matrix of vitreous (hard) endosperm is thicker than that of floury (soft) endosperm (Wang & Eckhoff, 2000) and forms a barrier that slows hydration and gelatinisation (Narváez-González *et al.*, 2006).

For each RVA test the viscosity (cP), temperature (°C), speed (rpm) and the heat-cool ratio are recorded every four seconds. The resulting curve, reporting the viscosity as a function of time (sometimes together with the temperature ramp, to improve interpretation), is called a viscogram as shown in Figure 2.5. Hard kernels thus reached peak viscosities sooner than soft kernels, but have lower peak viscosity times (Almeida-Dominguez *et al.*, 1997; Seetharaman *et al.*, 2001; Narváez-González *et al.*, 2006).

Direct and time consuming methods

A few researchers (Dombrink-Kurtzman & Knutson, 1997; Gaytán-Martínez *et al.*, 2006) separated parts of the maize kernel, in order to weigh and calculate respective percentages (usually of the pericarp, endosperm and germ). Mestres *et al.* (1991) also acknowledged that the cross-secional areas of the endosperm types, vitreous and floury, could be measured, but Blandino *et al*. (2010) did not agree with the practicality of this method, although they also went through this tedious process of **hand dissection**.

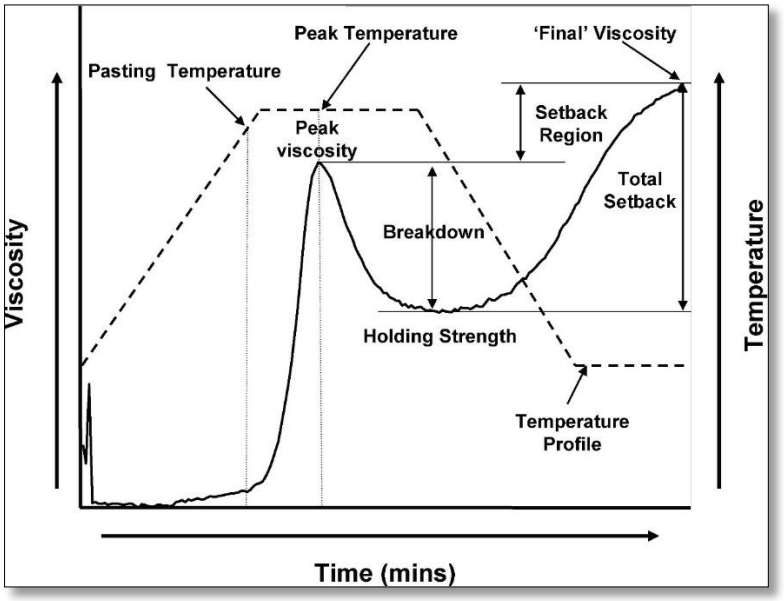

Figure 2.5. A Rapid Visco Analyser (RVA) viscogram (Agu *et al.*, 2006).

Mestres *et al.* (1991) found that vitreousness (as determined through hand-dissection) is not relevant for the prediction of dry-milling performance. It should have been significantly correlated with semolina recovery, a procedure similar to chop recovery, but it was not. In their study, ash content and sphericity explained most of the variation in semolina yield (Mestres *et al.*, 1991). In a prior study Paulsen and Hill (1985) found that tests for density and floaters usually correlate highly with the ratio of vitreous-to-floury endosperm.

Similar methods include the calculation of the percentage vitreousness by measuring the area from an enhanced photograph (Mestres *et al.*, 1991), or digital image analysis as in the study by Erasmus and Taylor (2004) who also used a light box to visually assess the endosperm types.

Micro-milling

To acquire an index of dry-milling performance, micro-milling can be considered as the total grit yield corresponding to the main products obtained in the conventional dry-milling industry (Blandino *et al.*, 2010). A micro-milling method novel to South Africa is the **Roff Milling** method, with the results known as the **Milling Index (MI)**. The Southern African Grain Laboratory (SAGL) applies this method, along with kernel whiteness and size tests, to assess milling performance. A roller mill system brakes the maize up into meal and bran fractions which are used to calculate the MI (Erasmus & Taylor, 2004). Van Loggerenberg and Pretorius (2004) used this method to develop a NIR transmittance calibration for whole grain predictions. These calibrations have in turn been used by Chiremba *et al.* (2011) for their characterisation of maize hardness.

Multivariate approach

A sensible summary to this section on different hardness methods, is to make reference to the conclusion of Blandino *et al.* (2010) where they described kernel hardness as a combination of physical and chemical characteristics and also state that there is no single method that describes dry-milling behaviour. They propose the use of a multivariate approach to take various properties into consideration. A multivariate approach was also followed by Chiremba *et al*. (2011) where principal component analysis revealed that a combination of TADD hardness and NIR Milling Index, or TADD hardness and test weight could be used to describe maize hardness.

A very useful summary (Table 2.1) of maize hardness testing methods used in Southern Africa, and their relevance to end-use quality, was published by Chiremba (2011). In this study it was found that TADD and test weight correlated (r = -0.64), as well as TADD and NIR transmittance (r = -0.66), and that the other hardness methods did not show any useful correlation. Two methods that are not depicted in Table 2.1 for maize hardness determination, are RVA and X-ray micro-computed tomography. Both these methods were used in the current study. Literature on the latter method will be reviewed in the following section.

Table 2.1. Simple methods used in Southern Africa for maize grain quality evaluation, their advantages, disadvantages and applicability (Chiremba *et al.*, 2011)

Method	Parameter/quality indicator measured	Advantages	Disadvantages	Applicability
Test weight Test weight per bushel or kg.hL^{-1}	Grain density	Inexpensive device, low maintenance cost, rapid, high repeatability and reproducibility, non-destructive method	Affected by grain packing in measuring apparatus, moisture content, kernel shape, broken kernels and foreign material, not suitable for early generation breeding	Applicable to breeding programs and cultivar evaluation with limited grain sample size, rapid test on dockage for commercial large and small- scale milling plants and grading for grain marketing
Thousand kernel weight (g)	Grain size and grain density	High repeatability and reproducibility, non-destructive indirect measure of grain density	Time consuming if done manually (without a seed counter)	Suitable for breeding programs with limited grain sample size. Also applicable in commercial grain quality control and processing, both large and small-scale
Abrasive Decortication Tangential Abrasive	Ease of grain to be abraded- indirect measure of grain hardness and	TADD is robust, high repeatability and reproducibility,	The abrasive disk may be worn out with the time and vary milling yields	Potential use at commercial level (both small and large scale),

Dehulling Device (TADD)	milling quality	low maintenance cost, equipment can be manufactured locally	although this can be monitored with the use of a standard sample of known yield	the multi-cup sample holder allows several samples to be decorticated simultaneously within a short time (5 to 10 min)
Stress cracks Light box	Proportion of grain with cracks and number of cracks	Apparatus cheap to set up, stress cracks may be quantified using the Stress Crack Index	Stress crack counting tedious and time consuming and to a degree subjective	Time consuming for routine analysis, but suitable for small sample size
Stein breakage susceptibility	Susceptibility of grain to break under stress	Allows quantification of the potential of grain to break, rapid analysis (4 min)	Apparatus is no longer manufactured, although other mills may be used	Suitable for commercial grain evaluation, destructive, could have limited use in breeding programs where grain sample size is limiting
Milling Index Near Infrared (NIR)Transmittance spectrometry	Grain milling quality	Automated and rapid analysis once a calibration is developed, calibration can be used by other users, non-destructive method	Requires calibration against physical or chemical data which could be time consuming and costly, very sensitive to sample preparation affecting precision and accuracy, high initial cost to purchase the instrument and operating software, regular software and service upgrade required, requires a relatively large grain sample size (approx. 500 g), limited use in breeding programs where grain sample size is limiting	Rapid for online processing at commercial milling plants and routine analysis in breeding programs and cultivar evaluation, skilled technical maintenance required, use could be limited to well established institutions; not economically appropriate for small-scale grain quality control and processing.
Kernel size: Set of sieves and sieve shaker	Kernel size	Analysis is relatively cheap, non-destructive, direct measure of kernel size, does not require a large grain sample size	Can be time-consuming especially if batches are very heterogeneous in terms of kernel size	Due to lengthy analysis time, it is not applicable in commercial grain quality analysis, applicable in research laboratories

X-ray micro-computed tomography scanning

The first use of X-rays was not for a medical application, but to produce a radiograph of a set of weights in a box. In later years (1907) John Radon generated the mathematical transformation algorithms that was later utilised to produce 3D reconstructed images from the X-ray scans (De Beer, 2005). A South African born American physicist, Alan M. Cormack, developed the diagnostic technique of computerised axial tomography (CAT) scanning in the 1970s (and received the Nobel Prize for Physiology in Medicine in 1979) (De Beer, 2005). This work of Cormack was further developed into X-ray computed tomography (CT), utilising the basic principles of CAT scanning (De Beer, 2005).

X-rays have a wavelength in the range of 0.01 to 10 nm, corresponding to frequencies from 30 to 30 000 Pentahertz and energies ranging from 120 eV to 120 keV (Kotwaliwale *et al.*, 2011). These are short electromagnetic waves and when they interact with matter, they behave like both particles (energy bundles, i.e. photons) and waves (Kotwaliwale *et al.*, 2011).

X-ray micro-computed tomography (µCT), or high-resolution CT, is a recent method that found use for the inspection of materials in many applications and settings (Singhal *et al.*, 2013). Information is gained of the micro-architecture or micro-structure of these materials, which leads to a better understanding of their performance or functionality (Singhal *et al.*, 2013). The high resolution (up to 300 nm) obtained, allows for the visualisation of fine-scale features (Singhal *et al.*, 2013). The data from the µCT results in a virtual rendering of the object under investigation, which allows one to travel through the volume in any direction and angle, revealing complex hidden and inaccessible structures within the object (Brunke, 2010; Singhal *et al.*, 2013).

The instrument

The fundamental components of any CT instrument, as seen in Figure 2.6 are (1) penetrating ionising radiation (X-ray radiation when using X-ray µCT), (2) a sample manipulator and (3) a detector (Duliu, 1999). The sample manipulator (or translation table) positions the sample in the path of the radiation beam and rotates it through a specific angle (usually 360°). The detector converts the attenuated radiation, which passes through the sample along a straight line, into a 2-D digital image, called a radiograph.

A radiograph

An X-ray radiograph image is essentially a map of the linear attenuation coefficient of every point in the sample (Singhal *et al.*, 2013). The radiograph consists of different scales of grey, depending on the different magnitudes of attenuation by the sample and components within the sample (Schena *et al.*, 2007). For 2-D visualisation, X-ray densities are mapped from black (low X-ray density = background) to white (high X-ray density = material). Therefore, a higher density phase appears brighter and is distinguishable from a lower density material.

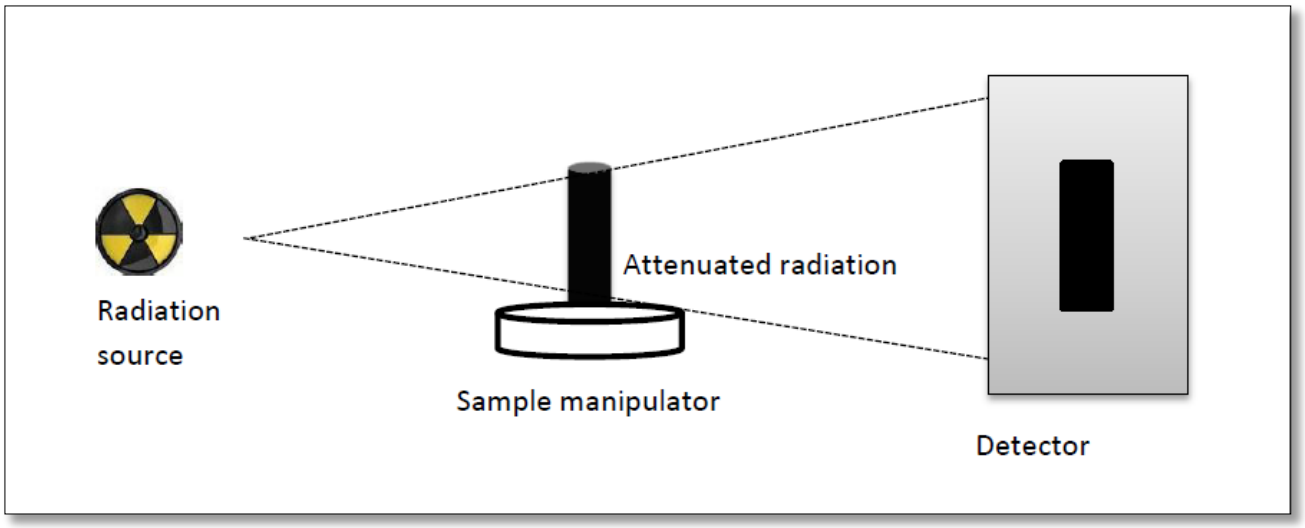

Figure 2.6. The fundamental components of any computed tomography instrument.

X-ray attenuation (μ) follows an exponential relationship with the incoming and outgoing X-rays from the sample. Differentiation of features within the sample is possible because of this linear attenuation coefficient that depends directly on the electron density (effective atomic number (Z) of the material comprising the sample) and the energy of the X-ray beam (E) (Lin & Miller, 2002).

A linear relationship exists between the sample-to-focal spot distance as a function of the voxel size achieved (Singhal *et al.*, 2013). Depending on the specific instrument used, the largest diameter and height of the object that can be imaged is 300 mm x 400 mm. The tube power (accelerating voltage x filament current) for any image acquisition is limited by the voxels size, because the tube has a focal spot size that dynamically increases with power. A focal spot size larger than the voxel size results in blurring of the pixels in the CT image (Singhal *et al.*, 2013). Therefore, for higher density objects, a lower resolution may be seen if a greater power penetration is required.

Reconstruction into a 3-D volume

Filtered back-projection algorithms are used to reconstruct the 3-D image volumes from the acquired 2-D data sets. Through this process a 3-D digital virtual volume of the sample is created from the series of radiographs through tomographic reconstruction (Schena *et al.*, 2007), as illustrated in Figure 2.7.

For a cone beam back-projection geometry, the reconstruction process requires that a whole 3-D data set is acquired within only one rotation of the sample (Lin & Miller, 2002). The projections displayed by the detector are proportional to the amount of radiation reaching the detector (Lin & Miller, 2002). Imaging is accomplished with a cone beam, providing a geometric magnification at the detector. For 3-D visualisation, the background will be rendered transparent, showing the material opaque white.

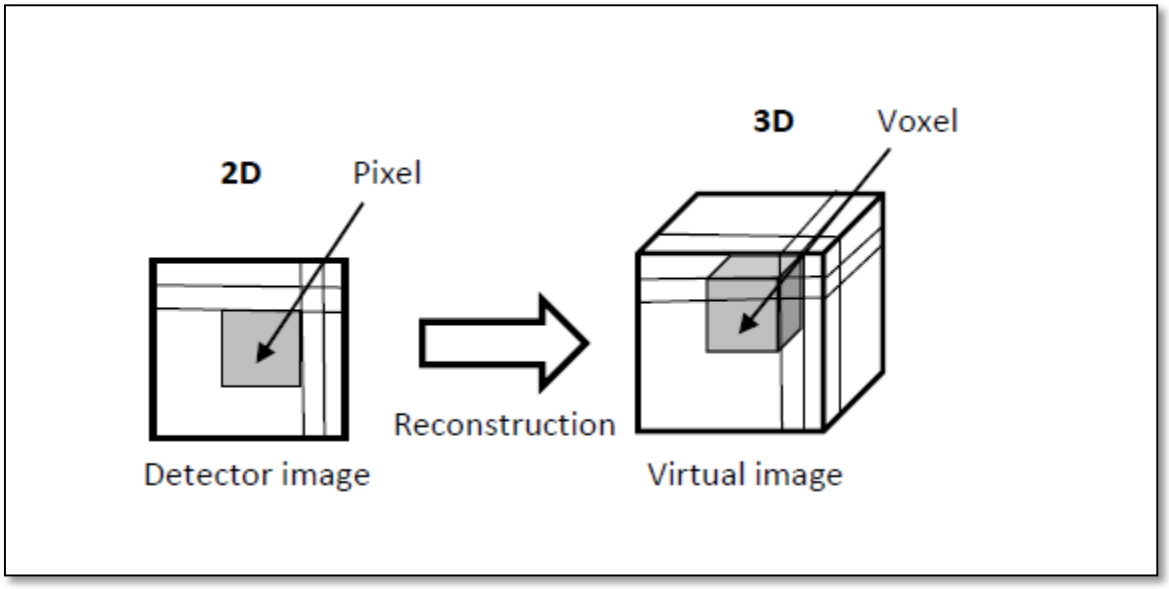

Figure 2.7. Schematic representation of tomographic reconstruction from 2-D to 3-D.

Analysis of the 3-D volume

Techniques to analyse µCT data sets are available in dedicated software packages such as VGStudio MAX software (Volume Graphics GmbH, Heidelberg, Germany). The measurement of specific areas or regions-of-interest (ROIs) can be accomplished by using a region grower tool that identifies voxels belonging to a selected grey value interval. In an example where the contact area of a thread from a capped bottle had to be measured, a ROI was created for the bottle (seen as the grey coloured area in Fig. 2.8). Another ROI was created for the bottle cap (coloured blue in Fig. 2.8), using the ROI of the bottle as the border. The result was the points of contact between the two ROIs and by using the option to extend the ROI of the cap with one voxel, this region extended into the bottle surface and points of contact could be displayed (seen as the red coloured area in Fig. 2.8) and quantified, using the Volume Analyser function. Using these analytical tools the exact contact area between bottle and cap of the closed bottle could be presented (Anon., 2014).

Other techniques available for µCT analysis are: defect detection (detection and analysis of pores/voids/cracks); nominal/actual comparison (compare geometries of two voxel data sets); wall thickness analysis and orientation analysis (orientation of fibers in 3-D and projected into a 2-D plane) (Singhal *et al.*, 2013).

Applications to maize

When considering X-ray µCT studies on maize, only few have been done, including Takhar *et al*. (2011) that focussed on moisture transport within maize kernels and De Carvalho *et al*. (1999) that studied stress cracks formation. The study of Gustin *et al.* (2013) recognised the potential of X-ray µCT as a method to determine kernel density and volume. Other cereal related studies are those

of Van Dalen *et al.* (2007) on pore structures of cereal products and that of Chaunier *et al.* (2007) that investigated the porosity of maize flakes.

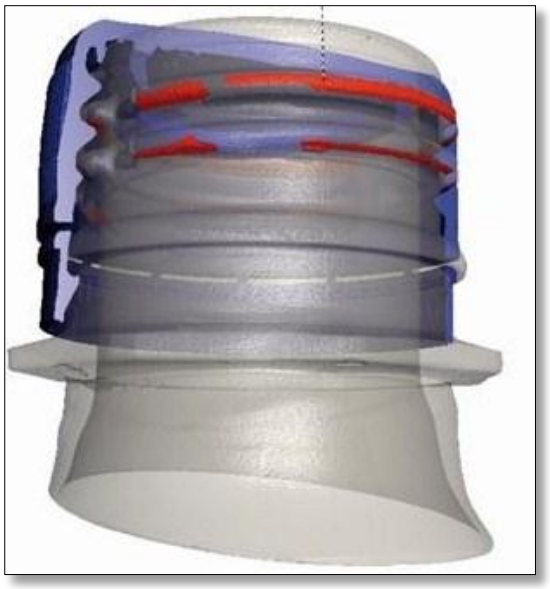

Figure 2.8. X-ray µCT segmentation of a bottle neck with screwed on bottle cap, creating regions-of-interest (ROIs): grey = bottle neck; blue = bottle cap and red = contact areas.

Statistical interpretation

When capturing data, a process is started with the aim to retrieve useful information and to draw a meaningful and significant conclusion. Statistics is crucial to complete the process, as it is through statistical analysis that the data can be interpreted and evaluated. Choosing the appropriate statistical method to fit a respective model, requires a lot of thought and consideration, a skill that is acquired through experience. When making use of single variables, the analysis is referred to as univariate statistical analysis, but when more than one variable is used simultaneously, multivariate data analyses are performed.

Univariate statistical analysis

Spearman's rank correlation coefficients

The correlation of ranks, as introduced by Spearman in the early 1900's, is a very appropriate procedure to use when non-parametric (values are replaced by ranks) results are expected (Zar, 1972). The Spearman correlation can be interpreted by its sign: the correlation will be positive (plus sign in front of the value) if the independent variable (Y) increases when the dependent variable (X) increases. If Y tends to decrease when X increase, the correlation will be indicated with a minus sign, and is thus negatively correlated. A Spearman correlation of zero indicates that there is no tendency for Y to either increase or decrease when X increases.

Intraclass correlation coefficients

When quantitative measurements of units within groups are made, the intraclass correlation coefficients (ICC) can be used to describe how strongly the units in the same groups resemble each other (Koch, 2004). The ICC assesses two factors: (a) the agreement that correlates the measurements with each other, while taking into account the differences in absolute values of the respective measurements, and (b) the consistency that only correlates the measurements (Bartko, 1976). If an ICC has a high agreement, very similar results are obtained from the comparing methods; a low agreement indicates a large bias amongst the methods (Bartko, 1976). ICC is thus a descriptive statistic and a useful tool to indicate the relationship among groups.

Analysis of variance

Analysis of variance (ANOVA) is a statistical model used to analyse variation among and between groups and to compare statistical significance thereof (Olson, 1976; Scheffe, 1999). ANOVA tests hypotheses from which decisions regarding the significance of a result can be made. Testing the null hypothesis, the result is seen as being statistically significant and the hypothesis will not be rejected, if it is deemed unlikely to have occurred by chance (Scheffe, 1999). For such a test, the probability (p-value) must be more than a threshold (significance level). To reject the null hypothesis, the p-value has to be less than the likely threshold value of 0.05, and is then seen as not significant (Olson, 1976).

Receiver operating characteristic curve

A receiver operating characteristic curve, or simply ROC curve, is a plot of the true positive rate or sensitivity against the false positive rate or 1 – specificity, at various threshold settings (DeLong *et al.*, 1988). The sensitivity defines how many correct positive results occur among all positive samples available during the test; 1 - specificity, on the other hand, defines how many incorrect positive results occur among all negative samples available during the test (Hanley & McNeil, 1983; DeLong *et al.*, 1988). The optimal threshold is determined by maximising the sum of sensitivity (no false negatives) and specificity (no false positives) and a tool is thus provided to select optimal models. The area under the ROC curve is also used to assess the fit of the logistic regression model and the closer the area value is to 1, the better the fit (Hanley & McNeil, 1983).

Multivariate statistical analysis

A multivariate statistical approach is followed when the simultaneous effect of many variables and the relationship amongst the samples are evaluated (Li Vigni *et al.*, 2013). In many instances, such as grain science, where instrumental analysis can provide many variables for each sample, the complexity of the data increases rapidly and requires multivariate data analysis techniques. Examples of multivariate statistical analysis are principal component analysis (PCA), used as an

instrument of descriptive statistics, and partial least squares (PLS) regression models, allowing predictions and classification accuracies. Multivariate image analysis (MIA), a technique developed to analyse hyperspectral imaging data incorporates both PCA and PLS, will also be explained.

Principal component analysis (PCA)

PCA was first introduced by Karl Pearson (1901) as "(a way of finding) lines and planes of closest fit to systems of points in the data space." PCA is a bi-linear decomposition technique which is responsible for reducing large amounts of data by creating principal components (PCs) (Massart, 1998). Also known as latent variables, these PCs capture the differences and similarities among the samples and variables of the modelled data (Li Vigni *et al.*, 2013). The decomposition of the data, using PCA, is as follows:

$$\mathbf{X} = \mathbf{T}_A\mathbf{V}_A^T + \mathbf{E}$$

where A is the number of PCs, **T** are the score vectors, **V** are the loading vectors and **E** represents the residual or noise. Another way to interpret the number of PCs, or A, is that they are the underlying structures or chemical rank of the matrix. In addition, the score vectors (T) give the coordinates of the samples in the PC space and allow the inspection of sample similarity/dissimilarity. Furthermore, the loadings vectors (V) represent the weight with which each original variable contributes to the PCs, enabling the inspection of the correlation structure among the variables through the loading scatter plots. The residual (E) is the part of the data that is not explained by the model and is used as an indicator of outlying samples and/or variables (Li Vigni *et al.*, 2013).

Partial least squares regression (PLS)

Regression is an approach where two or more sets of variables are associated with each other (Martens & Naes, 1991). When defining the variables to be modelled in a regression context, the Y-variable is seen as the dependent variable and the X-variables as the predictor or independent variables (Westad *et al.*, 2013). A regression technique such as partial least squares (PLS) is often used to build models that can be used to classify data or to make predictions. When using PLS, PCs are created which are associated with the maximum variance of **X,** as in PCA, but also incorporating the covariance associated with **Y** (Burger, 2006). These components are determined on the basis of decreasing significance, and with caution, as the incorrect number of PCs included in the calibration model will lead to unrealistic predictions (Burger, 2006).

When non-linearities in the relation between dependent and predictor variables occur (due to, e.g. clustering of the samples or different sub-populations), the global linear calibration models do not fit data correctly, leading to biased predictions. One way of dealing with this problem is to use a locally weighted (LW) regression approach (Martens & Næs, 1985) where, for each new sample to be predicted, a local model is developed based on its nearest neighbours, i.e. the calibration

objects nearest to it. LW regression based on PLS (Wold *et al.*, 1983) makes use of Euclidean distances on the original space variables and a uniform weighted scheme for the sample, as suggested by Centner and Massart (1998). In order to perform such a regression (LW-PLS2) for every new object (test), a different local calibration model must be built using only a defined number of closest samples, called nearest neighbours (n_{local}). To estimate the optimal number of neighbours to be considered in local modeling, together with the appropriate number of latent variables, a cross-validation procedure is normally used.

Multivariate image analysis

Simple multivariate statistical tools are not sufficient for hyperspectral imaging data analysis and these techniques need to be adapted for the large data sets produced by imaging (Burger & Geladi, 2006). A technique was developed to "unfold" the three dimensional image to create a two dimensional data set where second order analysis procedures (i.e. PCA) can be used (Geladi & Grahn, 1996). This technique involves the removal of spectra from a hyperspectral image, one row of pixels at a time, to create a long matrix of spectra. PLS is also often applied to spectral data to build models useful for making chemical classification or quantification predictions. However, when such models are applied to a single hyperspectral image as described above, over eighty thousand predictions will be produced (Burger, 2006). Again, the unfolding technique is used to simplify the data to achieve a successful calibration.

Conclusion

As maize hardness is an important quality trait for breeders, producers and processors, it is necessary to have access to reliable hardness methods. Up to date, no standardised hardness method exists, and therefore a wide range of methods, differing in methodologies and approaches, exist.

Hardness methods measure different properties, such as particle size subsequent to grinding and sieving, resistance to grinding and abrasion and the yield of grits. Other methods measure starch gelatinisation properties or polyphenol content to describe hardness. One of the older methods makes use of hand-dissection to determine the ratio of vitreous-to-floury endosperm. A similar method is machine vision technology that also quantifies the endosperm types in order to describe hardness.

NIR hyperspectral imaging can also be used to quantify endosperm types, whereas traditional NIR spectroscopy can predict maize hardness properties. Quality properties, such as protein, starch, fat and fiber contents are also seen as hardness descriptors, as well as kernel density. What is apparent from literature, is that many of these hardness methods do not correlate with each other, and that contradictory results are found between different studies.

X-ray µCT is an analytical technique that has found many applications in grain science and is increasingly used as a research tool. The 3-D visualisation of the imaged object permits functions

such as quantification and defect detection. Along with appropriate data analysis techniques and statistical methods, maize hardness can adequately be expressed.

References

Agu, R., Bringhurst, T. & Brosnan, J. (2006). Production of grain whisky and ethanol from wheat, maize and other cereals. *Journal of the Institute of Brewing*, **112**, 314-323.

Alcalà, M., Blanco, M., Moyano, D., Broad, N., O'Brien, N., Friedrich, D., Pfeifer, F. & Siesler, H. (2014). Qualitative and quantitative pharmaceutical analysis with a novel handheld miniature near-infrared spectrometer. *Journal of Near Infrared Spectroscopy*, **21**, 445-457.

Almeida-Dominguez, H.D., Suhendro, E.L. & Rooney, L.W. (1997). Factors affecting Rapid Visco-Analyser curves for the determination of maize kernel hardness. *Journal of Cereal Science*, **25**, 93-102.

Anonymous (1996). Corn: layers and structures of corn kernel. [Internet document]. URL http://www.britannica.com/EBchecked/media/162/The-outer-layers-and-internal-structures-of-a-kernel-of. Accessed 19/07/2013.

Anonymous (2008). Regulations relating to the grading, packing and marking of maize products intended for sale in the Republic of South Africa. Act No 119 of 1990, No. 30681. Johannesburg, South Africa: Goverment Gazette.

Anonymous (2014). Volume Graphics: Industrial applications. [Internet document]. URL http://www.volumegraphics.com/en/case-studies/industry/plastic-bottle-cap/. Accessed 22/05/2014.

Armstrong, P. (2006). Rapid single-kernel NIR measurement of grain and oil-seed attributes. *Applied Engineering in Agriculture*, **22**, 767.

Bartko, J.J. (1976). On various intraclass correlation reliability coefficients. *Psychological Bulletin*, **83**, 762-765.

Baye, T.M., Pearson, T.C. & Settles, A.M. (2006). Development of a calibration to predict maize seed composition using single kernel near infrared spectroscopy. *Journal of Cereal Science*, **43**, 236-243.

Bello, A., Waniska, R., Gomez, M. & Rooney, L. (1995). Starch solubilization and retrogradation during preparation of Tô (a Food Gel) from different sorghum cultivars. *Cereal Chemistry*, **72**, 80-84.

Berardo, N., Pisacane, V., Battilani, P., Scandolara, A., Pietri, A. & Marocco, A. (2005). Rapid detection of kernel rots and mycotoxins in maize by near-infrared reflectance spectroscopy. *Journal of Agricultural and Food Chemistry*, **53**, 8128-8134.

Blandino, M., Mancini, M.C., Peila, A., Rolle, L., Vanara, F. & Reyneri, A. (2010). Determination of maize kernel hardness: comparison of different laboratory tests to predict dry milling performance. *Journal of the Science of Food and Agriculture*, **90**, 1870-1878.

Brunke, O. (2010). High-resolution CT-based defect analysis and dimensional measurement. *Insight-Non-Destructive Testing and Condition Monitoring*, **52**, 91-93.

Burger, J. & Geladi, P. (2006). Hyperspectral NIR imaging for calibration and prediction: a comparison between image and spectrometer data for studying organic and biological samples. *Analyst*, **131**, 1152-1160.

Burger, J.E. (2006). Hyperspectral NIR image analysis: data exploration, correction and regression. PhD Thesis. Swedish University of Agricultural Sciences, Umeå, Sweden.

Centner, V. & Massart, D.L. (1998). Optimization in locally weighted regression. *Analytical Chemistry*, **70**, 4206-4211.

Chandrashekar, A. & Mazhar, H. (1999). The biochemical basis and implications of grain strength in sorghum and maize. *Journal of Cereal Science*, **30**, 193-207.

Chaunier, L., Della Valle, G. & Lourdin, D. (2007). Relationships between texture, mechanical properties and structure of cornflakes. *Food Research International*, **40**, 493-503.

Chiremba, C., Rooney, L.W. & Taylor, J.R.N. (2011). Relationships between simple grain quality parameters for the estimation of sorghum and maize hardness in commercial hybrid cultivars. *Cereal Chemistry*, **88**, 570-575.

Chiremba, C., Taylor, J., Rooney, L.W. & Beta, T. (2012). Phenolic acid content of sorghum and maize cultivars varying in hardness. *Food Chemistry*, **134**, 81-88.

De Beer, F. (2005). Characteristics of the neutron/X-ray tomography system at the SANRAD facility in South Africa. *Nuclear Instruments and Methods in Physics Research Section A: Accelerators, Spectrometers, Detectors and Associated Equipment*, **542**, 1-8.

De Carvalho, M.L.M., Van Aelst, A.C., Van Eck, J.W. & Hoekstra, F.A. (1999). Pre-harvest stress cracks in maize (*Zea mays* L.) kernels as characterized by visual, X-ray and low temperature scanning electron microscopical analysis: effect on kernel quality. *Seed Science Research*, **9**, 227-236.

Delcour, J. & Hoseney, R.C. (2010). *Principles of Cereal Science and Technology.* Pp. 1-22. Minnesota, USA: AACC International Press.

DeLong, E.R., DeLong, D.M. & Clarke-Pearson, D.L. (1988). Comparing the areas under two or more correlated receiver operating characteristic curves: a nonparametric approach. *Biometrics*, **44**, 837-845.

Dombrink-Kurtzman, M. & Knutson, C. (1997). A study of maize endosperm hardness in relation to amylose content and susceptibility to damage. *Cereal Chemistry*, **74**, 776-780.

Dombrink-Kurtzman, M.A. (1994). Examination of opaque mutants of maize by reversed-phase high-performance liquid chromatography and scanning electron microscopy. *Journal of Cereal Science*, **19**, 57-64.

Dombrink-Kurtzman, M.A. & Bietz, J.A. (1993). Zein composition in hard and soft endosperm of maize. *Cereal Chemistry*, **70**, 105-108.

Dorsey-Redding, H. & Johnson, F. (1991). Relationships among maize quality factors. *Cereal Chemistry*, **68**, 602-605.

Dowell, F., Maghirang, E., Graybosch, R., Baenziger, P., Baltensperger, D. & Hansen, L. (2006). An automated near-infrared system for selecting individual kernels based on specific quality characteristics. *Cereal Chemistry*, **83**, 537-543.

Downey, G., Byrne, S. & Dwyer, E. (1986). Wheat trading in the Republic of Ireland: The utility of a hardness index derived by near infrared reflectance spectroscopy. *Journal of the Science of Food and Agriculture*, **37**, 762-766.

Duarte, A.P., Mason, S.C., Jackson, D.S. & de C Kiehl, J. (2005). Grain quality of Brazilian maize genotypes as influenced by nitrogen level. *Crop Science*, **45**, 1958-1964.

Duliu, O.G. (1999). Computer axial tomography in geosciences: an overview. *Earth-Science Reviews*, **48**, 265-281.

Erasmus, C. (2003). Maize kernel translucency measurement by image analysis and its relationship to vitreousness and dry milling performance. PhD Thesis. University of Pretoria, Pretoria, South Africa.

Erasmus, C. & Taylor, J.R.N. (2004). Optimising the determination of maize endosperm vitreousness by a rapid non-destructive image analysis technique. *Journal of the Science of Food and Agriculture*, **84**, 920-930.

Eyherabide, G.H., Robutti, J.L. & Borras, F.S. (1996). Effect of near-infrared transmission-based selection on maize hardness and the composition of zeins. *Cereal Chemistry*, **73**, 775-778.

Fox, G. & Manley, M. (2009). Hardness methods for testing maize kernels. *Journal of Agricultural and Food Chemistry*, **57**, 5647-5657.

Gaytán-Martínez, M., Figueroa-Cárdenas, J., Reyes-Vega, M., Rincón-Sánchez, F. & Morales-Sánchez, E. (2006). Microstructure of starch granule related to kernel hardness in corn. *Revista Fitotecnia Mexicana*, **29**, 135-139.

Geladi, P. & Grahn, H. (1996). Multivariate Image Analysis. In: *Encyclopedia of Analytical Chemistry*. UK: Wiley Chichester.

Grahn, H.F. & Geladi, P. (2007). Multivariate images, hyperspectral imaging: background and equipment. In: *Techniques and Applications of Hyperspectral Image Analysis* (edited by P.L.M. Geladi, H.F. Grahn & J.E. Burger). Pp. 1-16. West Sussex, UK: John Wiley & Sons, Ltd.

Gustin, J.L., Jackson, S., Williams, C., Patel, A., Armstrong, P.R., Peter, G.F. & Settles, A.M. (2013). Analysis of maize (*Zea mays*) kernel density and volume using micro-computed tomography and single-kernel near infrared spectroscopy. *Journal of Agricultural and Food Chemistry*, **61**, 10872-10880.

Hanley, J.A. & McNeil, B.J. (1983). A method of comparing the areas under receiver operating characteristic curves derived from the same cases. *Radiology*, **148**, 839-843.

Hespell, R.B. (1998). Extraction and characterization of hemicellulose from the corn fiber produced by corn wet-milling processes. *Journal of Agricultural and Food Chemistry*, **46**, 2615-2619.

Janni, J., Weinstock, B.A., Hagen, L. & Wright, S. (2008). Novel near-infrared sampling apparatus for single kernel analysis of oil content in maize. *Applied spectroscopy*, **62**, 423-426.

Ji, Y., Wong, K., Hasjim, J., Pollak, L.M., Duvick, S., Jane, J. & White, P.J. (2003). Structure and function of starch from advanced generations of new corn lines. *Carbohydrate Polymers*, **54**, 305-319.

Kirleis, A. & Stroshine, R. (1990). Effects of hardness and drying air temperature on breakage susceptibility and dry-milling characteristics of yellow dent corn. *Cereal Chemistry*, **67**, 523-528.

Koch, G.G. (2004). Intraclass Correlation Coefficient. In: *Encyclopedia of Statistical Sciences*. UK: John Wiley & Sons, Inc.

Kotwaliwale, N., Singh, K., Kalne, A., Jha, S.N., Seth, N. & Kar, A. (2011). X-ray imaging methods for internal quality evaluation of agricultural produce. *Journal of Food Science and Technology*, **51**, 1-15.

Lee, E.A., Young, J.A., Frégeau-Reid, J.A. & Good, B.G. (2012). Genetic architecture underlying kernel quality in food-grade maize. *Crop Science*, **52**, 1561-1571.

Lee, K.M., Bean, S.R., Alavi, S., Herrman, T.J. & Waniska, R.D. (2006). Physical and biochemical properties of maize hardness and extrudates of selected hybrids. *Journal of Agricultural and Food Chemistry*, **54**, 4260-4269.

Lee, K.M., Herrman, T.J., Rooney, L.W., Jackson, D.S., Lingenfelser, J., Rausch, K.D., McKinney, J., Iiams, C., Byrum, L., Hurburgh, J.C.R., Johnson, L.A. & Fox, S.R. (2007). Corroborative study on maize quality, dry-milling and wet-milling properties of selected maize hybrids. *Journal of Agricultural and Food Chemistry*, **55**, 10751-10763.

Lending, C.R. & Larkins, B.A. (1989). Changes in the zein composition of protein bodies during maize endosperm development. *The Plant Cell Online*, **1**, 1011-1023.

Li, P.X.P., Hardacre, A.K., Campanella, H. & Kirkpatrick, K.J. (1996). Determination of endosperm characteristics of 38 corn hybrids using the Stenvert hardness test. *Cereal Chemestry*, **73**, 466-471.

Li Vigni, M., Durante, C. & Cocchi, M. (2013). Exploratory data analysis. In: *Chemometrics in Food Science*. Pp. 55-126. Oxford, England: Elsevier.

Lin, C. & Miller, J. (2002). Cone beam X-ray microtomography-a new facility for three-dimensional analysis of multiphase materials. *Minerals and Metallurgical Processing*, **19**, 65-71.

Manley, M., Williams, P., Nilsson, D. & Geladi, P. (2009). Near infrared hyperspectral imaging for the evaluation of endosperm texture in whole yellow maize (*Zea mays* L.) kernels. *Journal of Agricultural and Food Chemistry*, **57**, 8761-8769.

Martens, H. & Næs, T. (1985). Multivariate calibration. II. Cemometric methods. *Trends in Analytical Chemistry*, **3**, 266-271.

Martens, H. & Naes, T. (1991). *Multivariate calibration.* New York, USA: John Wiley & Sons Ltd.

Massart, D.L. (1998). Data handling in science and technology series, part A. In: *Handbook of Chemometrics and Qualimetrics* (edited by B. Vandeginste, L. Buydens, S. De Jong, P. Lewi & J. Smeyers-Verbeke). Pp. 519-556. Amsterdam: Elsevier.

McGoverin, C. & Manley, M. (2012). Classification of maize kernel hardness using near infrared hyperspectral imaging. *Journal of Near Infrared Spectroscopy*, **20**, 529-535.

Mestres, C., Louis-Alexandre, A., Matencio, F. & Lahlou, A. (1991). Dry-milling properties of maize. *Cereal Chemistry*, **68**, 51-56.

Mestres, C. & Matencio, F. (1996). Biochemical basis of kernel milling characteristics and endosperm vitreousness of maize. *Journal of Cereal Science*, **24**, 283-290.

Narváez-González, E.D., de Dios Figueroa-Cárdenas, J., Taba, S., Tostado, E.C., Peniche, R.Á.M. & Sánchez, F.R. (2006). Relationships between the microstructure, physical features, and chemical composition of different maize accessions from Latin America. *Cereal Chemistry*, **83**, 595-604.

O'Brien, N.A., Hulse, C.A., Friedrich, D.M., Van Milligen, F.J., von Gunten, M.K., Pfeifer, F. & Siesler, H.W. (2012). Miniature near-infrared (NIR) spectrometer engine for handheld applications. In: *Defense, Security, and Sensing SPIE*. Pp. 837404-837408.Baltimore, Maryland, USA.

O'Kennedy, K. (2011). Characterisation of zein from South African maize of varying endosperm texture. MSc Thesis. Stellenbosch University, South Africa.

Olson, C.L. (1976). On choosing a test statistic in multivariate analysis of variance. *Psychological Bulletin*, **83**, 579-586.

Orman, B.A. & Schumann Jr, R.A. (1991). Comparison of near-infrared spectroscopy calibration methods for the prediction of protein, oil, and starch in maize grain. *Journal of Agricultural and Food Chemistry*, **39**, 883-886.

Paiva, E., Kriz, A.L., Peixoto, M.J.V.V.D., Wallace, J.C. & Larkins, A.B. (1991). Quantitation and distribution of ã–zein in the endosperm of maize kernels. *Cereal Chemistry*, **68**, 276-279.

Paulsen, M. & Hill, L. (1985). Corn quality factors affecting dry milling performance. *Journal of Agricultural Engineering Research*, **31**, 255-263.

Pearson, K. (1901). LIII. On lines and planes of closest fit to systems of points in space. *The London, Edinburgh, and Dublin Philosophical Magazine and Journal of Science*, **2**, 559-572.

Pearson, T., Wicklow, D., Maghirang, E., Xie, F. & Dowell, F. (2001). Detecting aflatoxin in single corn kernels by transmittance and reflectance spectroscopy. *American Society of Agricultural Engineers*, **44**, 1247-1254.

Peplinski, A.J., Paulsen, M.R., Anderson, R.A. & Kwolek, W.F. (1989). Physical, chemical, and dry-milling characteristics of corn hybrids from various genotypes. *Cereal Chemisty*, **66**, 117-120.

Pomeranz, Y., Czuchajowska, Z., Martin, C. & Lai, F. (1985). Determination of corn hardness by the Stenvert hardness tester. *Cereal Chemistry*, **62**, 108-112.

Robutti, J.L., Borras, F., Ferrer, M.o., Percibaldi, M. & Knutson, C.A. (2000). Evaluation of quality factors in Argentine maize races. *Cereal Chemistry*, **77**, 24-26.

Robutti, J.L., Borras, F.S. & Eyherabide, G.H. (1997). Zein compositions of mechanically separated coarse and fine portions of maize kernels. *Cereal Chemistry*, **74**, 75-78.

Rotar, I., Dale, L.M., Vidican, R., Mogos, A. & Ceclan, O. (2009). Research on Protein Content and Total Nitrogen and a Cob of Maize Strains by FT-NIR Spectrometry. *Bulletin of University of Agricultural Sciences and Veterinary Medicine Cluj-Napoca. Agriculture*, **66**.

Sahai, D., Buendia, M. & Jackson, D. (2001). Analytical techniques for understanding nixtamalized corn flour: particle size and functionality relationships in a Masa flour Sample 1. *Cereal Chemistry*, **78**, 14-18.

Sandhu, K.S. & Singh, N. (2007). Some properties of corn starches II: Physicochemical, gelatinization, retrogradation, pasting and gel textural properties. *Food Chemistry*, **101**, 1499-1507.

Scheffe, H. (1999). *The Analysis of Variance.* New York, United States of America: John Wiley & Sons.

Schena, G., Santoro, L. & Favretto, S. (2007). Conceiving a high resolution and fast X-ray CT system for imaging fine multi-phase mineral particles and retrieving mineral liberation spectra. *International Journal of Mineral Processing*, **84**, 327-336.

Schweizer, S.M. & Moura, J.M.F. (2001). Efficient detection in hyperspectral imagery. *Image Processing*, **10**, 584-597.

Seetharaman, K., Tziotis, A., Borras, F., White, P.J., Ferrer, M. & Robutti, J. (2001). Thermal and functional characterization of starch from Argentinean Corn1. *Cereal Chemistry*, **78**, 379-386.

Serna-Saldivar, S.O. (2010). *Cereal Grains: Properties, Processing, and Nutritional Attributes.* Pp. 1-752. London, UK: CRC Press Inc.

Singhal, A., Grande, J.C. & Zhou, Z. (2013). Micro/Nano CT for visualization of internal structures. *Microscopy Today*, **21**, 16-22.

Spielbauer, G., Armstrong, P., Baier, J.W., Allen, W.B., Richardson, K., Shen, B. & Settles, A.M. (2009). High-throughput near-infrared reflectance spectroscopy for predicting quantitative and qualitative composition phenotypes of individual maize kernels. *Cereal Chemistry*, **86**, 556-564.

Sun, D. (2010). Principles of hyperspectral imaging technology. In: *Hyperspectral Imaging for Food Quality Analysis and Control* (edited by D.-W. Sun). Pp. 3-44. Oxford, UK: Elsevier.

Takhar, P.S., Maier, D.E., Campanella, O.H. & Chen, G. (2011). Hybrid mixture theory based moisture transport and stress development in corn kernels during drying: Validation and simulation results. *Journal of Food Engineering*, **106**, 275-282.

Tran, T., Deman, J. & Rasper, V. (1981). Measurement of corn kernel hardness. *Canadian Institute of Food Science and Technology Journal*, **14**, 42-48.

Van Dalen, G., Nootenboom, P. & Van Vliet, L.J. (2007). 3D Imaging and analysis of porous cereal products using X-ray microtomography. In: *The 12th International Congress for Stereology (ICSXII), 2007*. September 3-7, 2007.Saint-Etienne, France.

Van Loggerenberg, D. & Pretorius, A.J. (2004). Determining the milling index of maize with a NIT calibration. In: *Proceedings of the South African Society of Crop Producers Congress*. January 2004.Bloemfontein, South Africa.

Voca, N., Varga, B., Kricka, T., Curic, D., Jurisic, V. & Matin, A. (2009). Progress in ethanol production from corn kernel by applying cooking pre-treatment. *Bioresource Technology*, **100**, 2712-2718.

Wang, D. & Eckhoff, S.R. (2000). Effect of broken corn levels on water absorption and steepwater characteristics. *Cereal Chemistry*, **77**, 525-528.

Watson, S.A. (1987). Structure and Composition. In: *Corn Chemistry and Technology* (edited by S.A. Watson & P.E. Ramstad). Pp. 53-82. St. Paul, Minnesota, USA: American Association of Cereal Chemists, Inc.

Wehling, R., Jackson, D. & Hamaker, B. (1996). Prediction of corn dry-milling quality by Near-Infrared Spectroscopy. *Cereal Chemistry*, **73**, 543-546.

Westad, F., Bevilacqua, M. & Marini, F. (2013). Regression. In: *Chemometrics in Food Science*. Pp. 127-170. Oxford, UK: Elsevier.

Williams, P., Geladi, P., Fox, G. & Manley, M. (2009). Maize kernel hardness classification by near infrared (NIR) hyperspectral imaging and multivariate data analysis. *Analytica Chimica Acta*, **653**, 121-130.

Wold, S., Martens, H. & Wold, H. (1983). *The multivariate calibration problem in Chemistry 576 solved by the PLS method.* Heidelberg, Germany: Springer-Verlag.

Wolf, M.J., Buzan, C.L., MacMasters, M.M. & Rist, C.E. (1952). Structure of the mature corn kernel. I. Gross anatomy and structural relationships. *Cereal Chemistry*, **29**, 321-333.

Wu, Y.V. (1992). Corn hardness as related to yield and particle size of fractions from a micro hammer-cutter mill. *Cereal Chemistry*, **69**, 343-347.

Yamin, F., Lee, M., Pollak, L. & White, P. (1999). Thermal properties of starch in corn variants isolated after chemical mutagenesis of inbred line B73 1. *Cereal Chemistry*, **76**, 175-181.

Zar, J.H. (1972). Significance testing of the Spearman rank correlation coefficient. *Journal of the American Statistical Association*, **67**, 578-580.

Chapter 3

Application of Rapid Visco Analyser (RVA) viscograms and chemometrics for maize hardness characterisation*

Abstract

It has been established in this study that the Rapid Visco Analyser (RVA) can describe maize hardness, irrespective of the RVA profile, when used in association with appropriate multivariate data analysis techniques. Therefore, the RVA can complement or replace current and/or conventional methods as a hardness descriptor. Hardness modelling based on RVA viscograms was carried out using seven conventional hardness methods (hectoliter mass (HLM), hundred kernel mass (HKM), particle size index (PSI), percentage vitreous endosperm (%VE), protein content, percentage chop (%chop) and near infrared (NIR) spectroscopy) as references and three different RVA profiles (hard, soft and standard) as predictors. An approach using locally weighted partial least squares (LW-PLS) was followed to build the regression models. The resulted prediction errors (root mean square error of cross-validation (RMSECV) and root mean square error of prediction (RMSEP)) for the quantification of hardness values were always lower or in the same order of the laboratory error of the reference method.

*Published as: Guelpa A, Bevilacqua M, Marini F, O'Kennedy K, Geladi P & Manley M (2014). Application of Rapid Visco Analyser (RVA) viscograms and chemometrics for maize hardness characterisation. *Food Chemistry*, **173**, 1220–1227.

Introduction

Maize hardness is an important quality characteristic for the dry-milling industry. In South Africa, the dry-milling industry is significant as maize is the largest crop produced, of which two-thirds (*ca*. 4 million tons per annum) are processed into maize meal used to make porridge (SAGIS, 2013). For its definition, numerous aspects have to be considered. Even with careful consideration, the interpretation and measurement of maize hardness can still be confusing and needs further investigation. Nonetheless, the hardness of maize is important when determining the processing settings, such as for dry-milling. Similar to other grains, maize kernel hardness is principally a genetic characteristic (Johnson & Russell, 1982), although environmental influences (Hamilton *et al.*, 1951) and external factors such as postharvest handling (Peplinski *et al.*, 1989) will also affect the hardness. Maize (*Zea mays* L.) is anatomically made up of two types of endosperm, i.e. a harder (vitreous) endosperm situated to the outside of the kernel, and a softer (floury) endosperm found in the center of the kernel (Watson, 1987; Paiva *et al.*, 1991). It is known that hard kernels are favoured by industry as hard maize produces greater yield and a higher quality meals and grits than soft maize (Lee *et al.*, 2007).

There are many methods available to determine maize hardness, as extensively reviewed by Fox and Manley (2009). Yet, it is not clear which method best describes hardness. It is even more difficult to decide on a method that best describes milling quality. In this study, the samples were ranked according to their milling performance as measured during the actual milling process, although on pilot plant-scale. The outcome of good milling is indicated by a small percentage of hominy chop. Hominy chop (comprising the pericarp, tip cap, germ and some endosperm) is of lesser value than maize meal and grits and predominantly used as animal feed. Maize that mill poorly delivers a larger percentage chop (%chop) as soft endosperm is also included into the chop. Percentage chop is therefore used as an indication of the milling quality of maize, although it is not a recognised hardness measurement method as such. In this study, the relationship of %chop to other conventional hardness methods was investigated. These conventional methods were chosen to include many different descriptors, i.e. density, size and soundness (hectoliter mass and hundred kernel mass), particle size or breakage susceptibility (particle size index and near infrared absorbance) and quality properties (protein content and near infrared hyperspectral imaging).

Great financial losses experienced in the Australian wheat industry in the 1980's lead to the development of the Rapid Visco Analyser (RVA) (Ross *et al.*, 1987). This viscometric method has since found meaningful applications in a vast range of applications, especially in grain science due to the large amount of starch present in cereals (Doublier *et al.*, 1987; Agu *et al.*, 2006). The RVA measures the viscosity developed with hydration and subsequent gelatinisation of starch granules during heating and stirring in excess water (Almeida-Dominguez *et al.*, 1997). It has been reported that the RVA can be used to quantify maize hardness differences between maize hybrids (Yamin *et al.*, 1999; Seetharaman *et al.*, 2001; Ji *et al.*, 2003; Sandhu & Singh, 2007). This was due to hard

maize producing mainly coarse particles when milled, and soft maize smaller particles (Almeida-Dominguez *et al.*, 1997). Coarse particles have slower water diffusion, limited swelling of the starch granules and slow viscosity development (Sahai *et al.*, 2001; Narváez-González *et al.*, 2006). Smaller particles have bigger surface areas that result in better and more rapid hydration, thus better gelatinisation and higher viscosity (Almeida-Dominguez *et al.*, 1997). Furthermore, hard kernels show a more prominent protein-to-starch adhesion effect compared to soft kernels (Almeida-Dominguez *et al.*, 1997). The protein matrix of vitreous endosperm is thicker than that of floury endosperm (Wang & Eckhoff, 2000), and forms a barrier that slows hydration and gelatinisation (Almeida-Dominguez *et al.*, 1997; Narváez-González *et al.*, 2006).

Based on these considerations, determination of the usefulness of the RVA as a hardness descriptor was a key concern in the current study. With this aim, RVA viscograms were recorded on different maize samples which were also quantified and characterized for hardness by the seven conventional (reference) methods. The objective was to define whether it was possible to obtain information about properties (such as density, breakage susceptibility and protein content), that are commonly associated with hardness, from RVA curves obtained through single measurements. In order to analyse such a complex data set, the use of appropriate chemometrics techniques was required. At first, principal component analysis (PCA) was used to achieve a better understanding of the relations among the seven reference methods. Subsequently, the use of a non-linear regression technique, i.e. locally weighted partial least squares (LW-PLS) regression (Centner & Massart, 1998; Bevilacqua *et al.*, 2012) was used to build a regression model to predict maize hardness from the RVA curves. This was done for all seven reference methods individually.

Materials and methods

Maize samples

Nineteen pure hybrids of South African white maize, originating from maize breeding trials, were used. These hybrids, kindly supplied by PANNAR Seeds (Greytown, South Africa) came from three localities (Greytown, Delmas and Klerksdorp, South Africa) and two plantings in 2012 (early and late). A local farmer from Schweizer-Reneke also supplied some of the samples, resulting in a total of 49 samples. Before being milled, the samples were stored at ambient temperature in sealed plastic containers.

Methods

Pasting properties (acquisition of RVA data)

Maize samples were milled using a hammer type cyclone Laboratory Mill 3100 (Perten, Hägersten, Sweden) fitted with a 1 mm sieve. Milling was conducted on the same day as moisture content determination and RVA measurement. The moisture content of the milled maize samples was determined prior to RVA analysis according to a method used by Emvula (2012) which is an adapted method of the AACC modified vacuum oven method (AACC, 1999a).

Pasting properties of maize were determined using a Rapid Visco Analyser (RVA) model 4500 (Perten Instruments, Australia). Distilled water (25 ± 0.01 g) was added to the milled maize (3 ± 0.01 g, db) in an aluminium RVA canister to obtain a total constant sample weight of 28 ± 0.01 g. The masses of the dH_2O and maize were adjusted (± 0.01 g) to compensate for the differences in moisture content of each sample. In all the tests a moisture level of 15% was maintained, resulting in a relative high solid percentage. Clumping was prevented by stirring with a plastic paddle after which pre-programmed profiles were initiated.

The three profiles used to capture rheological information (RVA curves) were: a soft maize profile (Almeida-Dominguez *et al.*, 1997), a standard profile (AACC, 1999c) and a hard maize profile (Almeida-Dominguez *et al.*, 1997). The respective holding times, heating rates and final temperatures used are summarised in Table 3.1.

Table 3.1 Details of the RVA soft, standard and hard maize profiles (temperature and time)

Stage	Soft maize profile	Standard profile	Hard maize profile
Initial temperature (°C)	50	50	50
Initial holding time (min)	2:00	1:00	2:00
Heating time (min)	4:30	3:42	19:00
Max temperature (°C)	95	95	95
Hold at max temperature (min)	4:30	2:30	4:00
Cooling time (min)	4:00	3:48	-
Final temperature (°C)	50	50	95
Final holding time (min)	10:00	2:00	2:00
Total test time (min)	25:00	13:00	27:00

For each of the tests, viscosity (cP), temperature (°C), speed (rpm) and the heat-cool ratio were recorded every four seconds, therefore generating for each sample three measurement vectors of 376 (soft profile), 196 (standard profile), and 406 (hard profile) data points, respectively. The resulting

curve, reporting the viscosity (sometimes together with the temperature ramp, for the sake of better clarity) as a function of time, is called a viscogram. All the RVA tests were done in triplicate.

Determination of maize hardness by conventional reference methods

Seven conventional methods were used to explain the differences in kernel hardness: hectoliter mass (HLM), hundred kernel mass (HKM), protein content, %chop, particle size index (PSI), NIR hyperspectral imaging (percentage vitreous endosperm, %VE) and NIR absorbance value at 2230 nm.

Hectoliter mass

The HLM of the samples was determined using a German Kern 220/222 Grain Sampler (KERN & SOHN GmbH, Balingen-Frommern, Germany). The sampler was placed on a firm, non-flexible, vibration-free horizontal base. The scraper blade was inserted in the empty 1 L measuring container. The pre-filling measure was filled to the marked level with the maize. It was then emptied within 3 or 4 cm from the upper edge of the filling hopper in such a way that the maize could flow evenly into the middle of the filling hopper in 11 to 13 s. After filling, the straight edge was quickly pulled out, but without shaking the equipment. When the piston and the maize have fallen into the measuring container, the straight edge was placed back in the slit and pushed through the maize in a single stroke. If a kernel became jammed between the slit edges, the pouring was repeated. The excess maize lying on the straight edge was thrown out. The filling hopper and straight edge was removed. The maize was weighed (in g) and the HLM was read from the conversion chart supplied with the device in $kg.hL^{-1}$. This test was done in duplicate at the research and development facility of Sasko (Essential Foods, Division of Pioneer Foods (Pty.) Ltd., Paarl, South Africa).

Hundred kernel mass

The HKM of the samples was determined using an industry accepted method that provides a measure of grain size and density. One hundred whole maize kernels were obtained using a Numigral Seed Counter (Chopin Technologies, France) and weighed in grams. These determinations were done in triplicate at the research and development facility of Sasko (Essential Foods, Division of Pioneer Foods (Pty.) Ltd., Paarl, South Africa).

Protein content

The protein content was determined using the official method for crude protein (Dumas method) (AACC, 1999b). A LECO TruMac N (LECO Corporation, Saint Joseph, Michigan, USA) was used, which is a macro combustion nitrogen determinator that utilises a pure oxygen environment in a ceramic horizontal furnace operating at a high temperature (1200 ºC). Protein content was determined at 12 % moisture base (mb), and the results were expressed as nitrogen multiplied by the protein factor of 6.25. Duplicate determinations were done and the averaged results were used.

Protein content results were kindly supplied by Sasko (Essential Foods, Division of Pioneer Foods (Pty.) Ltd., Paarl, South Africa).

Percentage chop

The %chop was determined using a pilot plant scale de-germer and maize mill. De-germed maize was subjected to the milling process and the chop (combination of pericarp, germ and to a lesser extent endosperm) was calculated as a percentage of the total mass of the maize. The observed trend, when using this method, indicated that maize with a %chop below 22% was good milling maize, between 22% and 25% was good intermediate, between 26% and 30% was poor intermediate and above 30% was poor milling maize. Only single determinations were done. Results were kindly supplied by Sasko (Essential Foods, Division of Pioneer Foods (Pty.) Ltd., Paarl, South Africa). Due to the sensitivity of the data, the method cannot be described in detail.

Particle size index

The PSI method was used to differentiate between hard and soft maize samples. The samples were milled using a hammer type cyclone Laboratory Mill 3100 (Perten, Hägersten, Sweden) fitted with a 1 mm sieve. A two sieve method was used, where a 150 µm sieve was placed on a 75 µm sieve, fitted with a receiving pan (O'Kennedy, 2011). The pans and sieves (Retsch, Haan, Germany) were stacked on top of each other and placed in a Retsch AS 200 Tap Sieve Shaker for 10 min (Retsch, Haan, Germany). Three fractions, PSI_1 (particles > 150 µm), PSI_2 (particles < 150 µm, but > 75 µm) and PSI_3 (particles < 75 µm) were determined. The higher PSI_1 the harder the kernels; high PSI_2 and PSI_3 values indicate soft kernels. In addition, the ratio between larger (PSI_1) and smaller particle sizes (PSI_2 + PSI_3) was calculated to give a course over fine (c/f) ratio, where a higher number indicated harder samples (more dense) and vice versa. The PSI measurements were done in duplicate.

Percentage vitreous endosperm (%VE)

NIR hyperspectral images were acquired using an Umbio Inspector SWIR (short wave infrared) (Umbio AB, Umeå, Sweden) pushbroom hyperspectral imaging system. The Umbio pushbroom imager comprised an imaging spectrograph coupled to a 2-D array Mercury-Cadmium-Tellurium detector. Line illumination was obtained with two arrays of quartz-halogen lamps with regulated current. The samples were scanned on a moving belt. Individual images were acquired with a spectral range of 1151 – 2199 nm with 6 – 7 nm spacing. Images were made with a width of 320 pixels and variable length in 239 wavelength bands.

Six to ten maize kernels per sample were placed germ-down (endosperm rich) onto a plastic sample holder (75 mm x 110 mm) fitted with double sided tape. For each scanned sample an internal dark reference was measured. The external white reference was a Spectralon (ACAL BFi Nordic,

Uppsala, Sweden) strip measured just before the sample. The sample holders were put on the moving belt with the longest dimension in the direction of the movement.

The raw images were processed in Evince 2.5.5 (Umbio, Umeå, Sweden), converted to absorbance using the individual white and dark reference files and cleaned from unnecessary background. Absorbance images were subjected to PCA for further cleaning. PCA score plots, as well as the PCA score images, were used to identify outliers, bad pixels, illumination and shading errors, edge effects and background. Due to the huge number of pixels in these images, criteria normally used for smaller data sets (such as residuals and Hotelling's T^2 values) were not used in this case. Unwanted pixels were simply removed after visual inspection. PCA was recalculated using 6 PCs and all pairwise combinations of PC 1 to PC 6 were examined for any further pixel outliers. Outliers are usually found in the first two components, but after removal of the most obvious outliers, more components may be needed for further analysis. Six PCs were used for recalculating the models in order to obtain the best suited image for mosaic creation. No data pre-treatment (except mean centering) was used as multiplicative scatter correction (MSC) as an example of a pre-treatment method, would reduce information relating to scattering effects or differences which were necessary for this study.

A mosaic of the images of the samples was constructed. A mosaic is a number of images merged into a new single image. No pre-treatment was used and PCA was applied after mean centering. PCA score plots and images were used interactively to assign pixels (i.e. individual spectra) to endosperm (floury and vitreous) and non-endosperm (germ and pedicle) regions. After exclusion of the non-endosperm regions, PCA was re-applied. Two distinct clusters were observed in PC 1 vs PC 3 and these regions were identified as representing the respective endosperm types, i.e. vitreous and floury endosperm. The method of identification was based on selecting groups of points within the score plot and observing where the pixels were located within the score image. Two classes were subsequently created and the number of pixels within each class was determined for each individual kernel. The pixel counts were expressed as a percentage floury endosperm (%FE) and a percentage vitreous endosperm (%VE). Only the %VE results were used in this study as a measure of kernel hardness.

NIR absorbance at 2230 nm

This method, proposed by Downey *et al*. (1986), makes use of a wavelength (2230 nm), where reflectance is effectively independent of the samples' composition, but varies only with regards to the milled samples' particle size. Therefore, maize samples were ground using a hammer mill (Retsch, Haan, Germany) fitted with a 0.8 mm sieve. A BÜCHI NIRFlex N-500 Fourier transform near-infrared (FTNIR) spectrophotometer (BÜCHI Labortechnik GmbH, Flawil, Switzerland) with NIRLabWare (version 3.0) (BÜCHI Labortechnik GmbH, Flawil, Switzerland) near infrared (NIR) measurement software was used to perform the measurements of the ground maize samples in diffuse reflectance mode. The samples were presented to the instrument in rotating glass Petri

dishes, and the NIR spectra were collected from 1100 to 2500 nm (9090-4000 cm^{-1}) at an optical resolution of 32 cm^{-1}. The raw spectra (no pre-treatment) were used to measure the absorbance (log 1/R) at 2230 nm. Hardness values were derived by the following equation:

Hardness = a + b(log 1/R)

Values for a = -40 and b = 100 were selected arbitrarily to produce a scale of hardness from 0 to 15.

Chemometrics and statistical data analysis

Statistical analysis

Spearman's rank correlation coefficients were used to test the strength of the relationships between pairs of conventional methods (HLM, HKM, PSI, %VE, protein content, %chop and NIR at 2230 nm) in a bivariate fashion.

Principal component analysis

PCA reduces large data sets into fewer principal components (PCs) which are then used in the model. PC scores images and scores plots were used interactively to investigate samples for special features or irregularities and the observed explained variation studied by means of the accompanying PC loadings plots. The seven conventional methods (HLM, HKM, PSI, %VE, protein content, %chop and NIR at 2230 nm), used to assess the maize hardness, were compared using PCA to gain a holistic view of the entire reference data set.

Locally weighted partial least squares regression

When non-linearities in the relation between responses and predictors occur (due to, e.g. clustering of the samples or different sub-populations), the global linear calibration models do not fit data correctly, leading to biased predictions. One way of dealing with this problem is to use a locally weighted (LW) regression approach (Martens & Næs, 1985) where, for each new sample to be predicted a local model is developed based on its nearest neighbours, i.e. the calibration objects nearest to it. In this case, the use of LW regression based on partial least squares (PLS) (Wold *et al.*, 1983) using Euclidean distances on the original space variables and a uniform weighted scheme for the sample, was employed, as suggested by Centner and Massart (1998). In order to perform such a regression (LW-PLS2) for every new object (test), a different local calibration model must be built using only a defined number of closest samples, called nearest neighbours (n_{local}). To estimate the optimal number of neighbours to be considered in local modeling, together with the appropriate number of latent variables, a cross-validation procedure is normally used.

The hardness results from HLM, HKM, PSI, %VE, protein content, %chop and NIR at 2230 nm where used as reference when RVA viscograms were used to predict the same hardness descriptors. To present the results, error measures have been used, i.e. root mean square error of cross-validation (RMSECV) and root mean square error of prediction (RMSEP).

Software

Correlation analysis was performed using Microsoft Excel 2010 (Microsoft Corporation, Seattle, WA). Chemometric data processing was carried out by means of in-house functions and PLS Toolbox v 7.02 (Eigenvector Research Inc., Wenatchee, WA) running under MATLAB 2012b environment (The MathWorks, Natick, MA, USA).

Results and discussion

Descriptive statistics of the seven hardness related reference methods are summarised in Table S3.1.

PCA and correlations

A PCA model was built on the Y-block (reference data) to check for correlations and any possible relations between these variables (hardness methods). To account for the hardness indices being measured with different number of replicates (some in triplicate, some in duplicate and the remaining singular), the reference values for the respective hardness measurements (that was used for the PCA model) was taken as the averages of the respective number of replicates for each sample.

From the loadings plot (Fig. 3.1a) it can be seen that all the hardness measurement methods investigated were important in defining the characteristics of the samples, since no variables were lying in the center of the plot. At the same time, the PCA models showed that most of the reference methods correlated with each other, with respect to maize hardness properties. In particular, it can be observed how strongly correlated the variables in the rightmost part of plot (NIR, %VE, HLM and HKM) were and how they were negatively correlated with %chop. All these considerations were confirmed by the Spearman's rank correlation coefficients (Table 3.2).

Since, among these variables %chop is the more related to the actual quality of the milling process it was considered in this study as the true measure for milling quality. This assumption, and the practicality of %chop as reference method, was confirmed by the scores plot of the PCA model (Fig. 3.1b). In Figure 1b the dots have been coloured according to increasing (from blue to red) values of %chop. The progressive spread of the samples along the diagonal of the plot (thus both PCs 1 and 2 required to explain the direction of variation) can be seen as a further confirmation of how the samples differed in milling quality, and how all the variables shown in the PCA loadings plot (Fig.3.1a) contributed to describe this overall quality.

It can be seen from the histograms of the distribution of the reference data (Fig.S3.1) that for most of the variables, the values do not follow a normal distribution around their mean values. It is possible to clearly identify two different populations among the samples, in particular for %chop and PSI. These considerations led to the hypothesis of the presence of strong non-linearities in the data that could hinder the use of a linear method for building a regression model among the RVA curves and the reference values for maize kernel hardness.

Table 3.2. Spearman's rank correlation coefficients for the conventional reference hardness methods results

	HKM	Protein	%chop	PSI (c/f)	%VE	NIR @ 2230 nm
HLM	0.58	0.40	-0.71	0.38	0.77	0.75
HKM		0.27	-0.43	0.72	0.81	0.86
Protein			-0.51	0.11	0.44	0.48
%chop				-0.33	-0.55	-0.61
PSI (c/f)					0.63	0.69
%VE						0.84

HLM: Hectoliter mass ($g.hL^{-1}$)

HKM: Hundred kernel mass (g)

Protein: Protein content (Dumas method) %

PSI (c/f): Particle size index (coarse over fine ratio)

%VE: % vitreous endosperm as determined using NIR HSI

NIR @ 2230 nm: Near infrared spectroscopy (hardness index)

Based on observations made during unsupervised inspection of the reference methods (variables) by means of PCA loading and scores plots and the Spearman's rank correlation coefficients, the correlation structure of the Y-block (reference data) had to be taken into account. This indicated the need to use partial least squares – and, in particular the PLS2 algorithm – for building the regression models. To be able to deal with non-linearities among the reference data, a regression approach based on local modeling was chosen for the analysis. Therefore, the relation between the results of conventional hardness descriptors and RVA profile was expressed by means of a locally weighted-PLS2 approach.

RVA curves as hardness descriptor

In addition to the conventional methods, the RVA was investigated as another method to describe maize hardness. When using the RVA, the profile (length, heating and cooling rates, holding time) will influence the results. Therefore, three different profiles have been compared to determine an optimum profile for describing hardness. As expected, all three profiles resulted in different viscograms (Fig. 3.2a).

Hardness differences were evident for all three of the profiles. For example, from the standard profile variation in peak viscosity values (equilibrium point reached between viscosity increase or swelling and decrease or rupture) could easily be observed (Figs. 3.2b-2c). The hydration and gelatinisation process of starch from hard maize is slower than that of soft maize due to the thicker protein network present within hard maize (Wang & Eckhoff, 2000; Narváez-González *et al.*, 2006).

(a)

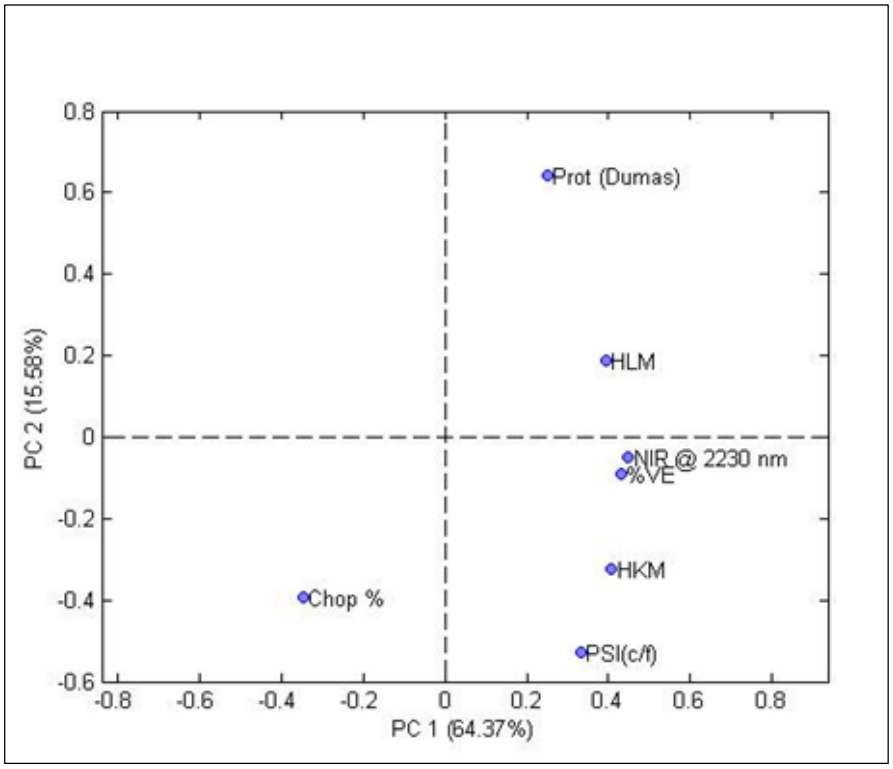

(b)

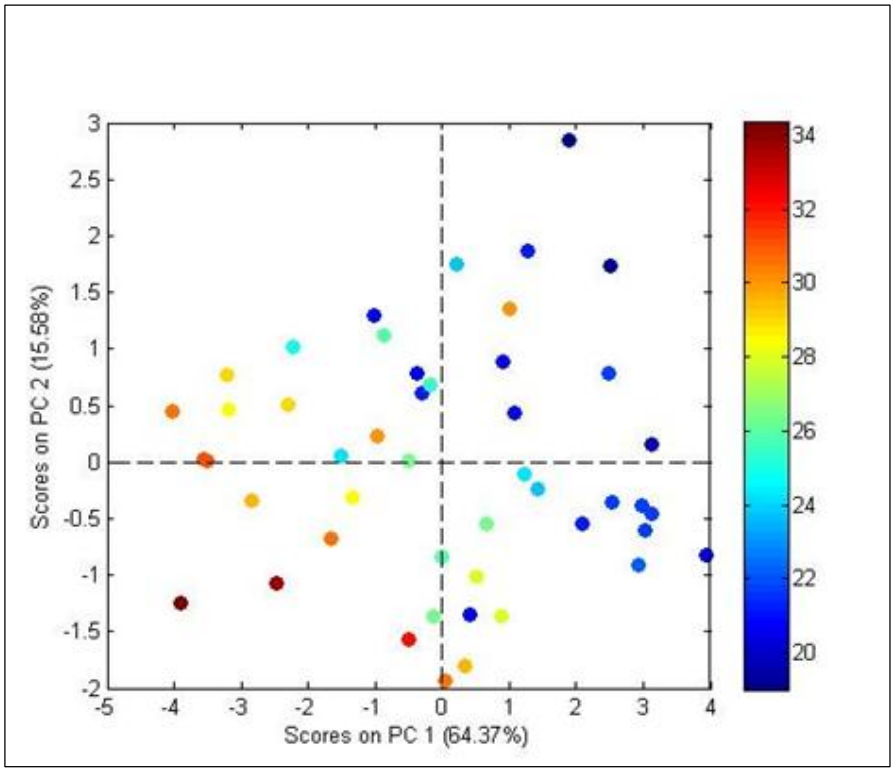

Figure 3.1. (a) Loading of the PCA on the Y block. (b) Score plot on the Y block. The dots are coloured as a function of the increasing %chop value. (HLM = hectoliter mass, HKM = hundred kernel mass, Prot (Dumas) = protein content, PSI (c/f) = particle size index (coarse/fine), %VE = % vitreous endosperm, NIR @ 2230 nm = near infrared absorbance at 2230 nm).

(a)

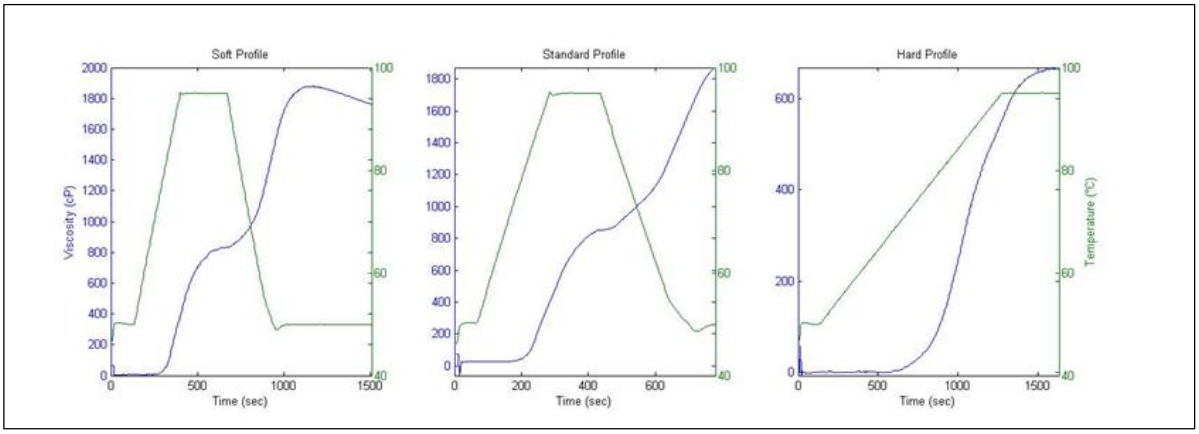

(b)

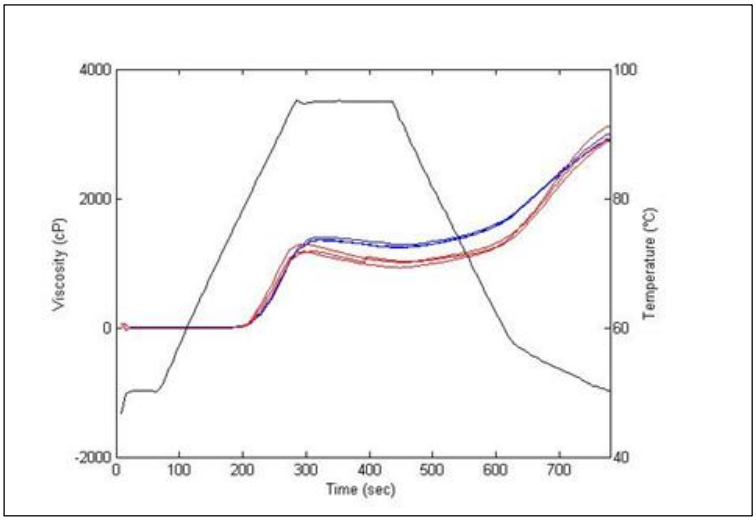

(c)

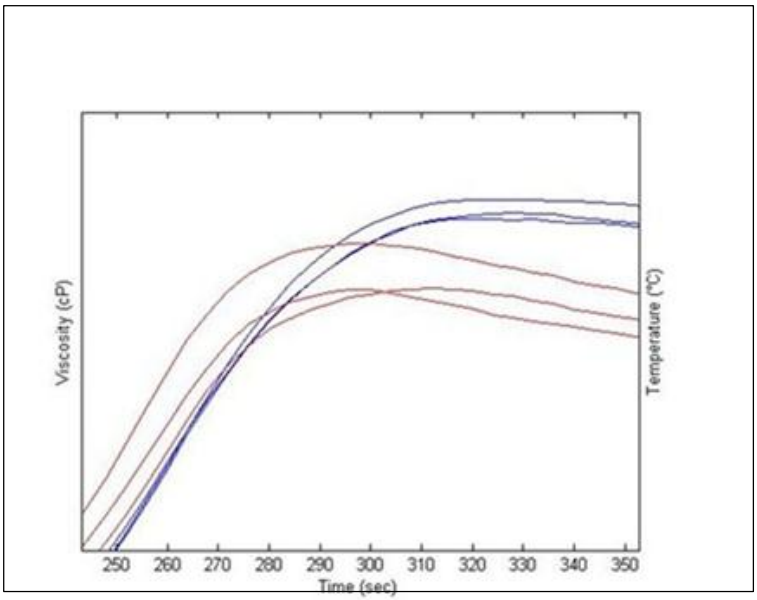

Figure 3.2. (a) RVA viscograms of a random maize sample, using the soft, standard and hard maize profile. (Green line = temperature; blue line = viscosity). (b) Viscograms using the standard profile for 3 hard (red curves) and 3 soft (blue curves) maize samples and (c) zoomed in to illustrate variability in peak viscosities.

The RVA curve data of all three the profiles showed promising results for RVA to be used for hardness characterisation and was subjected to further multivariate data analysis (chemometrics).

Quantification of hardness properties in maize samples

The collected RVA curves were pretreated with multiplicative scatter correction (Geladi *et al.*, 1985). The pretreated RVA viscograms were then used to build calibration models to predict the same hardness properties as those determined by the conventional methods. The correlations among the reference methods and the presence of non-linearities in the RVA data suggested the use of a non-linear method that can also take into account the correlation structure of the Y-block. For this reason, a LW-PLS2 approach was used to compute the regression models. This entailed correlating each of the three different RVA profiles to each of the seven conventional reference methods used to characterise maize hardness. In particular, LW-PLS2 regression was implemented using Euclidean distance to identify the neighbouring samples and a uniform weighting scheme (Bevilacqua *et al.*, 2012).

The optimal number of nearest neighbours and the optimal complexity of the PLS2 models have been chosen during a cross-validation procedure, i.e. choosing the numbers of these parameters as the ones leading to the minimum averaged RMSECV for the seven reference methods considered.

Since, for each RVA profile, three different analytical replicates have been collected for each sample, each of those had been considered as an individual measurement in building and validating the regression models. However, to be sure of not being prone to over-fitting when performing the cross-validation for model optimisation, the three measurements of each sample were always left out together. Leave-one-out cross-validation approach is normally used in LW-PLS2 regression to select the best number of nearest neighbours and latent variables, but in this case this would not represent the analytical replicates and thus the validation would not be performed at the correct level. Accordingly, in the present study, to deal with the presence of replicate measurements and to limit the risk of over-fitting, an alternative bootstrap-like scheme for cross-validation was adopted. At each splitting iteration 20% of the samples were randomly selected and left out as the cross-validation set (keeping together all the replicates corresponding to the same samples). For the training set, resampling with repetitions was adopted as occurs in the bootstrap procedure: a random subset of the samples not selected in the cross-validation set was chosen to constitute the training set, allowing the possibility of being selected multiple times. This was done to have all the samples included in the calibration and for a proper estimation of the optimal number of nearest neighbours. In this study, the procedure had been repeated 500 times in order to compute the average prediction error based on which model parameters were optimised.

Using the developed regression method, a different model for each RVA profile was computed, and each resulted in an error surface fit (Fig. S3.2), where the RMSECV is reported as a function of the latent variables and the number of nearest neighbours. Based on the results in cross-validation, the optimal number of latent variables was set at 1 for all three the RVA profiles and the number of

nearest neighbours at 100 for the soft and standard profile, and 71 for the hard profile. The difference in milling quality could be considered as one of the factors that introduce a non-linear response. Therefore, once the PLS model became linear in the local space of the nearest neighbours, the impact of this source of variability was limited, if not absent. This was consistent with the observation that in LW-PLS only 1 LV was selected for the local models. The corresponding RMSECV for each of the models are summarised in Table 3.3.

Optimisation of the regression model required the selection of the number of nearest neighbours and latent variables on the basis of the minimum error in cross-validation. In spite of the limited number of samples available, the data set was split into a training and test set to account for an external validation of the results. For this purpose, and also to take into account that the same test samples should be used to validate the predictions for each of the three RVA profiles, an ad hoc procedure based on the duplex algorithm was used for representative splitting. A duplex algorithm (Snee, 1977) was run on each of the data sets with a splitting ratio of 7:1. The relatively high splitting ratio was chosen, given the overall number of samples, to have enough training objects to build a reliable non-linear model. The need to adopt a non-linear approach required a higher number of training samples than what would have been necessary when using standard PLS regression. An intelligent criterion based on the duplex algorithm was adopted to choose the samples to be included in the test set. This included the same diversity as the training data, in order to limit the bias toward over-optimistic results. All the samples which were selected at least twice were included in the final test set. Accordingly, 41 samples constituted the training set and the remaining 6 were left out as external validation samples. For the three RVA profiles and the seven conventional hardness methods the LW-PLS2 prediction statistics for cross- and external validation are summarised in Table 3.4.

The RMSECV and RMSEP obtained when the RVA regression models were used to predict the reference values were quite low. They were often lower than those of the respective analytical reference methods. Although the seven Y variables all express hardness, each of them is based on a particular instrumental determination, with different associated errors and produces a result which is defined on a different scale. The order of magnitude of the errors would thus be expected to differ. Similar results were obtained when estimating the RMSEP in double cross-validation. When the same accuracy could not be reached, the errors of the RVA regression methods were always comparable with the laboratory errors of the reference methods. In particular, the developed RVA regression models allowed higher accuracies than those associated with the reference data for HLM and HKM, for which an error of 2.0 $g.hL^{-1}$ and 4.0 g can be expected (Voca *et al.*, 2009). The PSI method can be associated with a laboratory error of 2.24% (Manley *et al.*, 2002) although this error was reported for mean PSI results and not the ratio between the PSI fractions as in this study.

Table 3.3. RMSECV results for the conventional hardness methods, using three different RVA profiles.

	HLM	HKM	Protein	%chop	PSI (c/f)	%VE	NIR @ 2230 nm
RVA Soft profile	0.8	3.54	0.39	1.71	0.49	3.69	1.52
RVA Standard profile	0.82	3.37	0.38	1.7	0.47	3.53	1.45
RVA Hard profile	0.83	3.71	0.36	1.79	0.52	3.78	1.65

HLM: Hectoliter mass ($g.hL^{-1}$)

HKM: Hundred kernel mass (g)

Protein: Protein content (Dumas method) %

PSI (c/f): Particle size index (coarse over fine ratio)

%VE: % vitreous endosperm as determined using NIR HSI

NIR @ 2230 nm: Near infrared spectroscopy (hardness index)

Table 3.4. LW-PLS2 prediction statistics for cross-validation (n = 41) and external (n = 6) validation for the conventional hardness methods, using the three RVA profiles

	RVA soft profile		RVA standard profile		RVA hard profile	
	RMSECV	RMSEP	RMSECV	RMSEP	RMSECV	RMSEP
HLM	0.91	1.5	0.92	1.45	0.9	2.09
HKM	3.74	3.78	3.81	3.92	4.09	4.94
Protein	0.45	0.35	0.43	0.36	0.42	0.28
%chop	1.87	1.9	1.91	2.1	1.91	2.75
PSI (c/f)	0.54	0.62	0.58	0.64	0.58	0.82
%VE	4.15	6.52	4.46	6.55	4.48	7.78
NIR @ 2230 nm	1.64	1.99	1.74	1.89	1.84	2.84

HLM: Hectoliter mass ($g.hL^{-1}$)

HKM: Hundred kernel mass (g)

Protein: Protein content (Dumas method) %

PSI (c/f): Particle size index (coarse over fine ratio)

%VE: % vitreous endosperm as determined using NIR HSI

NIR @ 2230 nm: Near infrared spectroscopy (hardness index)

At the same time, the method under study enabled an objective measure of the %VE whose reference method is known to be very subjective to the operator and, consequently, affected by a high uncertainty of the results. On the contrary, the Dumas protein method is known to be very accurate and reproducible with an expected error of 0.2%. The accuracy of the %chop reference method has been found to be 0.6%, by repeating the same measure 7 times. It should, however, be stressed that this method requires big and expensive equipment, large samples and is also time-consuming. The method proposed in this work allows an accurate estimation (with only a slightly higher error) of the same parameters without any further measure. NIR absorbance values at 2230 nm were only single measurements with no known errors.

These results confirm the assumption that the RVA viscograms used with chemometrics offer an easy and simple way to predict the hardness of maize samples which can be related to milling quality. The results obtained from the three respective profiles did not differ. Irrespective of the RVA profile prediction of hardness properties should be possible.

Finally, as a further validation, a hybrid double cross-validation procedure was followed to assess whether the model could also be applicable to the crops harvested in different locations. Four cancelation groups were considered, each corresponding to a different geographical location. To take into account the relatively low number of samples available, each of the different locations was in turn selected to constitute the external validation set. The remaining samples were used to build the model, whose optimal complexity and dimension of the local neighbourhood were estimated according to a bootstrap procedure similar to that described earlier.

The prediction errors obtained by this procedure are summarised in Table S3.2. These results are comparable to those obtained from the use of a single representative test set (Table 3.4) and also to the results of the internal validation only (Table 3.3). This suggests that the proposed approach could be in principle applicable also to samples coming from different locations.

Conclusion

This study attempted to provide a solution to the problem of selecting the most appropriate method that best describe maize hardness milling quality. The different conventional methods were all shown to contribute towards describing hardness with %chop being the most appropriate to determine milling quality. The RVA was shown as being useful, not only for describing pasting properties of starch, but also to characterise maize hardness. Using LW-PLS2 regression, calibration models were developed that predicted the conventional hardness methods with accuracies lower or, at least, comparable to the laboratory error. Using different RVA profiles did not influence the RMSECV and RMSEP results thus, any RVA profile could be used to predict the hardness of maize samples once a regression model has been developed and appropriately validated.

References

AACC (1999a). Approved Methods of Analysis, 11 th Ed. Method 44-40.01. Moisture - Modified Vacuum-Oven Method. Approved November 3, 1999. St Paul, MN, U.S.A.: AACC International.

AACC (1999b). Approved Methods of Analysis, 11th Ed. Method 46-30.10. Crude Protein - Combustion Method. Approved November 3, 1999.: St. Paul, MN, U.S.A.: AACC International.

AACC (1999c). Approved Methods of Analysis, 11th Ed. Method 76-21.01. General Pasting Method for Wheat or Rye Flour or Starch Using the Rapid Visco Analyser. Approved November 3, 1999.: St. Paul, MN, U.S.A.: AACC International.

Agu, R., Bringhurst, T. & Brosnan, J. (2006). Production of grain whisky and ethanol from wheat, maize and other cereals. *Journal of the Institute of Brewing*, **112**, 314-323.

Almeida-Dominguez, H.D., Suhendro, E.L. & Rooney, L.W. (1997). Factors affecting Rapid Visco-Analyser curves for the determination of maize kernel hardness. *Journal of Cereal Science*, **25**, 93-102.

Bevilacqua, M., Bucci, R., Materazzi, S. & Marini, F. (2012). Application of near infrared (NIR) spectroscopy coupled to chemometrics for dried egg-pasta characterization and egg content quantification. *Food Chemistry*, **140**, 726-734.

Centner, V. & Massart, D.L. (1998). Optimization in locally weighted regression. *Analytical Chemistry*, **70**, 4206-4211.

Doublier, J.L., Llamas, G. & Le Meur, M. (1987). A rheological investigation of cereal starch pastes and gels. Effect of pasting procedures. *Carbohydrate Polymers*, **7**, 251-275.

Downey, G., Byrne, S. & Dwyer, E. (1986). Wheat trading in the Republic of Ireland: The utility of a hardness index derived by near infrared reflectance spectroscopy. *Journal of the Science of Food and Agriculture*, **37**, 762-766.

Emvula, S. (2012). Assessment of hectolitre mass (HLM) equipment and HLM measurements of oats. Masters. Stellenbosch University,

Fox, G. & Manley, M. (2009). Hardness methods for testing maize kernels. *Journal of Agricultural and Food Chemistry*, **57**, 5647-5657.

Geladi, P., MacDougall, D. & Martens, H. (1985). Linearization and scatter-correction for near-infrared reflectance spectra of meat. *Applied spectroscopy*, **39**, 491-500.

Hamilton, T., Hamilton, B.C., Johnson, B.C. & Mitchell, H. (1951). The dependence of the physical and chemical composition of the corn kernel on soil fertility and cropping system. *Cereal Chemistry*, **28**, 163-176.

Ji, Y., Wong, K., Hasjim, J., Pollak, L.M., Duvick, S., Jane, J. & White, P.J. (2003). Structure and function of starch from advanced generations of new corn lines. *Carbohydrate Polymers*, **54**, 305-319.

Johnson, D.Q. & Russell, W.A. (1982). Genetic variability and relationships of physical grain-quality traits in the BSSS population of maize. *Crop Science*, **22**, 805-809.

Lee, K.M., Herrman, T.J., Rooney, L.W., Jackson, D.S., Lingenfelser, J., Rausch, K.D., McKinney, J., Iiams, C., Byrum, L., Hurburgh, J.C.R., Johnson, L.A. & Fox, S.R. (2007). Corroborative study on maize quality, dry-milling and wet-milling properties of selected maize hybrids. *Journal of Agricultural and Food Chemistry*, **55**, 10751-10763.

Manley, M., Van Zyl, L. & Osborne, B. (2002). Using Fourier transform near infrared spectroscopy in determining kernel hardness, protein and moisture content of whole wheat flour. *Journal of Near Infrared Spectroscopy*, **10**, 71-76.

Martens, H. & Næs, T. (1985). Multivariate calibration. II. Cemometric methods. *Trends in Analytical Chemistry*, **3**, 266-271.

Narváez-González, E.D., de Dios Figueroa-Cárdenas, J., Taba, S., Tostado, E.C., Peniche, R.Á.M. & Sánchez, F.R. (2006). Relationships between the microstructure, physical features, and chemical composition of different maize accessions from Latin America. *Cereal Chemistry*, **83**, 595-604.

O'Kennedy, K. (2011). Characterisation of zein from South African maize of varying endosperm texture. Masters Thesis in Food Science. Stellenbosch University, South Africa.

Paiva, E., Kriz, A.L., Peixoto, M.J.V.V.D., Wallace, J.C. & Larkins, A.B. (1991). Quantitation and distribution of ã–zein in the endosperm of maize kernels. *Cereal Chemistry*, **68**, 276-279.

Peplinski, A.J., Paulsen, M.R., Anderson, R.A. & Kwolek, W.F. (1989). Physical, chemical, and dry-milling characteristics of corn hybrids from various genotypes. *Cereal Chemisty*, **66**, 117-120.

Ross, A., Walker, C., Booth, R., Orth, R. & Wrigley, C. (1987). The Rapid Visco-Analyzer: a new technique for the estimation of sprout damage. *Cereal Foods World*, **32**, 827-829.

Anonymous (2013). SAGIS (South African Grain Information Services). Demand and supply table. [Internet document]. http://www.sagis.org.za/Flatpages/SMB%20Summary.asp. 29.7.2013.

Sahai, D., Buendia, M. & Jackson, D. (2001). Analytical techniques for understanding nixtamalized corn flour: particle size and functionality relationships in a Masa flour Sample 1. *Cereal Chemistry*, **78**, 14-18.

Sandhu, K.S. & Singh, N. (2007). Some properties of corn starches II: Physicochemical, gelatinization, retrogradation, pasting and gel textural properties. *Food Chemistry*, **101**, 1499-1507.

Seetharaman, K., Tziotis, A., Borras, F., White, P.J., Ferrer, M. & Robutti, J. (2001). Thermal and functional characterization of starch from Argentinean Corn1. *Cereal Chemistry*, **78**, 379-386.

Snee, R.D. (1977). Validation of regression models: methods and examples. *Technometrics*, **19**, 415-428.

Voca, N., Varga, B., Kricka, T., Curic, D., Jurisic, V. & Matin, A. (2009). Progress in ethanol production from corn kernel by applying cooking pre-treatment. *Bioresource Technology*, **100**, 2712-2718.

Wang, D. & Eckhoff, S.R. (2000). Effect of broken corn levels on water absorption and steepwater characteristics. *Cereal Chemistry*, **77**, 525-528.

Watson, S.A. (1987). Structure and composition. In: *Corn chemistry and technology* (edited by S.A. Watson & P.E. Ramstad). Pp. 53-82. St. Paul, Minnesota, USA: American Association of Cereal Chemists, Inc.

Wold, S., Martens, H. & Wold, H. (1983). *The multivariate calibration problem in Chemistry 576 solved by the PLS method.* Heidelberg, Germany: Springer-Verlag.

Yamin, F., Lee, M., Pollak, L. & White, P. (1999). Thermal properties of starch in corn variants isolated after chemical mutagenesis of inbred line B73 1. *Cereal Chemistry*, **76**, 175-181.

Supplementary material:

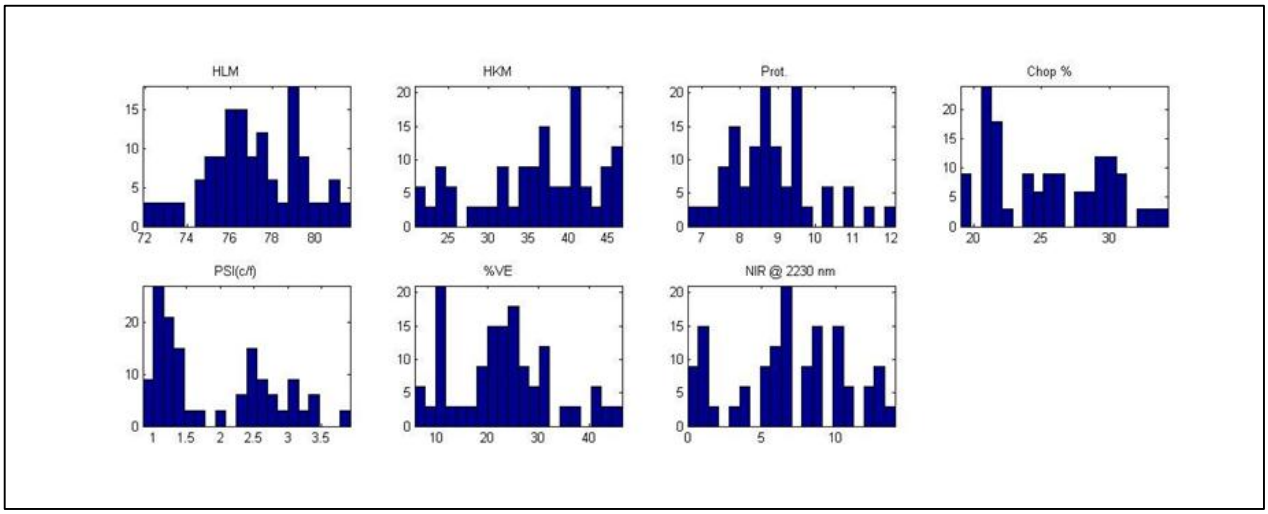

Figure S3.1. Histograms of the distribution of the values for each variable. (HLM = hectoliter mass, HKM = hundred kernel mass, Protein = protein content (Dumas method) %, PSI (c/f) = particle size index (coarse/fine), %VE = % vitreous endosperm, NIR @ 2230 nm = near infrared spectroscopy (hardness index).

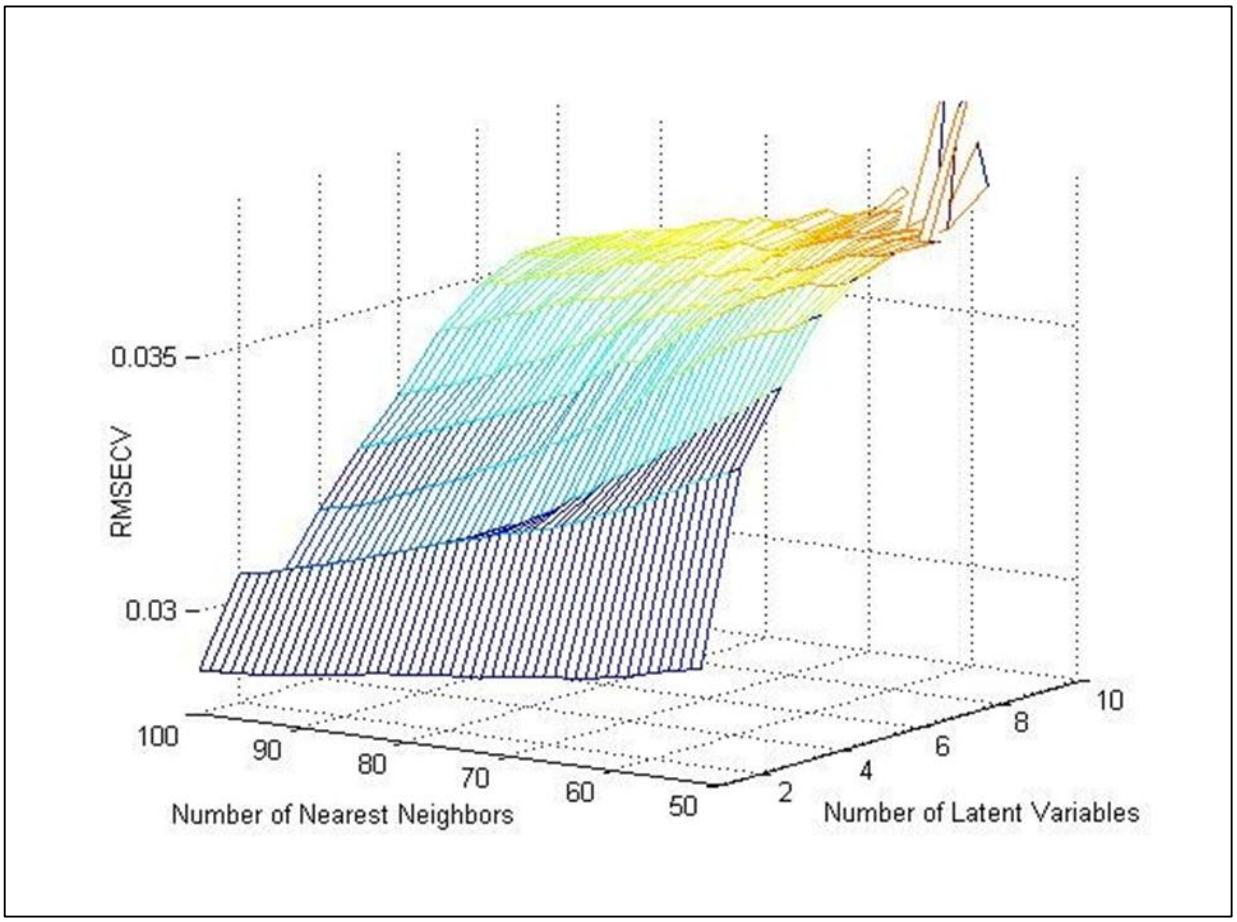

Figure S3.2. LW-PLS2 modeling: plot of the error surface, reporting the RMSECV of the model built with the RVA curves for the standard profile as a function of the number of nearest neighbours and the number of latent variables, used for the selection of optimal model parameters.

Table S3.1. Descriptive statistics of the conventional reference hardness methods results

	Unit	n	Range	Mean	SD
Hectoliter mass	$g.hL^{-1}$	48	71.9 – 81.7	77.05	2.18
Hundred kernel mass	g	49	20.7 – 46.7	36.13	0.58
Protein content	%	45	6.6 – 12.1	8.13	1.14
Chop content	%	49	19 – 34.33	22.55	4.19
Particle size index (coarse/fine)		49	0.9 – 3.9	1.9	0.86
Vitreous endosperm content	%	49	5.59 – 46.49	23.17	9.78
NIR absorbance at 2230 nm		49	0 – 13.68	6.97	3.84

Table S3.2. LW-PLS2 prediction statistics for the conventional hardness methods, using the three RVA profiles, as estimated by double cross-validation across the four localities

	Unit	RVA soft profile	RVA standard profile	RVA hard profile
		RMSEP	RMSEP	RMSEP
Hectoliter mass	$g.hL^{-1}$	1.66	1.65	1.79
Hundred kernel mass	g	3.91	4.01	5.02
Protein content	%	0.37	0.36	0.32
Chop content	%	1.93	2.15	2.97
Particle size index (coarse/fine)		0.63	0.70	0.81
Vitreous endosperm content	%	6.49	6.80	7.98
NIR absorbance at 2230 nm		1.87	1.97	2.87

Chapter 4

Non-destructive estimation of maize (*Zea mays* L.) kernel hardness by means of an X-ray micro-computed tomography (µCT) density calibration*

Abstract

An X-ray micro-computed tomography (µCT) density calibration was constructed for whole maize (*Zea mays* L.) kernels from polymers ranging in absolute densities from 0.9 to 2.2 g.cm^{-3}. The resulting linear equation was used to estimate the densities of two regions-of-interest, i.e. vitreous and floury endosperm, as well as that of the entire maize kernel. The sample set comprised 16 maize kernels (8 hard and 8 soft). Validation of entire kernel density was performed by comparing estimated and measured (actual) masses (r = 0.99; standard error of measurement = 0.01 g). In addition percentage cavity (%cavity) and percentage porosity (%porosity) were quantified from the X-ray images. As determined with ANOVA, floury, vitreous and entire kernel endosperm densities as well as %cavity and %porosity significantly ($P < 0.05$) contributed to the variation within the hardness classes. Hardness classification was attempted using a receiver operating characteristic (ROC) curve. Threshold values of 1.48 g.cm^{-3}, 1.67 g.cm^{-3} and 1.30 g.cm^{-3} were determined for the entire kernel, vitreous and floury endosperm densities, respectively at a maximum of 100% sensitivity and specificity. Classification was possible from % porosity values of the entire kernel, which are easier to determine, at 88% accuracy. Efficient maize kernel hardness classification is required by the dry-milling industry when maize is milled into a meal and used as a food source. Optimum quality and yield can only be obtained during the milling process if maize of appropriate hardness is used as raw material.

*Submitted for publication as: Guelpa A, Du Plessis A, Kidd M & Manley M (2014). Non-destructive estimation of maize (*Zea mays* L.) kernel hardness by means of an X-ray micro-computed tomography (µCT) density calibration. *Food and Bioprocess Technology*.

Introduction

Maize (*Zea mays* L.) is a vital source of energy and one of the most important dietary staple foods globally. It is used for human consumption in different forms, from specialised foods in developed countries to staple food in undeveloped countries (Malvar *et al.*, 2008). Maize is predominantly processed into maize meal using dry-milling, comprising milling into different particle sizes, after de-germing (removal of germ and pericarp).

Two types of endosperm, vitreous and floury, are present in maize kernels (Watson, 1987; Paiva *et al.*, 1991). The vitreous endosperm is harder, of higher density, more translucent and situated to the outside of the kernel, whereas the floury endosperm is softer, of lower density, mealy textured and found in the center of the kernel (Watson, 1987; Paiva *et al.*, 1991). Due to the starch granules of the floury endosperm being less compacted, many intergranular air spaces are present. These are absent in vitreous endosperm (Robutti *et al.*, 1974; Dombrink-Kurtzman & Knutson, 1997). Furthermore, cavities (or cracks) exist within maize kernels (Chang, 1988; Huber & BeMiller, 1997; De Carvalho *et al.*, 1999; Huber & BeMiller, 2000; Gustin *et al.*, 2013), predominantly due to dehydration when the endosperm collapses to leave relative large air spaces. It is thus apparent that the microstructure of the endosperm types present in maize kernels differs.

Hard maize kernels have better milling quality (resulting in a higher milling yield) compared to softer maize. Many methods have been used since the 1950's to determine the hardness of maize. These methods have been extensively reviewed by Fox and Manley (2009) and include measuring resistance to grinding and abrasion (Lee *et al.*, 2007); yield of grits (Wu, 1992); starch gelatinisation properties (Almeida-Dominguez *et al.*, 1997); as well as determination of particle size index (PSI) subsequent to grinding and sieving (Pomeranz *et al.*, 1984; Wu, 1992). The use of near infrared (NIR) reflectance and NIR transmittance spectroscopy have also been widely investigated (Pomeranz *et al.*, 1984; Robutti, 1995; Eyherabide *et al.*, 1996). Other methods include hand dissection which determines the ratio of vitreous and floury endosperm and machine vision technology for non-destructive classification of maize kernels (Erasmus, 2003). Near infrared hyperspectral imaging (NIR HSI) has been used to distinguish between individual maize kernels differing in hardness (Manley *et al.*, 2009; Williams *et al.*, 2009). It was also shown that NIR HSI could be used to classify maize kernels without the need for hardness reference data (McGoverin & Manley, 2012). This was possible due to the spatial dimension, in addition to the spectral dimension, offered by NIR HSI. Quality properties such as protein, starch, fat and fiber contents (Blandino *et al.*, 2010); kernel density (Blandino *et al.*, 2010) and protein (zein) composition (Dombrink-Kurtzman & Bietz, 1993; Robutti *et al.*, 1997) have also been used to characterise kernel hardness and thus dry-milling performance. Density measurements were performed by means of a floating test where a variable density solution separated the kernels based on density differences (Blandino *et al.*, 2010; Blandino *et al.*, 2012). A similar method, i.e. gas pycnometry was used to characterise genotypic and phenotypic diversity in maize (Siska & Hurburgh, 1995).

Micro-computed tomography uses the differences in X-ray attenuation arising principally from differences in density and atomic composition within the material (Chawanji *et al.*, 2012; Zhu *et al.*, 2012; Cnudde & Boone, 2013). For a particular material (at a specific energy) the X-ray attenuation is approximately proportional to the material's density (Sinka *et al.*, 2004). The main advantage of the X-ray µCT technique is the ability to perform non-destructive and non-invasive capturing of high-resolution three dimensional (3-D) detail, thus visualising and characterising microstructural features.

Measurement of density variation in pharmaceutical tablets (Sinka *et al.*, 2004; Busignies *et al.*, 2006), wood test pieces (Lindgren *et al.*, 1992), commercial plastics (Du Plessis *et al.*, 2013) and compacted parts, i.e. ceramics (Burch, 2002) has been investigated using X-ray µCT. In the case of pharmaceutical tablets compaction of the tablets may impact on efficient packaging and storage. This was effectively measured in terms of density variation using X-ray µCT (Sinka *et al.*, 2004). Similarly, Meincken and Du Plessis (2013) observed the impact of forest fires on the decomposition of major chemical components in wood by determining the density and dimension of the wood samples.

X-ray µCT has been successfully applied in food studies, i.e. Italian salami (Frisullo *et al.*, 2009), mayonnaise (Laverse *et al.*, 2012), cream cheese (Laverse *et al.*, 2011b) and yoghurt (Laverse *et al.*, 2011a). The microstructure of loose-packed and compacted milk powders has also been studied (Chawanji *et al.*, 2012). The increasing number of X-ray imaging applications for food and agricultural produce have been illustrated recently in reviews by Donis-González *et al.* (2014) and Kotwaliwale *et al.* (2011). X-ray µCT has been applied to whole grain rice specifically to study kernel structure of high-amylose and wild-type rice (Zhu *et al.*, 2012). The structure of porous cereal products (Van Dalen *et al.*, 2007) and maize flakes (Chaunier *et al.*, 2007) has also been evaluated. The study of porous products is possible since X-ray µCT enables imaging of cavities and thus real density variations within a kernel; this is not possible with other imaging methods. The development of a density calibration and subsequent measurement of densities have not been considered in these food studies, although a recent study by Gustin *et al.* (2013) demonstrated that individual kernel density and volume could be accurately measured using X-ray µCT. It is not clear how the latter measurements were made. It is assumed that the pycnometer was used as reference method. Gustin *et al*. (2013) showed that the embryo (germ) had little impact on overall kernel density and that grain fill showed a strong correlation with density. The usefulness of single kernel near infrared (NIR) predictions of density and volume was also illustrated.

X-ray µCT poses to be very useful when a region within a sample under investigation needs to be excluded (i.e. germ and cavities) non-destructively. X-ray µCT therefore allows for true determination of volumes and densities of desired regions-of-interest (ROIs). The most prominent maize kernel characteristics, along with size, that determines kernel quality are density which are closely related with kernel hardness (Lee *et al.*, 2006). Mestres et al. (1991) showed that maize hardness could be evaluated through density measurements with almost 90% accuracy. Similarly,

Wu and Bergquist (1991) reported that grit yield (an indicator of maize hardness) correlated with density (r = 0.89).

This paper presents the application of an X-ray µCT density calibration to non-destructively estimate kernel hardness from calculated density, percentage porosity (%porosity) and percentage cavity (%cavity) of the entire maize kernel as well as that of the selected ROIs (vitreous and floury endosperm).

Material and methods

Maize samples

Sixteen whole maize kernels (eight kernels from each hybrid) were randomly selected from two white maize hybrids, PAN6Q445B and H2D1 (not released as commercial hybrid as yet), differing in kernel hardness. These two hybrids were chosen, as extremes based on hardness determinations, from a sample set of 49. The hybrids originated from the 2012 harvest maize breeding trials and were kindly supplied by PANNAR Seeds (Greytown, South Africa).

Polymers used for density calibration

The polymers, used as calibration standards, were acquired from Maizey Plastics (Cape Town, South Africa) and each was cut into a cylinder of 10 mm thickness and 25 mm diameter. These polymers included: polytetrafluoroethylene (PTFE) (2.15 $g.cm^{-3}$); sustanat polycarbonate (PC) (1.2 $g.cm^{-3}$); ultra-high molecular weight polyethylene (UHMW PE) (0.92 $g.cm^{-3}$); polypropylene (PP) (0.91 $g.cm^{-3}$); high density polyethylene (HDPE) (0.91 $g.cm^{-3}$); polyethylene terephthalate (PET) (1.38 $g.cm^{-3}$); and sustarin C acetal / nylon (1.15 $g.cm^{-3}$) (Du Plessis *et al.*, 2013). The polymers used to construct the linear density calibration were selected as such that their densities (0.9 to 2.2 $g.cm^{-3}$) overlapped with typical densities of whole maize kernels (*ca*. 1.18 to 1.36 $g.mL^{-1}$) as determined with the floating test.

Hardness determination of maize kernels

Particle size index

The particle size index (PSI) method, using milling followed by sieving, was used to differentiate between hard and soft maize hybrids. The samples were milled using a cyclone Laboratory Mill 3100 (Perten, Hägersten, Sweden) fitted with a 1 mm sieve. A two sieve method (O'Kennedy, 2011) was used, where a 150 µm sieve was placed on a 75 µm sieve, fitted with a receiving pan and lid. Two sets of pans and sieves (Retsch, Haan, Germany) were stacked on top of each other and placed in a Retsch AS 200 Tap Sieve Shaker (Retsch, Haan, Germany) for 10 minutes. Three fractions, PSI_1, PSI_2 and PSI_3 were determined. For the determination of the first fraction (PSI_1), the 150 µm sieve was weighed ($W_{150\ \mu m\ sieve}$) to the nearest 0.001 g. Thereafter, 10 ± 0.01 g of ground maize was weighed (W_{maize}) into the 150 µm sieve together with 10 ± 0.01 g whole wheat ($W_{wheat\ on\ 150\ \mu m}$

$_{sieve}$). Whole wheat was added to facilitate efficient sieving. After the sieving and tapping process, the fine maize meal adhering to the bottom of the 150 µm sieve was gently brushed off into the 75 µm sieve and the 150 µm sieve was weighed (W_1). Equation 1 was used to determine PSI_1:

$$PSI_1 = (W_1 – (W_{150\ \mu m\ sieve} + W_{wheat\ on\ the\ 150\ \mu m\ sieve})) / W_{maize} \quad [\ldots eq.\ 1]$$

Thereafter, the fine maize meal adhering to the bottom of the 75 µm sieve was gently brushed off into the receiving pan and the 75 µm sieve was weighed (W_2). The weight of the 75 µm sieve was recorded (to the nearest 0.001g) when it was still empty ($W_{75\ \mu m\ sieve}$) as well as that of the whole wheat 10 ± 0.01 g placed on the 75 µm sieve ($W_{wheat\ on\ 75\ \mu m\ sieve}$). The second PSI fraction (PSI_2) was determined according to equation 2:

$$PSI_2 = (W_2 - (W_{75\ \mu m\ sieve} + W_{wheat\ on\ the\ 75\ \mu m\ sieve})) / W_{maize} \quad [\ldots eq.\ 2]$$

For the determination of PSI_3 (eq. 3), the empty receiving pan weight (W_{pan}) (to the nearest 0.001g) was deducted from that of the pan, weighed after the sieving and shaking step (W_3).

$$PSI_3 = (W_3 – W_{pan}) / W_{maize} \quad [\ldots eq.\ 3]$$

The higher the value of PSI_1 the harder the kernels; high PSI_2 and PSI_3 values indicated soft kernels. In addition, the ratio between larger (PSI_1) and smaller particle sizes ($PSI_2 + PSI_3$) was calculated to give a course over fine (c/f) ratio, where a higher value indicated harder (more dense) samples and vice versa (eq. 4):

$$c/f = PSI_1 / (PSI_2 + PSI_3) \quad [\ldots eq.\ 4]$$

The PSI measurements were done in duplicate for each sample.

Floating test

A floating test (Blandino *et al.*, 2010; Blandino *et al.*, 2012) was used to determine the densities ($g.mL^{-1}$) of the whole maize kernel samples (n = 16). Each individual kernel was placed in a 120 mL tetrachloroethylene (Kimix, Epping Industrial, South Africa; density 1.62 $g.mL^{-1}$) and 40 mL petroleum ether (Kimix, Epping Industrial, South Africa; density 0.653 $g.mL^{-1}$) solution in individual Erlenmeyer flasks (250 mL). Petroleum ether was added, after a twenty second waiting period, in 5 mL increments to each flask in order to gradually decrease the solution's density. The moment a kernel sank to the bottom of the flask, the density of that solution was calculated which equated the density of the kernel. After sufficient drying of the kernel with a paper towel the test was repeated with the

same kernel (duplicate measurements). After completion of the floating test, the same 16 kernels were subjected to X-ray µCT scanning.

Scanning electron microscopy

A thin slice (*ca*. 1 mm) of a maize kernel (sliced with a Solingen blade) was mounted onto double sided carbon tape. The slice was coated with gold dust, using a 5150A sputter coater (HHV, Crawley, United Kingdom). The scanning electron microscopy (SEM) micrographs were taken with a LEO1430 VP Scanning electron microscope (Zeiss, Germany) at a voltage of 7 kV and 4500 times magnification.

X-ray micro computed tomography scanning

X-ray scans were acquired using a commercial micro-focus X-ray computed tomography system, i.e. the Phoenix V|Tome|X L240 (General Electric Sensing and Inspection Technologies / Phoenix X-ray, Wunstorff, Germany), equipped with a nano-focus tube at the Stellenbosch University CT Scanner facility (www.sun.ac.za/ctscanner). The system was integrated with Phoenix Datos acquisition and reconstruction software (General Electric Sensing and Inspection Technologies / Phoenix X-ray, Wunstorff, Germany). Image acquisition was set at 1 s per image with 1300 images recorded in one rotation at 13.4 µm voxel size. A scan took approximately 30 minutes to complete. In this work 60 kV was used for X-ray generation after it was determined that the grey value differences at each of two different energies (60 and 230 kV) resulted in normalised values close to one for both the polymers and maize kernels as explained earlier by (Du Plessis *et al.*, 2013). This also enabled the use of polymers for the calibration construction.

The polymer discs were stacked on top of each other and placed on florist oasis, along with 8 single maize kernels, also mounted in florist oasis as illustrated in Figure 4.1. The low density of florist oasis makes it a suitable mounting material due to it being easily distinguishable from the subjects of interest. The mounted samples were placed on the specimen stage and rotated along the axis, perpendicular to the beam direction. Two such scans were required to collect the images of all 16 kernels (8 kernels per scan), according to the method of Du Plessis (2013). The aim of scanning 8 kernels in one scan volume at lower resolution was to demonstrate the possibility of having high throughput µCT scans.

A further high resolution scan was acquired from one of the 16 maize kernels, using a Phoenix Nanotom S system (General Electric Sensing and Inspection Technologies / Phoenix X-ray, Wunstorff, Germany) with Molybdenum target. Energies of 50 kV accelerating voltage was needed to obtain a 6 µm resolution for the entire kernel. Averaging and skipping of images were included to improve image quality resulting in scan time of 2 h. In addition a 3 µm resolution scan of a sub-volume of the kernel was also done.

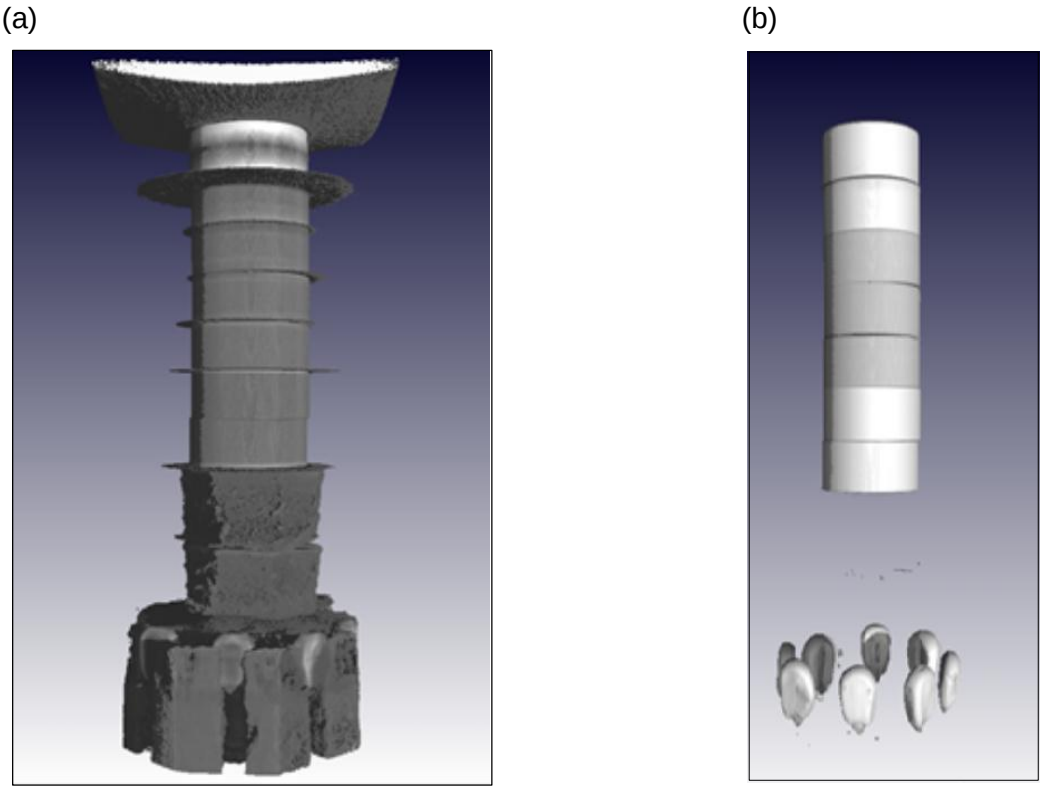

Figure 4.1. Stack of 7 polymer discs, used for the density calibration, along with 8 maize kernels with (a) showing the florist oasis, used for mounting and (b) with the mounting material removed.

Data processing

A series of two-dimensional (2-D) X-ray projection images were obtained from a sample rotating through 360 degrees. The projections images are reconstructed into a volume data set using General Electric Datos software. The process of reconstruction comprises filtered back-projection algorithms and the grey values in a rendered CT image then represent the attenuation in each pixel (Singhal *et al.*, 2013). This relates to a higher density phase that appears brighter compared to the darker representation of the lower density material. This 3-D data set was rendered and analyzed using VGStudio MAX 2.2 (Volume Graphics, Heidelberg, Germany).

During the image processing step, the maize kernels were scanned simultaneously with the polymer discs to facilitate calibration and direct comparison of different scans. In µCT the resulting grey values depend on the densest object in the scan volume (in this case the PTFE disc with a density of 2.15 $g.cm^{-3}$). This is because the filtered back projection reconstruction algorithm normalises the grey values within the range, from minimum to maximum (Kak & Slaney, 1988). By using the same densest object in subsequent scans, and using that object for normalisation, the grey values between scans could be directly compared.

The grey values of the polymer discs were acquired by selecting a representative volume from each disk. Each voxel had an associated grey value depending on the material's density and atomic number. The average grey value of each homogeneous polymer disk was therefore a measure of its density. To generate the calibration function, a linear function (eq. 5) was used:

Actual density ($g.cm^{-3}$) = m x grey value + c […eq. 5]

where, m = the slope and c = intercept.

The average grey values for the entire kernels and ROIs were obtained from VGStudio MAX 2.2 after excluding the germ (Fig. 4.2). The densities of the germ and vitreous endosperm regions were very similar and prevented accurate separation between the vitreous and floury endosperm regions. Therefore, the germ region was manually removed for each of the maize kernels, using the VGStudio Max 2.2 Drawing tool.

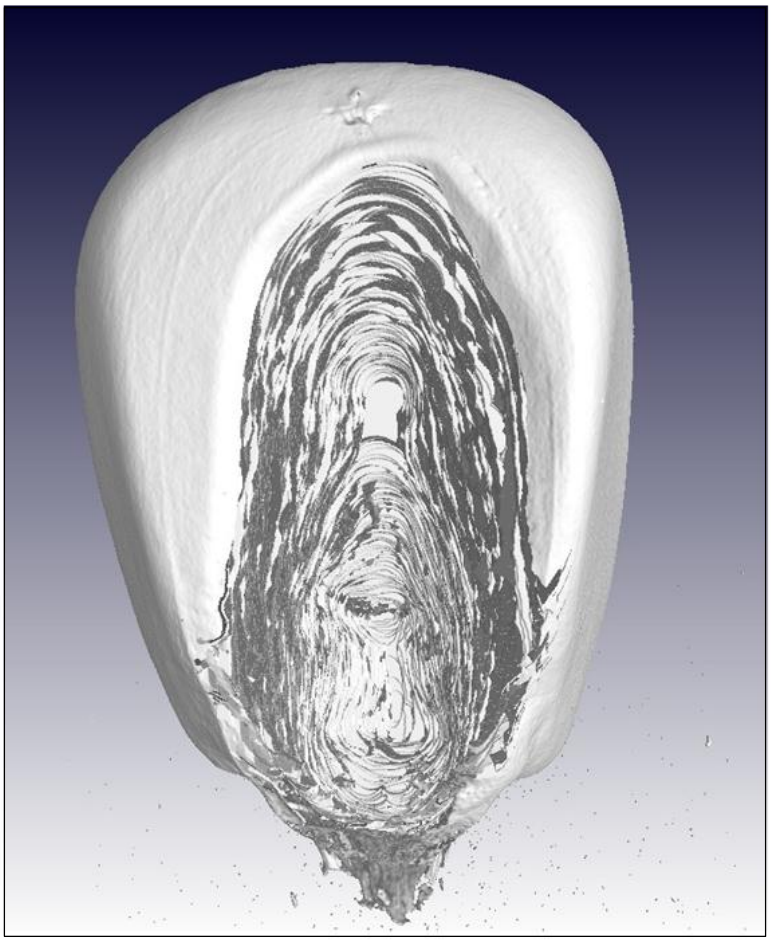

Figure 4.2. 3-D µCT image of a maize kernel with its germ removed.

Large air spaces (cavities) present in whole maize kernels were selected using the Region growing tool (VGStudio MAX 2.2). These areas were selected manually and the volumes were acquired on the 13.4 µm scans, using the Volume analyser function (VGStudio MAX 2.2). For each kernel the cavities were calculated as a percentage of the total volume of the entire kernel (%cavaties).

To indicate the arrangement and quantity of pores (intergranular air pockets) present in the endosperm, the Thresholding function (VGStudio MAX 2.2) was used in combination with the Defect detection module (VGStudio MAX 2.2). These functions were also applied to the 13.4 µm scans

after the cavities were excluded. Air pore volumes comprising more than 8 adjacent dark voxels were seen as pores. Hence, minimum detectable pore size is dependent on scan resolution, making typical spherical pores of approximately 27 µm in diameter detectable in the 13.4 µm scan. For each kernel the porosity was calculated as a percentage of the total volume of the entire kernel (%porosity) (Gondek *et al.*, 2013).

Statistical procedures

Analysis of variance

One-way analysis of variance (ANOVA) was performed to compare average measurements for the respective measures (%cavity, %porosity, entire kernel density, vitreous endosperm density and floury endosperm density) with respect to hardness classes, i.e. hard and soft. ANOVA analyses were performed using STATISTICA version 11 (StatSoft, Inc., Tulsa, USA).

Comparison of density measurements (µCT and floating test)

The floating test and X-ray scans were performed on the same 16 kernels. In spite of the results not recorded in the same units ($g.mL^{-1}$ and $g.cm^{-3}$, respectively), were they comparable and the intraclass correlation (ICC) coefficients could be determined. The ICC coefficients were determined as the ICC agreement that correlates measurements with each other, while taking into account the differences in absolute values of the respective measurements, and the ICC consistency that only correlates measurements. The ICC agreement was determined to express variation in density measured with the two respective density measurement methods (µCT and floating test). The ICC consistency, on the other hand, was determined to reflect the correlation between the two density measurement methods. All ICC calculations were done using the R statistical programming language (R Package Concord). The correlation coefficient (r), which is a less strict correlation method than the ICC, and the standard error of measurement (SE) between the two measurement methods were determined using STATISTICA version 11 (StatSoft, Inc., Tulsa, USA).

Validation of density calibration

The density calibration was validated by measuring the mass of each of the 16 kernels, using a laboratory scale (Precisa, Instrulab, Johannesburg, South Africa) (accurate to 3 decimals) and comparing these to the estimated masses (Gustin *et al.*, 2013). The mass of each kernel was calculated from the volume (mm^3) and density ($g.cm^{-3}$) as determined from the µCT images. The respective volumes were determined using the Volume analysis tool (VGStudio MAX 2.2) and the densities were acquired from the density calibration. The mathematical relationship between mass, volume and density was used to calculate the predicted masses (eq. 6):

$$\text{Mass} = \text{volume} \times \text{density} \qquad \text{[…eq. 6]}$$

Correlation coefficients

Spearman's rank correlation coefficients were used to test the strength of the relationships between pairs of microstructural traits: %cavity, %porosity, entire kernel density, vitreous endosperm density and floury endosperm density. Correlation analysis was performed using Microsoft Excel 2010 (Microsoft Corporation, Seattle, WA).

Classification models

A receiver operating characteristic (ROC) curve was used to separate the maize kernels into hard and soft hybrid classes based on entire kernel density, vitreous and floury endosperm densities as well as %cavity and %porosity. An ROC curve is a plot of sensitivity on the *y*-axis against 1-specificity on the *x*-axis for varying values of the threshold. The optimal threshold is determined by maximising the sum of sensitivity and specificity. Sensitivity is the percentage hard kernels correctly classified and specificity is the percentage soft kernels correctly classified. ROC analyses were performed using STATISTICA version 11 (StatSoft, Inc., Tulsa, USA).

Principal component analysis

Principal component analysis (PCA) was performed on the X-ray µCT derived variables (entire kernel density, vitreous and floury endosperm densities as well as %cavities and %porosity). To determine the relationship amongst the variables, a PCA bi-plot, which combines the scores and loadings, were used. PCA analyses was performed using STATISTICA version 11 (StatSoft, Inc., Tulsa, USA).

Results and discussion

Although originally used to determine wheat hardness, the PSI method (AACC, 1999) is also recognised as a suitable method for maize hardness measurements (Pomeranz *et al.*, 1984; Wu, 1992). For maize hardness PSI determinations, a two sieve method is however more appropriate. Also, the c/f ratio correlated better with milling quality compared to other conventional tests such as the floating test, hectolitre mass and the Stenvert test, probably due to the efficient separation of the vitreous and floury fractions (Blandino *et al.*, 2010). In the current study the c/f ratio ($c/f = PSI_1 / (PSI_2 + PSI_3)$) was thus used to select two maize hybrids which differed maximally in hardness properties and thus kernel density, from a set of 49 samples. The c/f ratio for the 49 samples was 1.92±0.88 (mean±SD) with that of the selected hard and soft hybrids determined as 3.90±0.37 and 1.56±0.31, respectively (Table 4.1).

Table 4.1. The results from PSI (n = 49) that was used to select two hybrids that differs maximally in hardness

	Range	Mean±SD
PSI_1	0.47 – 0.80	0.64±0.09
PSI_2	0.12 – 0.33	0.20±0.06
PSI_3	0.08 – 0.26	0.18±0.06
c/f	0.85 – 3.92	1.92±0.88

SD: Standard deviation

Microstructure of maize kernels

In the 2-D µCT slices, taken longitudinally from approximately the same plane and region (center of the kernel) of both the hard (Fig. 4.3a) and soft (Fig. 4.3b) hybrids, large cavities in the floury endosperm were evident. This was observed in all 16 scanned kernels, but much more prominent in the soft hybrid kernels (Table 4.2). Proportionally, soft kernels have more floury endosperm that is prone to form cracks, than in the case of hard kernels. When moisture loss is experienced the absence of a thick continues protein matrix covering the starch granules in the floury endosperm causes the formation of these cracks that later develop into cavities. Such cavities have been reported to account for up to 13% of the volume of some hybrid kernels (Chang, 1988; Gustin *et al.*, 2013). The %cavities quantified for all 16 kernels (1.79%), as determined in this study, are depicted in Table 4.2. The %cavities of the soft hybrid (2.68%) was significantly ($P < 0.05$) higher than that of the hard hybrid (0.89%) (Table 4.3). The %porosity for the 16 kernels was 0.0116% (Table 4.2). As expected %porosity of the soft hybrid (0.0164%) was significantly ($P < 0.01$) higher than that of the hard hybrid (0.0069%) (Table 4.3). A good relationship existed between %cavity and %porosity (r = 0.78).

The digital image in Figure 4.4a of a longitudinal slice of a maize kernel depicts the vitreous (glassy) and the floury (powdery) endosperm as the translucent and white areas, respectively. In the 2-D X-ray µCT image (Fig. 4.4b), the brighter grey region represents the denser vitreous endosperm and the darker region the less dense floury endosperm. In the SEM micrographs pores and air pockets could be observed in the soft endosperm on the surface and between the loosely packed, less structured starch granules (Fig. 4.5a). Due to the air pockets and the granules not as tightly packed, light is reflected and the endosperm appears opaque (Dombrink-Kurtzman & Knutson, 1997) as illustrated in the digital image (Fig. 4.4a). The protein matrix covering the starch granules is thin and shrinks easily, consequently not covering the granules completely (Fig. 4.5a) (Delcour & Hoseney, 2010; O'Kennedy, 2011). The polygonal more structured starch granules of the vitreous endosperm were shown to be tightly packed with no or very little air pockets (Fig.4.5b). The vitreous endosperm thus appeared translucent (Fig. 4.4a) due to no light being reflected (Figueroa-Cárdenas *et al.*, 2006; Lee *et al.*, 2006; Delcour & Hoseney, 2010). A continuous protein matrix covered the

starch granules in the vitreous endosperm with the small, round protein (zein) bodies clearly visible (Fig. 4.5b). This microstructural difference between floury and vitreous endosperm could now be quantified by means of %porosity determinations from X-ray µCT scans.

(a) (b)

Figure 4.3. 2-D X-ray µCT slice images of (a) a hard and (b) a soft maize kernel illustrating the presence of distinct, large cavities (marked with white circles) present in mostly the soft endosperm. Cavities are shown as black in X-ray images.

Table 4.2. %Cavity, %porosity, entire kernels density, vitreous endosperm density and floury endosperm density results of 16 maize kernels as derived by X-ray µCT

	Range	**Mean±SD**
Cavities (%)	0.17 – 6.1	1.79±1.55
Porosity (%)	0.0014 – 0.0298	0.0116±0.0069
Entire kernel density ($g.cm^{-3}$)	1.28 – 1.62	1.49±0.12
Vitreous endosperm density ($g.cm^{-3}$)	1.60 – 1.75	1.67±0.07
Floury endosperm density ($g.cm^{-3}$)	1.21 – 1.53	1.34±0.11

SD: Standard deviation

Table 4.3. Cavity and porosity percentages as well as entire kernel, vitreous endosperm and floury endosperm densities as derived by X-ray µCT for hard (n = 8) and soft (n = 8) maize hybrids

	Hard maize hybrid Mean±SD	**Soft maize hybrid** Mean± SD	**P-values**
Cavity (%)	0.89±0.62	2.68±1.72	0.01
Porosity (%)	0.0069±0.0039	0.0164±0.0060	< 0.01
Entire kernel density ($g.cm^{-3}$)	1.6±0.03	1.37±0.05	< 0.01
Vitreous endosperm density ($g.cm^{-3}$)	1.74±0.01	1.61±0.01	< 0.01
Floury endosperm density ($g.cm^{-3}$)	1.43±0.07	1.25±0.03	< 0.01

SD: Standard deviation

Figure 4.6a shows a CT image obtained at a resolution of 6 µm and Figure 4.6b an internal sub-volume image of the same maize kernel at a resolution of 3 µm. Microstructural detail could be observed when the Nanotom S system was used that was not detectable with the µCT instrument (13.4 µm resolution). In particular, the endosperm "bridges" that cross the cavity areas were visible. The results of the Defect detection function applied on the high resolution image, also revealed in very clear manner the porosity within the kernel's floury endosperm (Fig. 4.6c). The higher resolution made it possible to visualise pores as small as 6 µm in diameter (coloured blue in Fig. 4.6c). At 13.4 µm resolution, the smallest detectable pore was 30 µm. The mean %porosity was calculated to be 0.0152% for this specific kernel.

Density calculations using X-ray µCT

For true estimation of maize kernel density, a density function was constructed where the average grey values (arbitrary units) produced by the scans of the 7 polymers at 60 kV were used. Since the 16 kernels were scanned in 2 batches of 8 kernels each, two equations (eq. 7 and eq. 8) were required:

$$\text{Density } (g.cm^{-3}) = 4.98909 \times 10^{-5} \times \text{grey value} - 0.28237 \quad \text{[…eq. 7]}$$

$$\text{Density } (g.cm^{-3}) = 4.83039 \times 10^{-5} \times \text{grey value} - 0.40171 \quad \text{[…eq. 8]}$$

Mean kernel density of all 16 kernels was 1.49 (Table 4.2) with the entire kernel density for the hard hybrid (1.6 $g.cm^{-3}$) significantly ($P < 0.01$) higher than that of the soft hybrid (1.37 $g.cm^{-3}$) (Table 4.3). These densities were in the same range than those obtained by Gustin *et al.* (2013), i.e. 1.50 $g.cm^{-3}$ for entire kernel density estimations.

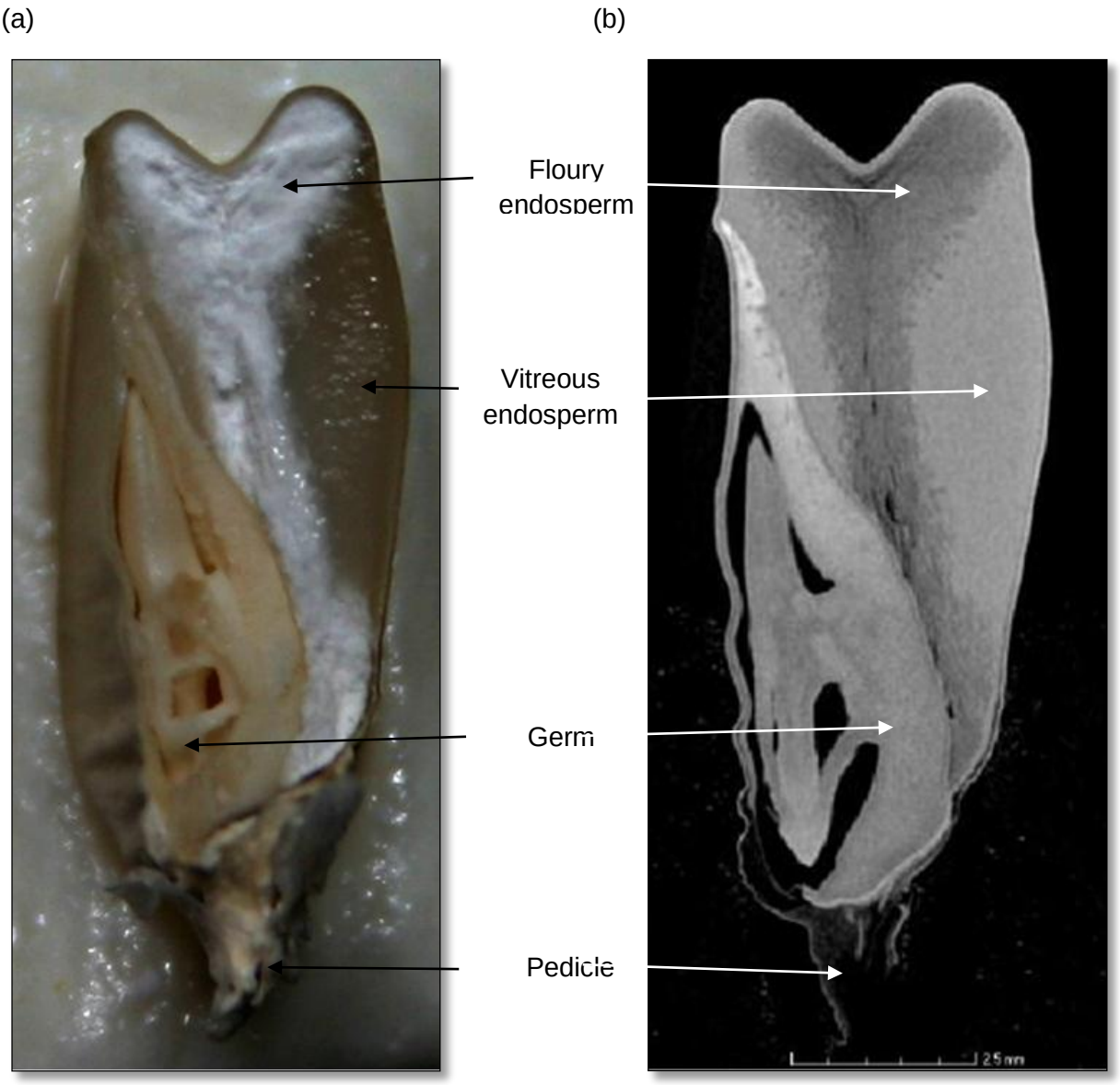

Figure 4.4. (a) A longitudinal digital image (Canon EOS 300D digital camera, fitted with a Canon 30 – 80 mm lens) and (b) 2-D X-ray µCT image slice of the same maize kernel, depicting the internal structure of the maize kernel, i.e. flour and vitreous endosperm, germ and pedicle.

When attempting to select the two respective ROIs, it was observed that the density of the germ was similar to that of the vitreous endosperm. It was thus required to manually select the germ region and excluded it from each image, using the Drawing tool (VGStudio MAX 2.2). Similar densities interfere with thresholding as the interface between the ROIs (germ and vitreous endosperm) is not well defined. After the removal of the germ region, the automated Region growing tool was applied to separate the remaining ROIs (vitreous and floury endosperm) for density determination. Both the vitreous and floury endosperm regions of the hard hybrid were subsequently determined to be significantly ($P < 0.01$) higher in density than those of the soft hybrid (Table 4.3).

(a)

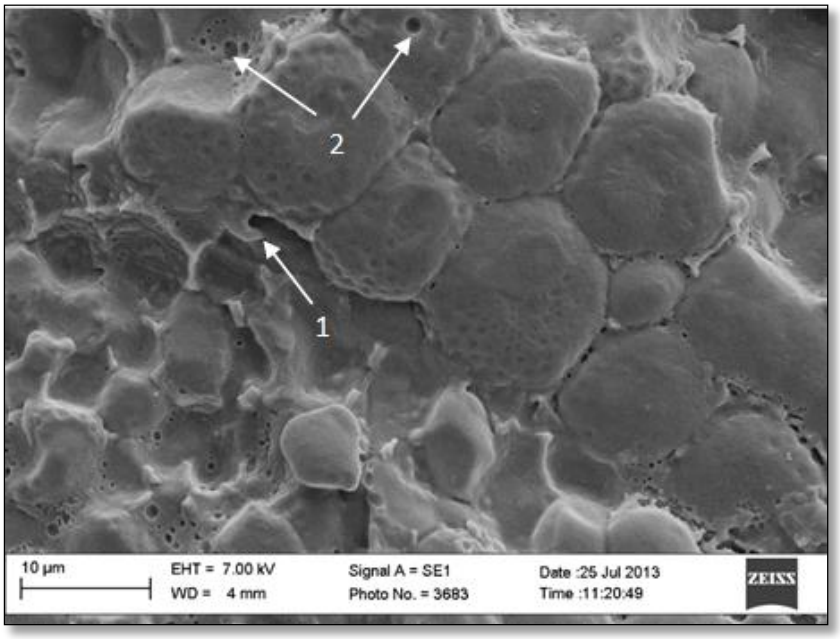

(b)

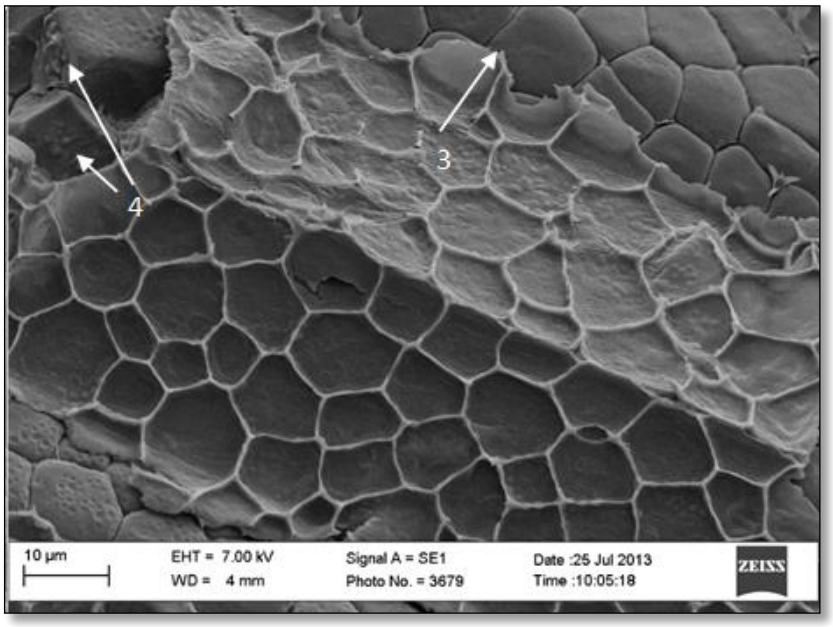

Figure 4.5. Scanning electron microscopy (SEM) micrographs (4500X) of (a) loosely packed irregularly shaped starch granules covered with a thin protein matrix (1) from floury endosperm with pores and air pockets (2) around and embedded into the granules and; (b) the tightly packed polygonal shaped starch granules from vitreous endosperm covered in a thick protein matrix (3) with protein (zein) bodies (4) visible.

(a) (b)

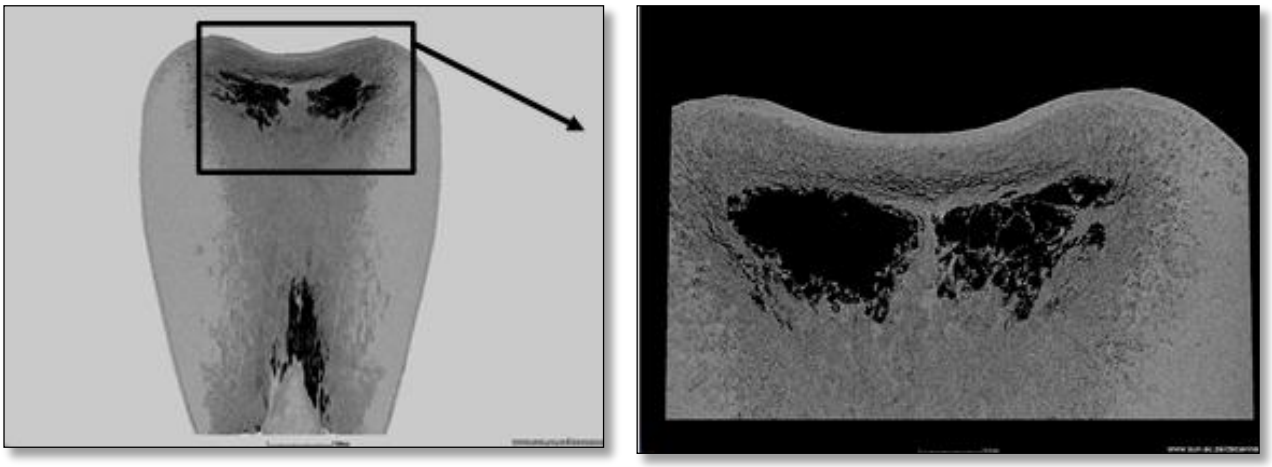

(c)

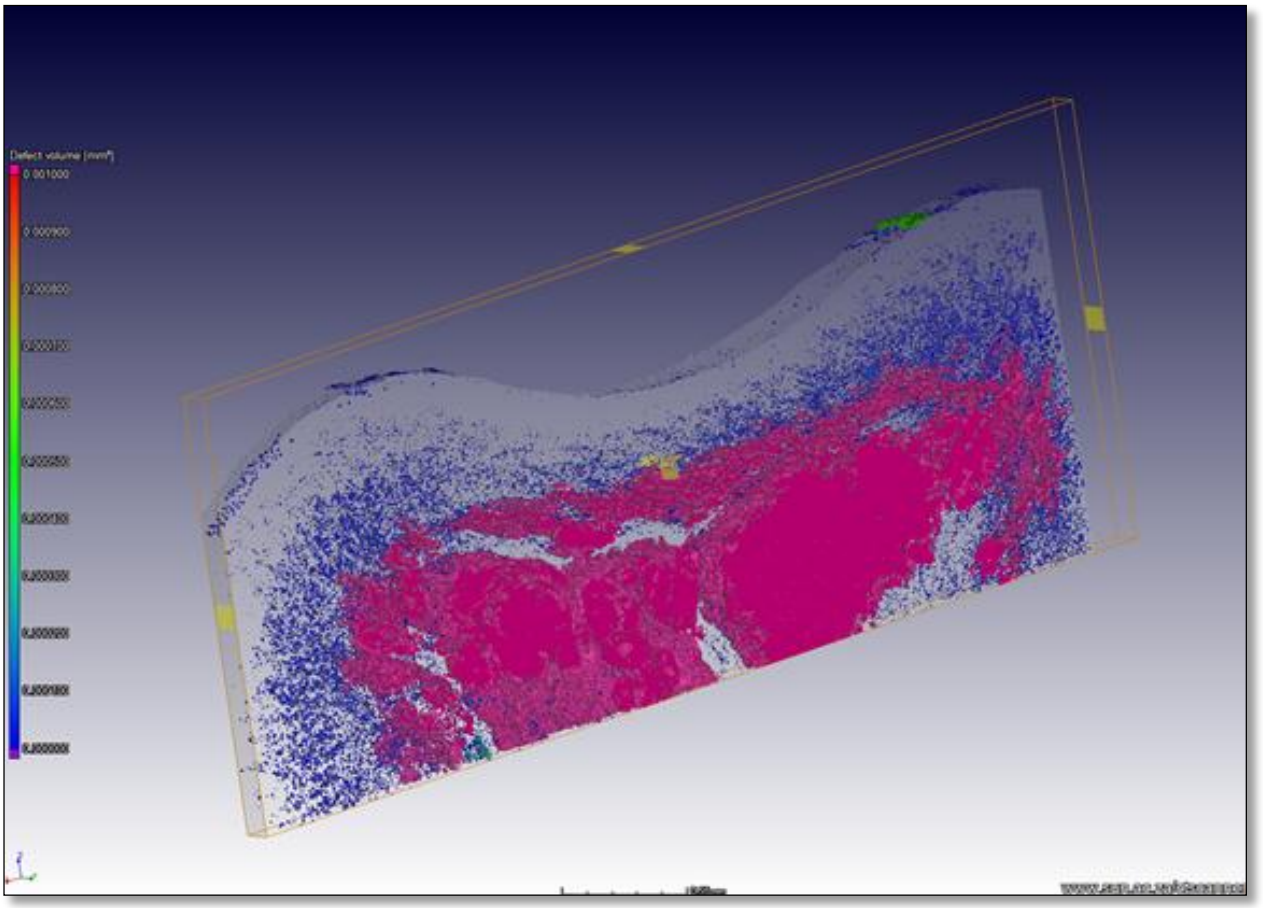

Figure 4.6. 2-D X-ray µCT slice image illustrating the endosperm microstructure of (a) a whole maize kernel acquired at 6 µm resolution and (b) a sub-volume of the same kernel acquired at 3 µm resolution. (c) 3-D X-ray µCT image of the sub-volume of the maize kernel (acquired at 3 µm resolution) with the larger cavities visualised in magenta and the smaller pores in blue. The colour bar indicates the size (mm^3) of the cavities (large; magenta) and pores (small; blue).

Validating the accuracy of X-ray µCT density calculations

The accuracy of the µCT density measurements (validation of density calibration) was tested by comparing the estimated (µCT) kernel mass with the measured (weighed) mass (Gustin *et al.*, 2013). The estimated masses ranged from 0.234 to 0.704 g (mean±SD; 0.396±0.114 g) with the actual masses ranging from 0.220 to 0.633 g (0.368±0.101 g). The high ICC consistency (0.99) and agreement (0.96) and low SE of measurement (0.01) confirmed that the two methods resulted in very similar masses and indicated the accuracy of the X-ray µCT method. This confirms the use of X-ray µCT to predict whole maize kernel densities by means of a density calibration developed from polymers.

Conventional density measurements

Conventionally, the density of whole maize kernels is determined using pycnometry (Siska and Hurburgh 1995) or the floating test (Blandino et al. 2012). The floating test and X-ray scans were performed on the same 16 kernels. Maize kernel densities results obtained with the floating test were constantly lower than those obtained with µCT. The average density of all 16 maize kernels were recorded as 1.29±0.05 (mean±SD) $g.mL^{-1}$ with that of the hard and soft hybrids recorded as 1.32±0.02 $g.mL^{-1}$ and 1.26±0.05 $g.mL^{-1}$, respectively. Although the results were not recorded in the same units ($g.mL^{-1}$ and $g.cm^{-3}$, respectively), were they comparable and the intraclass correlation (ICC) coefficients could be determined. While the two methods correlated (r = 0.78; ICC consistency = 0.74), the very low ICC agreement (0.035) indicated a large bias. This was expected due to the distinct cavities observed in the kernels (Fig. 4.3). These cavities were not included in the µCT density measurements. The feasibility of using X-ray µCT is evident from the ability of this method to exclude cavities, that would negatively influence results (Gustin *et al.*, 2013). Because of the reasonable high r and ICC consistency results it appeared possible that the results from the respective density methods could be made comparable by means of correction factors. The SE between the two measurement methods was 0.023 $g.mL^{-1}$ (or $g.cm^{-3}$).

Principal component analysis for variable interpretation

The interaction of the X-ray µCT derived variables is illustrated in the PCA bi-plot (Fig. 4.7). The first two principal components (PCs) described 91% of the variation within the model, with PC 1 describing the major percentage (78%). The hard kernels are found on the left of PC 1, whereas the soft kernels are found on the right of PC 1. The loadings indicated the relationship between the variables, and in particular, it can be observed that a stronger correlation existed between entire kernel density, vitreous endosperm density and floury endosperm density, whereas %porosity and %cavity were correlated. All these considerations were confirmed by the Spearman's rank correlation coefficients (Table 4.4), with the strongest correlation (r = 0.92, $P < 0.01$) indicated to be that between the entire kernel density and vitreous endosperm density. This strong correlation was expected as

the vitreous endosperm is the denser endosperm present in a maize kernel. Hard kernels also consisted of a higher percentage vitreous endosperm than soft kernels.

A larger variance was found between the soft kernels than the hard kernels, predominantly due to a bigger range in %cavities for the soft kernels (2.68±1.72%) compared to that of the hard kernels (0.89±0.62%). The outlier, also a soft kernel, had an exceptionally high %cavities (6.1%). It was important to note that, although the variance between the density measurements were not as large as that of the %cavities and %porosity, there were still significant differences ($P < 0.05$) between all the variables. The density variables, as well as the %cavity and %porosity variables, all contributed towards describing the hardness of individual maize kernels. The variance between the hard kernels were more pronounced by the density variables, whereas the soft kernels were better described by %cavities and %porosity.

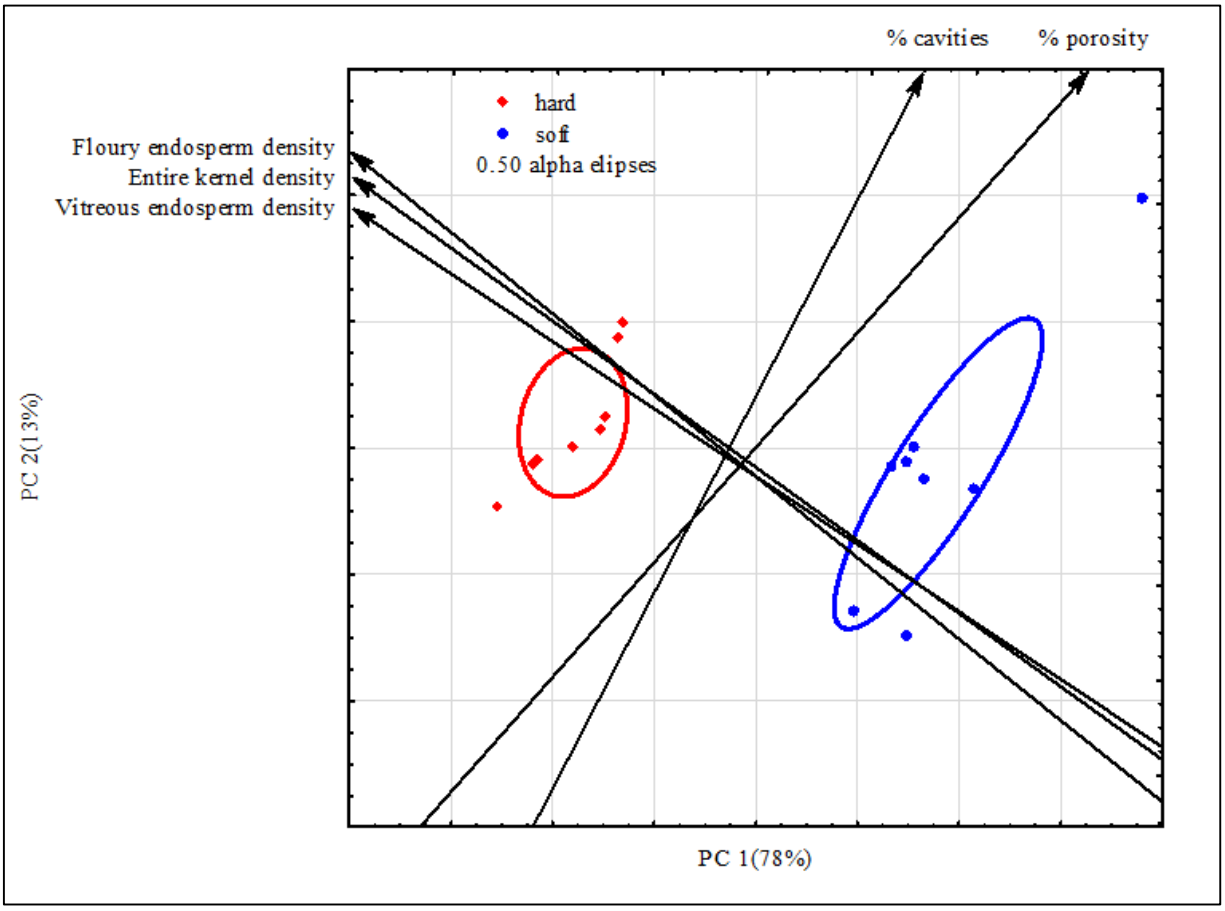

Figure 4.7. Principal component analysis bi-plot illustrating the interaction of the X-ray µCT derived variables.

Table 4.4. Spearman's rank correlation coefficients for the X-ray µCT derived variables

	Cavity (%)	**EKD**	**VED**	**FED**
Porosity (%)	0.78*	-0.63*	-0.71*	-0.68*
Cavity (%)		-0.62**	-0.58**	-0.55**
EKD			0.92*	0.89*
VED				0.85*

*: P < 0.01

**: P < 0.05

EKD: Entire kernel density (g.cm^{-3})

VED: Vitreous endosperm density (g.cm^{-3})

FED: Floury endosperm density (g.cm^{-3})

Hardness classification

Based on the observations made during the inspection of the variables by means of the PCA bi-plot and the Spearman's rank correlation coefficients, hardness classification was attempted. Threshold values could be obtained at classification accuracies of 100% sensitivity and 100% specificity for all density measurements (Table 4.5). For %porosity and %cavities, threshold values could be obtained at classification accuracies of 88% and 75%, respectively. Although hardness classification based on %porosity was not as accurate as those based on entire kernel or endosperm densities, in practice it would be a feasible and faster alternative.

Table 4.5 Receiver operating characteristic (ROC) curve results for hardness classification using X-ray µCT derived variables

	Sensitivity (%)	**Specificity** (%)	**Threshold value**	**Area under curve** (%)
Porosity (%)	88	100	0.01	97
Cavity (%)	75	100	2.02	88
EKD	100	100	1.48	100
VED	100	100	1.67	100
FED	100	100	1.30	100

EKD: Entire kernel density (g.cm^{-3})

VED: Vitreous endosperm density (g.cm^{-3})

FED: Floury endosperm density (g.cm^{-3})

Conclusion

This study attempted to provide a potential solution to classify maize kernels based on hardness. Conventional density hardness methods, such as the floating test, unintentionally overlook the influence of the cavities present in kernels. In this study, µCT scanning allowed the estimation of the true densities of the two endosperm types, vitreous and floury, as well as the density of entire maize kernels, using an appropriate density calibration. Hardness classification was possible based on ROC curve threshold values. Entire kernel density, as well as both vitreous and floury endosperm densities contributed to the variation. Additionally, X-ray µCT was shown to enable quantification of endosperm microstructural properties such as porosity and cavities. Hardness classification was also possible based on these variables with %porosity being more accurate and thus the preferred X-ray µCT measurement for this purpose.

References

AACC (1999). Approved Methods of Analysis, 11th Ed. Method 55-30.01. Particle Size Index for Wheat Hardness. Approved November 3, 1999. AACC International: St. Paul, MN, U.S.A.

Almeida-Dominguez, H.D., Suhendro, E.L. & Rooney, L.W. (1997). Factors Affecting Rapid Visco Analyser Curves for the Determination of Maize Kernel Hardness. *Journal of Cereal Science*, **25**, 93-102.

Blandino, M., Mancini, M.C., Peila, A., Rolle, L., Vanara, F. & Reyneri, A. (2010). Determination of maize kernel hardness: comparison of different laboratory tests to predict dry milling performance. *Journal of the Science of Food and Agriculture*, **90**, 1870-1878.

Blandino, M., Sacco, D. & Reyneri, A. (2012). Prediction of the dry milling performance of maize hybrids through hardness associated properties. *Journal of the Science of Food and Agriculture*, **93**, 1356-1364.

Burch, S. (2002). Measurement of density variations in compacted parts using X-ray computerised tomography. *Metal Powder Report*, **57**, 24-28.

Busignies, V., Leclerc, B., Porion, P., Evesque, P., Couarraze, G. & Tchoreloff, P. (2006). Quantitative measurements of localized density variations in cylindrical tablets using X-ray microtomography. *European Journal of Pharmaceutics and Biopharmaceutics*, **64**, 38-50.

Chang, C.S. (1988). Measuring density and porosity of grain kernels using a gas pycnometer. *Cereal Chemistry*, **65**, 13-15.

Chaunier, L., Della Valle, G. & Lourdin, D. (2007). Relationships between texture, mechanical properties and structure of cornflakes. *Food Research International*, **40**, 493-503.

Chawanji, A.S., Baldwin, A.J., Brisson, G. & Webster, E. (2012). Use of X-ray micro tomography to study the microstructure of loose-packed and compacted milk powders. *Journal of Microscopy*, **248**, 49-57.

Cnudde, V. & Boone, M.N. (2013). High-resolution X-ray computed tomography in geosciences: A review of the current technology and applications. *Earth-Science Reviews*, **123**, 1-17.

De Carvalho, M.L.M., Van Aelst, A.C., Van Eck, J.W. & Hoekstra, F.A. (1999). Pre-harvest stress cracks in maize (*Zea mays* L.) kernels as characterized by visual, X-ray and low temperature scanning electron microscopical analysis: effect on kernel quality. *Seed Science Research*, **9**, 227-236.

Delcour, J. & Hoseney, R.C. (2010). *Principles of Cereal Science and Technology.* Pp. 1-22. Minnesota, USA: AACC International Press.

Dombrink-Kurtzman, M. & Knutson, C. (1997). A study of maize endosperm hardness in relation to amylose content and susceptibility to damage. *Cereal Chemistry*, **74**, 776-780.

Dombrink-Kurtzman, M.A. & Bietz, J.A. (1993). Zein composition in hard and soft endosperm of maize. *Cereal Chemistry*, **70**, 105-108.

Donis-González, I.R., Guyer, D.E., Pease, A. & Barthel, F. (2014). Internal characterisation of fresh agricultural products using traditional and ultrafast electron beam X-ray computed tomography imaging. *Biosystems Engineering*, **117**, 104-113.

Du Plessis, A., Meincken, M. & Seifert, T. (2013). Quantitative determination of density and mass of polymeric materials using microfocus computed tomography. *Journal of Nondestructive Evaluation*, **32**, 413-417.

Erasmus, C. (2003). Maize kernel translucency measurement by image analysis and its relationship to vitreousness and dry milling performance. PhD Thesis. University of Pretoria, Pretoria, South Africa.

Eyherabide, G.H., Robutti, J.L. & Borras, F.S. (1996). Effect of near-infrared transmission-based selection on maize hardness and the composition of zeins. *Cereal Chemistry*, **73**, 775-778.

Figueroa-Cárdenas, J.D., Reyes-Vega, M.L., Rincón-Sánchez, F., Gaytán-Martínez, M. & Morales-Sánchez, E. (2006). Microstructure of starch granule related to kernel hardness in corn. *Revista Fitotecnia Mexicana*, **29**, 135-139.

Fox, G. & Manley, M. (2009). Hardness methods for testing maize kernels. *Journal of Agricultural and Food Chemistry*, **57**, 5647-5657.

Frisullo, P., Laverse, J., Marino, R. & Nobile, M.A.D. (2009). X-ray computed tomography to study processed meat microstructure. *Journal of Food Engineering*, **94**, 283-289.

Gondek, E., Jakubczyk, E., Herremans, E., Verlinden, B., Hertog, M., Vandendriessche, T., Verboven, P., Antoniuk, A., Bongaers, E. & Estrade, P. (2013). Acoustic, mechanical and microstructural properties of extruded crisp bread. *Journal of Cereal Science*, **58**, 132-139.

Gustin, J.L., Jackson, S., Williams, C., Patel, A., Armstrong, P.R., Peter, G.F. & Settles, A.M. (2013). Analysis of maize (*Zea mays*) kernel density and volume using micro-computed tomography and single-kernel near infrared spectroscopy. *Journal of Agricultural and Food Chemistry*, **61**, 10872-10880.

Huber, K.C. & BeMiller, J.N. (1997). Visualization of channels and cavities of corn and sorghum starch granules. *Cereal Chemistry*, **74**, 537-541.

Huber, K.C. & BeMiller, J.N. (2000). Channels of maize and sorghum starch granules. *Carbohydrate Polymers*, **41**, 269-276.

Kak, A.C. & Slaney, M. (1988). *Principles of computerized tomographic imaging* Pp. 104-107. New York: IEEE Press.

Kotwaliwale, N., Singh, K., Kalne, A., Jha, S.N., Seth, N. & Kar, A. (2011). X-ray imaging methods for internal quality evaluation of agricultural produce. *Journal of Food Science and Technology*, **51**, 1-15.

Laverse, J., Mastromatteo, M., Frisullo, P., Albenzio, M., Gammariello, D. & Del Nobile, M.A. (2011a). Fat microstructure of yogurt as assessed by X-ray microtomography. *Journal of Dairy Science*, **94**, 668-675.

Laverse, J., Mastromatteo, M., Frisullo, P. & Del Nobile, M.A. (2011b). X-ray microtomography to study the microstructure of cream cheese-type products. *Journal of Dairy Science*, **94**, 43-50.

Laverse, J., Mastromatteo, M., Frisullo, P. & Del Nobile, M.A. (2012). X-ray microtomography to study the microstructure of mayonnaise. *Journal of Food Engineering*, **108**, 225-231.

Lee, K.M., Bean, S.R., Alavi, S., Herrman, T.J. & Waniska, R.D. (2006). Physical and biochemical properties of maize hardness and extrudates of selected hybrids. *Journal of Agricultural and Food Chemistry*, **54**, 4260-4269.

Lee, K.M., Herrman, T.J., Rooney, L.W., Jackson, D.S., Lingenfelser, J., Rausch, K.D., McKinney, J., Iiams, C., Byrum, L., Hurburgh, J.C.R., Johnson, L.A. & Fox, S.R. (2007). Corroborative study on maize quality, dry-milling and wet-milling properties of selected maize hybrids. *Journal of Agricultural and Food Chemistry*, **55**, 10751-10763.

Lindgren, O., Davis, J., Wells, P. & Shadbolt, P. (1992). Non-destructive wood density distribution measurements using computed tomography. *Holz als Roh-und Werkstoff*, **50**, 295-299.

Malvar, R.A., Revilla, P., Moreno-González, J., Butrón, A., Sotelo, J. & Ordás, A. (2008). White maize: genetics of quality and agronomic performance. *Crop Science*, **48**, 1373-1381.

Manley, M., Williams, P., Nilsson, D. & Geladi, P. (2009). Near infrared hyperspectral imaging for the evaluation of endosperm texture in whole yellow maize (*Zea mays* L.) kernels. *Journal of Agricultural and Food Chemistry*, **57**, 8761-8769.

McGoverin, C. & Manley, M. (2012). Classification of maize kernel hardness using near infrared hyperspectral imaging. *Journal of Near Infrared Spectroscopy*, **20**, 529-535.

Meincken, M. & du Plessis, A. (2013). Visualising and quantifying thermal degradation of wood by computed tomography. *European Journal of Wood and Wood Products*, **71**, 387-389.

Mestres, C., Louis-Alexandre, A., Matencio, F. & Lahlou, A. (1991). Dry-milling properties of maize. *Cereal Chemistry*, **68**, 51-56.

O'Kennedy, K. (2011). Characterisation of zein from South African maize of varying endosperm texture. MSc Thesis. Stellenbosch University, South Africa.

Paiva, E., Kriz, A.L., Peixoto, M.J.V.V.D., Wallace, J.C. & Larkins, A.B. (1991). Quantitation and distribution of ã–zein in the endosperm of maize kernels. *Cereal Chemistry*, **68**, 276-279.

Pomeranz, Y., Martin, C.R., Traylor, D.D. & Lai, F.S. (1984). Corn hardness determination. *Cereal Chemistry*, **61**, 147-150.

Robutti, J.L. (1995). Maize kernel hardness estimation in breeding by near-infrared transmission analysis. *Cereal Chemistry*, **72**, 632-636.

Robutti, J.L., Borras, F.S. & Eyherabide, G.H. (1997). Zein compositions of mechanically separated coarse and fine portions of maize kernels. *Cereal Chemistry*, **74**, 75-78.

Robutti, J.L., Hoseney, R.C. & Wassom, C.E. (1974). Modified opaque-2 corn endosperms. ll. Structure viewed with a scanning electron microscope. *Cereal Chemistry*, **51**, 173-180.

Singhal, A., Grande, J.C. & Zhou, Z. (2013). Micro/Nano CT for visualization of internal structures. *Microscopy Today*, **21**, 16-22.

Sinka, I.C., Burch, S.F., Tweed, J.H. & Cunningham, J.C. (2004). Measurement of density variations in tablets using X-ray computed tomography. *International Journal of Pharmaceutics*, **271**, 215-224.

Siska, J. & Hurburgh, C.R. (1995). Corn density measurement by near-infrared transmittance. *Transactions of the ASAE*, **38**, 1821-1824.

Van Dalen, G., Nootenboom, P. & Van Vliet, L.J. (2007). 3D Imaging and analysis of porous cereal products using X-ray microtomography. In: *The 12th International Congress for Stereology (ICSXII), 2007*. September 3-7, 2007.Saint-Etienne, France.

Watson, S.A. (1987). Structure and Composition. In: *Corn Chemistry and Technology* (edited by S.A. Watson & P.E. Ramstad). Pp. 53-82. St. Paul, Minnesota, USA: American Association of Cereal Chemists, Inc.

Williams, P., Geladi, P., Fox, G. & Manley, M. (2009). Maize kernel hardness classification by near infrared (NIR) hyperspectral imaging and multivariate data analysis. *Analytica Chimica Acta*, **653**, 121-130.

Wu, Y.V. (1992). Corn hardness as related to yield and particle size of fractions from a micro hammer-cutter mill. *Cereal Chemistry*, **69**, 343-347.

Wu, Y.V. & Bergquist, R.R. (1991). Relation of corn grain density to yields of dry-milling products. *Cereal Chemistry*, **68**, 542-544.

Zhu, L.J., Dogan, H., Gajula, H., Gu, M.H., Liu, Q.Q. & Shi, Y.C. (2012). Study of kernel structure of high-amylose and wild-type rice by X-ray microtomography and SEM. *Journal of Cereal Science*, **55**, 1-5.

Chapter 5

Milling quality classification of maize (*Zea mays* L.) using X-ray micro-computed tomography (µCT)

Abstract

This study has shown that good classification of maize hybrids, differing in milling quality, was possible when using X-ray µCT derived density and volume measurements. These variables were obtained from low resolution (80 µm) µCT scans as 150 kernels were imaged at once, thereby reducing acquisition time and cost. When using entire kernel density (EKD) and vitreous-to-floury endosperm ratio (V:F) measurements, good classification accuracies of 93% and 92% were obtained respectively. Furthermore, it was established that milling quality could not be described without the inclusion of density measurements. Conventional hardness methods should therefore be used with caution when intended to describe milling quality, as they intrinsically contribute towards volume related properties. A conventional density hardness method, such as the floating test, is also not adequate for describing milling quality, as this method overlooks the influence of cavities present in maize kernels.

Introduction

Kernel hardness is one of the most important factors in determining the functionality of grains. Hardness is a characteristic often used in the milling industry to identify the varieties or hybrids desirable for milling (Neethirajan *et al.*, 2006). Dry-milling is the industrial practise used to process maize (*Zea mays* L.) into maize flour, and is dependent on the hardness of the maize for optimal yield. Due to the complexity of maize hardness, the interpretation and measurement thereof can be difficult. As yet, no standardised hardness method exists, resulting in an extensive range in approaches (Fox & Manley, 2009).

In an earlier study, percentage chop (%chop) was used as milling quality descriptor where de-germed maize was subjected to the milling process and the chop (combination of pericarp, germ and to a lesser extent endosperm) was calculated as a percentage of the total mass of maize (Guelpa *et al.*, 2014a). It had been established that hectoliter mass (HLM) correlated (r = -0.71) with %chop and that the coarse-over-fine ratio as derived from the particle size index (PSI) method, milling index (from near infrared (NIR) absorbance values), percentage vitreous endosperm (based on NIR hyperspectral imaging) and hundred kernel mass (HKM) all contributed to describing the overall milling quality of the respective hybrids (Guelpa *et al.*, 2014a).

Eighty percent of the volume of a typical maize kernel consists of two types of starch tissue, i.e. vitreous and floury endosperm (Paiva *et al.*, 1991). The vitreous endosperm is hard and translucent (glassy) and lies mainly at the sides and back of the kernel, whereas the floury endosperm is softer and mealy textured and found in the centre of the kernel (Watson, 1987; Paiva *et al.*, 1991). White maize is classed as dent maize, which is a cross between flint and flour types (Benson & Pearce, 1987) and intermediate between flour (soft) and popcorn (hard) with respect to hardness (Wolf *et al.*, 1952). The ratio of vitreous and floury endosperm volume averages about 2:1 in dent maize (Wolf *et al.*, 1952), but variations occur due to genetic make-up (Johnson & Russell, 1982), environmental influences (Hamilton *et al.*, 1951) and postharvest handling (Peplinski *et al.*, 1989).

With the discovery of X-rays by Prof Wilhelm Röntgen in 1895 (Cnudde & Boone, 2013), this type of radiation has become a prominent technique for medical diagnostics (Kotwaliwale *et al.*, 2011). As X-rays are capable of penetrating material in varying degrees as expressed by Beer's law (Cnudde & Boone, 2013), this attenuated radiation can be converted by a detector into a two dimensional (2-D) digital image, called a radiograph. Only with the development of modern computer technology in the 1960s, computed tomography became feasible (Kalender, 2006). Computed tomography (CT) refers to the reconstruction of 2-D images mathematically, to display and archive them in digital three dimensional (3-D) format (Kalender, 2006). In the 1980's a new research field emerged as high-resolution X-ray tomography, or commonly called micro-CT (µCT) was first discussed (Cnudde & Boone, 2013). X-ray µCT has seen a period of rapid growth over the last 15 years, mainly due to considerable improvements in spatial resolution and image reconstruction times (Maire & Withers, 2014).

In a study on a limited number of maize kernels, it was shown how X-ray µCT could estimate maize hardness when constructing a density calibration (Guelpa *et al.*, 2014b). Threshold values were determined for entire kernel density, and vitreous and floury endosperm densities, respectively which allowed for hardness classification (Guelpa *et al.*, 2014b). When considering other X-ray µCT studies on maize, Takhar *et al*. (2011) focussed on moisture transport within maize kernels and De Carvalho *et al*. (1999) studied stress cracks formation. Both found the technique of X-ray µCT to be successful to be applied in food processing studies. The study of Gustin *et al.* (2013), recognised the potential of X-ray µCT as a method to determine kernel density and volume. They also demonstrated that single kernel density correlated (r = 0.8) with test weight (Gustin *et al.*, 2013), which in turn is seen as a conventional method of describing maize hardness (Lee *et al.*, 2006).

The aim of this study was to perform milling quality classification based on X-ray µCT densities and volumes (entire kernel, vitreous and floury endosperm).

Material and methods

Samples and preparation

From a set of 49 samples, consisting of 19 hybrids, four localities and three plantings, 300 maize kernels were selected, as depicted in Table 5.1. The sample set (n = 49) originated from maize breeding trials of South African white maize, either supplied by PANNAR Seeds (Greytown, South Africa) or a farmer from Schweizer-Reneke. The four localities represented in the sample set were Greytown, Delmas, Klerksdorp and Schweizer-Reneke and the three plantings refer to an early, normal and late planting of the 2012 harvest.

The sample set was ranked according to the samples' milling performance, using an industrial guideline known as percentage chop (%chop). To determine the %chop, a pilot plant scale de-germer was used and the de-germed maize was subjected to the milling process, also on a pilot plant scale. The chop (combination of pericarp, germ and endosperm) was then calculated as a percentage of the total mass of the maize. A %chop below 22% indicated good milling maize, between 22% and 25% was good intermediate, between 26% and 30% was poor intermediate and above 30% was poor milling maize.

Consequently, 150 maize kernels were selected from the 10 samples that illustrated the best milling performance (15 kernels per sample), and another 150 kernels were selected from the 10 samples that showed poorest milling performance (again 15 kernels per sample).

Florist oasis discs (10 cm diameter; 2 cm height) were prepared in order to facilitate simultaneous X-ray µCT scanning of multiple kernels. The low density of the florist oasis provided for clear distinction from the subjects of interest and was therefore a suitable medium for mounting purposes. Thirty maize kernels were placed in a specific order in each of 10 florist oasis discs, without touching each other (Fig. 5.1). Polymer discs (25 mm in diameter and 10 mm in height) that were used for the density calibrations were also placed in the florist oasis discs. Five discs were stacked on top of each

other (150 kernels) and secured with a wooden stick to prevent any movement during X-ray acquisition.

Table 5.1. List of white maize hybrids, localities and plantings from the 2012 harvest

	Kernels	Hybrid	Locality	Planting
Good milling	1 – 15	1	Greytown	Early
	16 – 30	2	Delmas	Early
	31 – 45	3	Greytown	Early
	46 – 60	3	Greytown	Late
	61 – 75	2	Greytown	Early
	76 – 90	2	Greytown	Late
	91 – 105	11	Schweizer-Reneke	Normal
	106 – 120	1	Delmas	Early
	121 – 135	16	Schweizer-Reneke	Normal
	135 – 150	3	Delmas	Early
Poor milling	1 – 15	8	Greytown	Early
	16 – 30	10	Greytown	Early
	31 – 45	19	Schweizer-Reneke	Normal
	46 – 60	17	Schweizer-Reneke	Normal
	61 – 75	18	Schweizer-Reneke	Normal
	76 – 90	8	Greytown	Late
	91 – 105	10	Delmas	Late
	106 – 120	5	Delmas	Late
	121 – 135	5	Delmas	Early
	135 – 150	12	Schweizer-Reneke	Normal

Conventional hardness methods

The particle size index (PSI) coarse-over-fine (c/f) ratio, hundred kernel mass (HKM), hectoliter mass (HLM), protein content as determined with the Dumas method, a NIR spectroscopy hardness index and a vitreous endosperm percentage value derived from NIR hyperspectral imaging (HSI) were determined for each of the 20 samples as described in Guelpa *et al.* (2014a).

X-ray micro-computed tomography scanning

X-ray scans were acquired using a commercial micro-focus X-ray computed tomography system, i.e. Phoenix V|Tome|X L240 (General Electric Sensing and Inspection Technologies / Phoenix X-ray, Wunstorff, Germany). The system depicted in Fig. 5.2 is located at the CT Scanner Facility of the Central Analytical Facility (CAF), Stellenbosch University, South Africa. It comprises of a lead-lined cabinet that houses the X-ray direct tube and the sample manipulator, along with a cooling unit

and an external control module. Image acquisition was set at 500 ms per image with 2000 images recorded in one rotation at 80 µm voxel size or resolution. A 0.1 mm copper filter was used to reduce beam hardening artefacts and a scan took 1 h to complete. In this work a tungsten target, 60 kV and 240 µA was used for X-ray generation.

The florist oasis stacks containing 150 maize kernels each were placed one at a time on the specimen stage and rotated along the axis, perpendicular to the beam direction. Two scans were required to image all 300 kernels, illustrating a cost-effective and time-saving application of µCT.

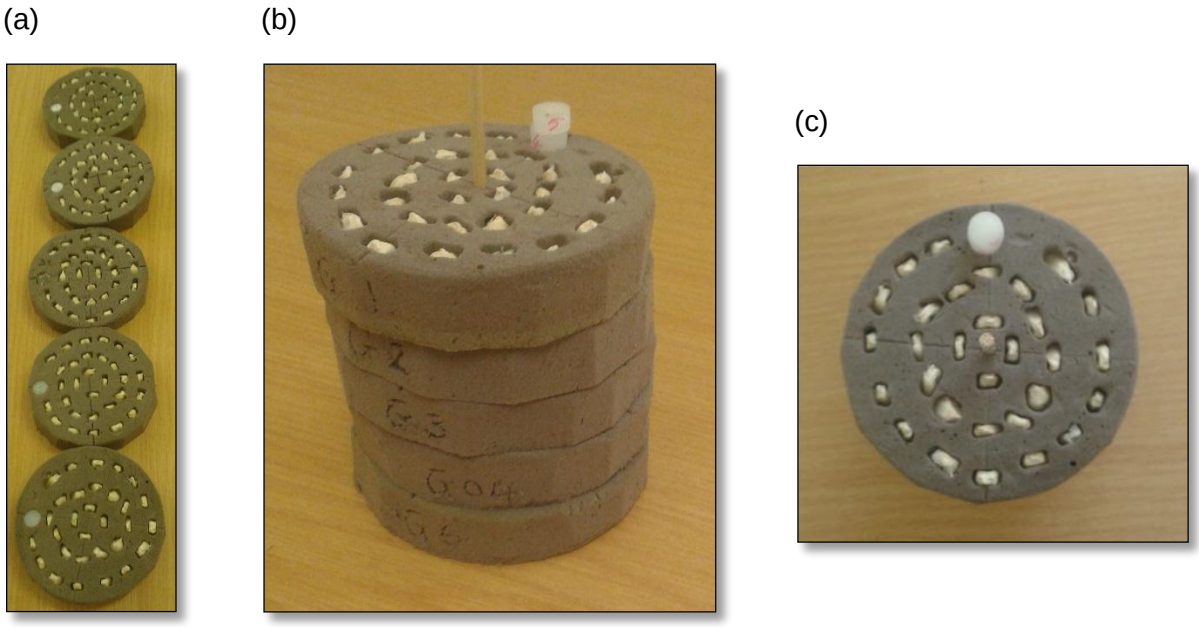

Figure 5.1. Digital images illustrating sample preparation: (a) five florist oasis discs used as mounting material for the 150 good milling maize kernels, (b) the stack of discs, held upright with a wooden stick and (c) a top view of the stack. The polymer discs used for the density calibration are also visible in these images.

Image processing and analysis

The acquired 2-D X-ray images were rendered into 3-D volumes, using the integrated Phoenix Datos acquisition and reconstruction software (General Electric Sensing and Inspection Technologies / Phoenix X-ray, Wunstorff, Germany). The process of reconstruction comprises of filtered back-projection algorithms where the grey values in a rendered CT image represent the attenuation in each pixel (Singhal *et al.*, 2013) (Fig. 5.3). The 3-D images were further analysed with VGStudio Max 2.2 (Volume Graphics, Heidelberg, Germany).

Each maize kernel was analysed independently as sub volume extraction was possible. Therefore, density calculations, as well as volume analysis, were performed per kernel.

(a) (b) (c)

Figure 5.2. The Phoenix V|Tome|X L240 micro-computed tomography scanner showcasing the (a) direct tube and the sample manipulator, (b) lead-line cabinet with cooling unit and (c) the control monitor.

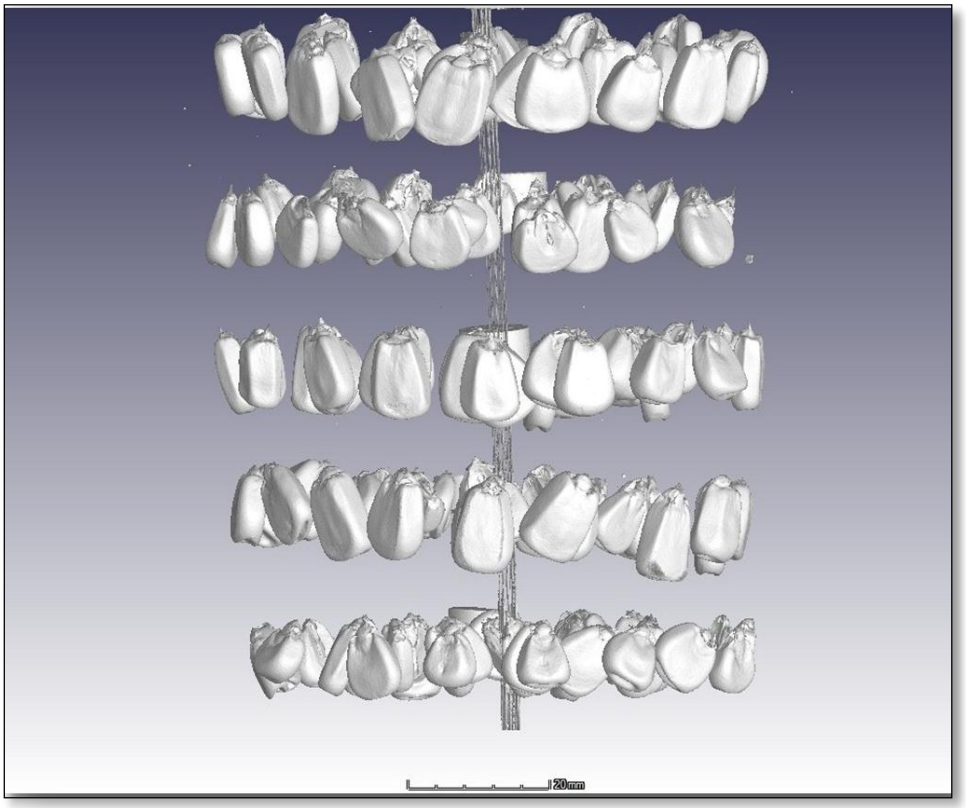

Figure 5.3. The 3-D X-ray µCT image of a stack of five discs, containing 30 kernels each and with the mounting material removed.

Density calculations

Densities of entire maize kernels (EKD), as well as two regions of interest (ROIs) i.e. the vitreous endosperm (VED) and the floury endosperm (FED), were calculated using a density calibration method as described in Guelpa *et al*. (2014b). EKD did not include cavities (large air spaces). This

method made use of a set of polymers with known densities that was included in each X-ray scan to facilitate the construction of a density calibration. To generate the calibration function (eq. 1), the average grey values of each polymer disk, as well as their actual density values, were used.

Actual density ($g.cm^{-3}$) = m x grey value + c …[eq. 1]

Where:
m: is the slope
c: is the intercept

It was found that the densities of the germ and vitreous endosperm regions were very similar and thus prevented accurate separation. Therefore, the germ region was removed, slice by slice, for each kernel (Guelpa *et al.*, 2014b) as illustrated in Figure 5.4. After the manual removal of the germ, the remaining endosperm could be separated and mean grey values for the respective ROIs could be obtained. Mean grey values for the entire kernel were acquired prior to the separation. The grey values were substituted into the calibration equations (one for each X-ray scan) and subsequent densities could be calculated, expressed as $g.cm^{-3}$.

(a) (b)

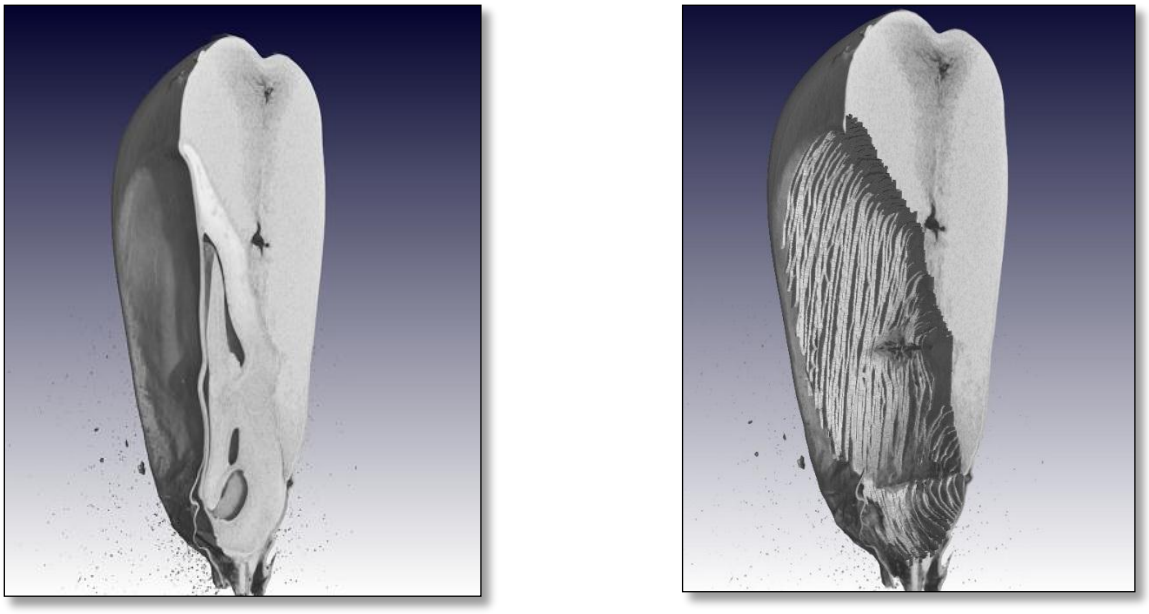

Figure 5.4. X-ray µCT slice images of (a) maize kernel with germ intact, and (b) with germ removed, slice by slice.

Volume analysis

Entire kernel volume (EKV) and the volumes of the two endosperm types, i.e. vitreous (VEV) and floury endosperm (FEV), was determined using the automated Region growing tool, in combination

with the Volume analyser function of VGStudio Max 2.2. The endosperm type volumes (VEV and FEV) were expressed as a percentage of the total volume of endosperm per kernel. Additionally, a vitreous-to-floury endosperm ratio (V:F) was calculated from the VEV and FEV. Figure 5.5 illustrates the segmentation into respective regions, allowing quantification, non-destructively.

(a) (b)

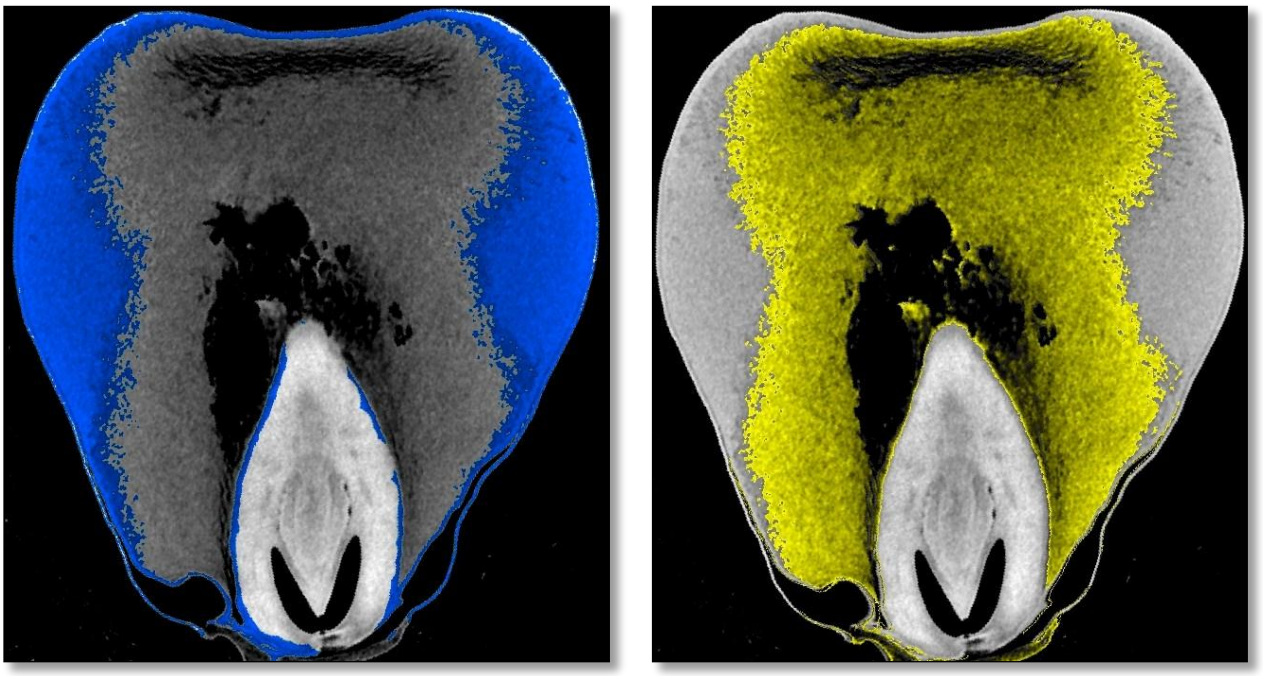

Figure 5.5. 2-D X-ray µCT slice images of the (a) vitreous endosperm (blue) and (b) floury endosperm (yellow) present within a maize kernel.

Statistical procedures

Univariate methods

Mean differences for the X-ray µCT derived variables (densities: entire kernel, vitreous and floury endosperm and volumes: entire kernel, vitreous and floury endosperm, also vitreous-to-floury endosperm volume ratio) were evaluated by one-way analysis of variance (ANOVA) using STATISTICA version 11 (StatSoft, Inc., Tulsa, USA).

Furthermore, a receiver operating characteristic (ROC) curve was used to classify the maize kernels into good milling and poor milling classes, based on the respective constituents, using STATISTICA version 11 (StatSoft, Inc., Tulsa, USA). An ROC curve is a plot of sensitivity on the *y*-axis against 1-specificity on the *x*-axis, for varying values of the threshold. The optimal threshold is determined by maximising the sum of sensitivity and specificity. Sensitivity is the percentage good milling kernels correctly classified and specificity is the percentage poor milling kernels correctly classified.

Spearman's rank correlation coefficients were used to test the strength of the relationships between pairs of X-ray µCT derived results (densities: entire kernel, vitreous and floury endosperm

and volumes: cavities, entire kernel, vitreous and floury endosperm, also vitreous-to-floury endosperm volume ration), using STATISTICA version 11 (StatSoft, Inc., Tulsa, USA).

Multivariate method: principal component analysis

Principal component analysis (PCA) was performed on X-ray µCT derived variables (densities: entire kernel, vitreous and floury endosperm and volumes: entire kernel, vitreous and floury endosperm, also vitreous-to-floury endosperm volume ration) and variables derived from 6 conventional hardness methods. To inspect the relationship between the variables, PCA bi-plots were used as it combines the scores and the loadings. STATISTICA version 11 (StatSoft, Inc., Tulsa, USA) was used to perform the PCA.

Results and discussion

X-ray µCT density calculations

When considering the accuracy of conventional density measurements, it was reasoned that internal air spaces or cavities would greatly influence the result, possibly dominate the important density differences found between the endosperm types and in doing so, cause misleading results. This was seen when floating test densities of the same kernels were compared to densities calculated with X-ray µCT data (Guelpa *et al.*, 2014b). The floating test consistently produced lower densities than the latter method and a large bias was apparent.

Based on an advantage of X-ray µCT, i.e. allowing the exclusion of undesired regions (such as cavities), this method was seen as more suited for accurate density measurements (Gustin *et al.*, 2013). Another advantage being each voxel having an associated grey value depending on the material's density and atomic number. Areas of low density cause less attenuation of the X-ray beams and are portrayed as darker regions. Black areas represents air that do not attenuate at all. Areas of high density causes lots of attenuation and therefore fewer X-rays can reach the detector.

It has been considered that the structural arrangement of the starch, of which endosperm predominantly consist of, affects maize hardness more than any other morphological features within maize kernels (Figueroa Cárdenas *et al.*, 2006). The different starch granule patterns of vitreous endosperm, tightly packed within the protein matrix, as opposed to the loosely packed floury endosperm with intergranular air spaces (or pores) were revealed by scanning electron microscopy (Figueroa Cárdenas *et al.*, 2006). A 2-D µCT slice image of a maize kernel, acquired at 13.4 µm resolution, revealed similar endosperm textural properties as the vitreous endosperm was portrayed as the denser endosperm with tightly packed starch granules, whereas the floury endosperm revealed loosely packed granules (Fig. 5.6).

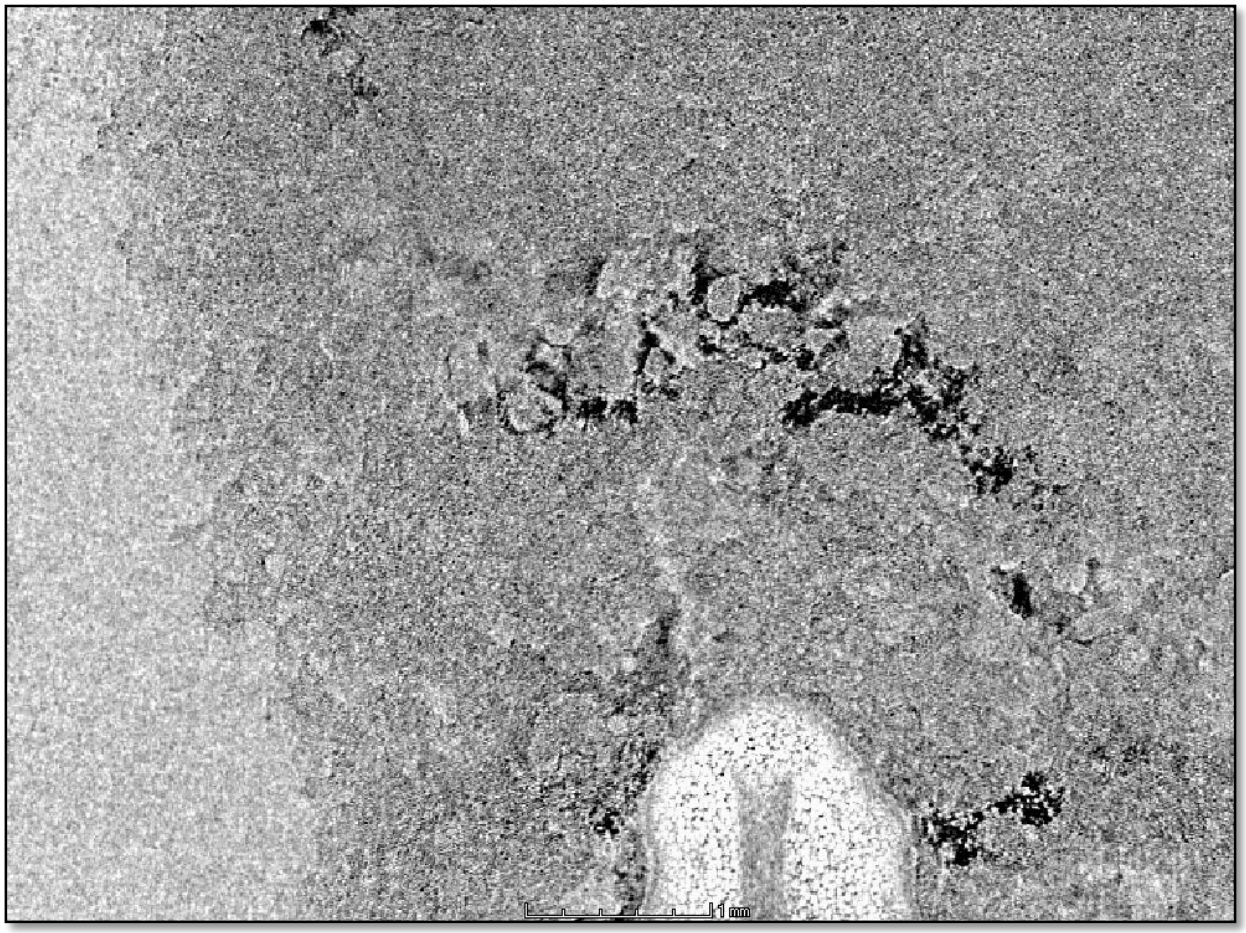

Figure 5.6. A zoomed in 2-D X-ray µCT slice image acquired at a 13.4 µm resolution of the internal structures of a maize kernel. The light grey (more dense) region on the left is the vitreous endosperm, whereas a section of the germ is visible at the bottom (white) and the loosely packed floury endosperm is visible in darker grey (less dense) with intracellular airspaces (black).

Figueroa-Cárdenas *et al*. (2006) saw a significant ($P < 0.05$) correlation (r = 0.69) between kernel density (determined using water replacement and a floating test) and hardness (as expressed by a puncture test). Similarly, Guelpa *et al*. (2014b) showed a significant correlation ($P < 0.05$) between kernel density (determined using X-ray µCT) and hardness (using the PSI (c/f)). In the latter study, 16 maize kernels scanned at a resolution of 13.4 µm, were used for density calculations. The same was attempted, using 300 maize kernels acquired at 80 µm resolution.

The respective densities were calculated in a similar fashion as explained in Guelpa *et al.* (2014b). EKD, VED and FED were determined by obtaining grey values from each respective region-of-interest (ROI) and substituting these values into density equations (eq. 2 and 3). The mean grey values obtained for EKD did not include cavities, which was possible by setting an appropriate threshold to exclude air spaces. After manual exclusion of the germ region, a higher grey value threshold was applied to select the vitreous endosperm region, while excluding the floury endosperm region. Consequently, the mean grey value for the vitreous endosperm ROI was obtained. The

mean grey value for the floury endosperm ROI was obtained in a similar fashion, but by selecting the higher grey value interval in the histogram.

Two scans were required to image all 300 kernels (150 kernels per scan), therefore two linear equations had to be constructed, as shown in equations 2 and 3:

Density ($g.cm^{-3}$) = 3.58158 x 10^{-5} x grey value – 0.11004 …[eq. 2]

Density ($g.cm^{-3}$) = 3.52309 x 10^{-5} x grey value – 0.0659 …[eq. 3]

As a result of artifacts that were present in three of the imaged maize kernels, these respective kernels could not be used for image analysis. Consequently, there were only 297 samples used throughout this study.

The average EKD of all 297 maize kernels were 1.30 $g.cm^{-3}$, while that of the VED and FED were 1.36 $g.cm^{-3}$ and 1.12 $g.cm^{-3}$, respectively. Mean EKD of the good milling hybrids (1.31 $g.cm^{-3}$) was significantly ($P < 0.05$) higher than that of the poor milling hybrids (1.23 $g.cm^{-3}$) (Table 5.2) as expected with the higher proportion of vitreous endosperm present within good milling (or hard) hybrids (Watson, 1987), which would increase the density. The protein matrix within this endosperm type keeps the starch granules tightly packed, thus dense, as opposed to more intracellular air spaces found within the loosely packed floury endosperm (Robutti *et al.*, 1997). The same trend was found for the mean VED and FED, as these values were also significantly higher for the good milling hybrids (1.38 $g.cm^{-3}$ and 1.14 $g.cm^{-3}$, respectively) compared to the poor milling hybrids (1.35 $g.cm^{-3}$ and 1.10 $g.cm^{-3}$, respectively) (Table 5.2). It was expected that the VED would be significantly higher for the hybrids with the higher proportion of vitreous endosperm, i.e. the good milling hybrids.

Table 5.2. Entire kernel density, vitreous endosperm density and floury endosperm density results as derived by X-ray µCT for the two milling classes, good (n = 150) and poor (n = 147), also indicating ANOVA results

	Good milling hybrids		**Poor milling hybrids**		***P*-value**
	Range	Mean±SD	Range	Mean±SD	
EKD ($g.cm^{-3}$)	1.22 – 1.36	1.31±0.03	0.97 – 1.32	1.23±0.05	< 0.01
VED ($g.cm^{-3}$)	1.26 – 1.42	1.38±0.03	1.23 – 1.40	1.35±0.03	< 0.01
FED ($g.cm^{-3}$)	1.04 – 1.26	1.14±0.04	0.89 – 1.27	1.10±0.04	< 0.01

SD: Standard deviation

EKD: Entire kernel density

VED: Vitreous endosperm density

FED: Floury endosperm density

(a)

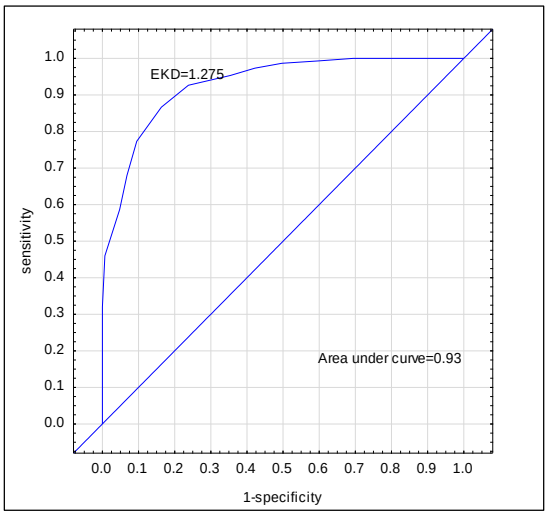

(b)

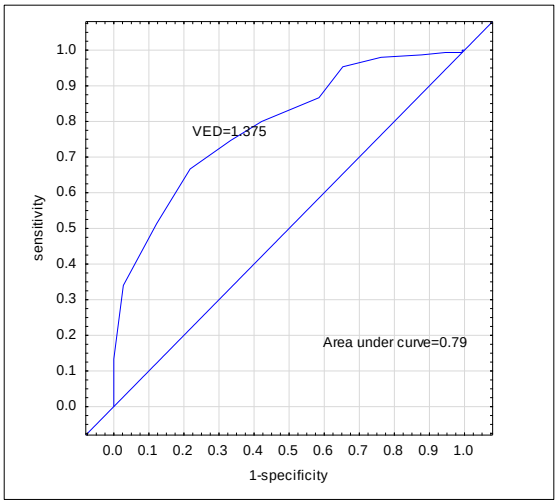

(c)

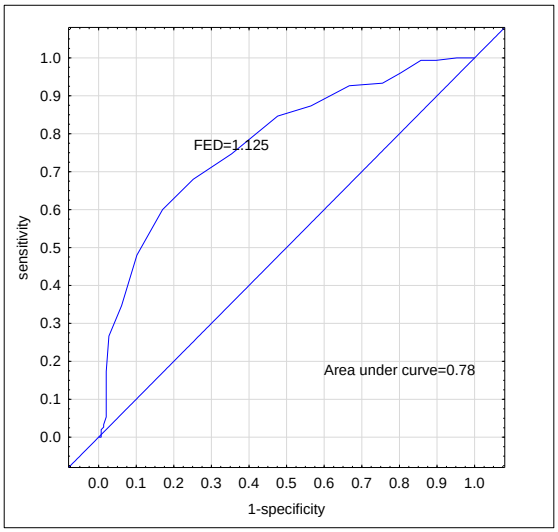

Figure 5.7. ROC curves indicating milling quality classification, using (a) EKD, (b) VED and (c) FED.

Using an appropriate statistical method, i.e. ROC curves, classification based on milling quality was possible (Table 5.3). The highest classification accuracy was obtained for EKD (Fig. 5.7a) (area under curve = 93%) with a threshold value of 1.28 g.cm^{-3} classifying kernels with higher densities as

good milling hybrids (with 85% sensitivity) and with lower densities as the threshold value as poor milling hybrid (with 88% specificity) (Table 5.3). VED (Fig. 6.7b) and FED (Fig. 5.7c) were also responsible for good classifications (area under curve = 79% and 78%, respectively).

Better classification accuracies (100% sensitivity and 100% specificity) were observed in an earlier study (Guelpa *et al.*, 2014b), but it must be noted that a significantly higher resolution (13.4 µm) was used for the image acquisition, resulting in more density variation being captured. However, the classification accuracies obtained at the lower resolution (80 µm) were still good (78% - 93%), while simultaneously scanning 150 kernels. Consequently, a more robust classification model was obtained, as well as a faster (as 300 vs. 16 kernels were scanned in the same time frame) and more cost effective method of estimating maize kernel densities, therefore making it more applicable for industry.

Table 5.3. ROC curve classification results when using X-ray µCT densities

	Sensitivity (%)	**Specificity** (%)	**Threshold** ($g.cm^{-3}$)	**Area under curve** (%)
EKD ($g.cm^{-3}$)	85	88	1.28	93
VED ($g.cm^{-3}$)	68	77	1.37	79
FED ($g.cm^{-3}$)	71	74	1.12	78

EKD: Entire kernel density

VED: Vitreous endosperm density

FED: Floury endosperm density

X-ray µCT volume analysis

X-ray µCT allowed the quantification of the following volumes: EKV, VEV and FEV, based on grey value thresholding of the respective ROIs. EKV included all volume inside the contour lines drawn around the entire kernel, after removal of cavities. To segment the other 2 ROIs, the germ region had to be excluded manually. Thereafter, a higher grey value threshold was applied to select the vitreous endosperm region, while excluding the floury endosperm region. A region growing tool identified voxels belonging to the selected grey value interval and respectively quantified the volumes, using a volume analyser tool. Floury endosperm was quantified using the same method, although a higher grey value interval had to be selected for segmentation.

Mean volumes for the entire sample set were: 251.64 mm^3, 161.85 mm^3 and 90.28 mm^3 for EKV, VEV and FEV, respectively. This is in accordance with an earlier finding of Wolf *et al.* (1952) that the vitreous endosperm is approximately double the volume of floury endosperm in dent maize. Wolf *et al.* (1952) made use of hand dissection to quantify the endosperm types.

For the two milling classes, it was evident that the EKV of the good milling hybrids were significantly ($P < 0.01$) bigger (321.50 mm^3) than that of the poor milling hybrids (255.56 mm^3) (Table

5.4). The mean VEV (199.70 mm^3) for the good milling hybrids were significantly ($P < 0.01$) bigger than that of the poor milling hybrids (123.23 mm^3), whereas the mean FEV (78.88 mm^3) for the good milling hybrids were significantly ($P < 0.01$) smaller than that of the poor milling hybrids (101.91 mm^3). The obtained results agree with the higher proportion of vitreous endosperm present in good milling kernels (Weber *et al.*, 2014).

Numerous studies inspected the ratio of vitreous-to-floury endosperm (V:F) (Pomeranz *et al.*, 1984; Watson, 1987; Robutti, 1995; Siska & Hurburgh, 1995) as this ratio expresses maize hardness (Delcour & Hoseney, 2010). Only few of these studies make use of non-destructive techniques, as demonstrated by Erasmus and Taylor (2004) that developed a maize translucency detection instrument and Weber *et al.* (2014) that used biospeckle and fuzzy granularity to quantify vitreous and floury endosperm proportions. Near infrared (NIR) hyperspectral imaging (HSI) has also shown to quantify the respective endosperm types (McGoverin & Manley, 2012), non-destructively. The V:F was calculated for the X-ray µCT derived densities and the results obtained indicated a significantly ($P < 0.01$) higher V:F for the good milling kernels (2.77) compared to that of the poor milling kernels (1.27) (Table 5.4).

Table 5.4. Entire kernel volume, vitreous endosperm volume and floury endosperm volume results as derived by X-ray µCT for the two milling classes, good (n = 150) and poor (n = 147), also indicating ANOVA results

	Good milling hybrids		**Poor milling hybrids**		***P*-value**
	Range	Mean±SD	Range	Mean±SD	
EKV (mm^3)	158.41 – 147.68	321.50±51.42	143.09 – 443.96	255.56±70.09	< 0.01
VEV (mm^3)	66.36 – 313.67	199.70±39.72	35.92 – 282.79	123.23±51.79	< 0.01
FEV (mm^3)	34.51 – 188.42	78.88±23.51	51.98 – 218.14	101.91±26.67	< 0.01
V:F	0.69 – 7.18	2.77±1.04	0.2 – 3.71	1.27±0.58	< 0.01

SD: Standard deviation

EKD: Entire kernel density

VED: Vitreous endosperm density

FED: Floury endosperm density

V:F: Vitreous-to-floury endosperm ratio

As volume measurements were easier to obtain than density measurements, classification using ROC curves was attempted based on volumes and summarised in Table 5.5. Very good classification accuracies of 87% and 92% were obtained for VEV and V:F, respectively (Figs. 6.8a and b). The fact that V:F was an excellent descriptor of maize hardness in many previous studies, it was also shown that this ratio was equally useful in describing maize milling quality. The efficacy of X-ray µCT as a non-destructive quantitative method was also shown. Slightly poorer classification accuracies were obtained for EKV (75%) and FEV (77%) (Figs. 5.8c and d).

Table 5.5. ROC curve classification results when using X-ray µCT volumes

	Sensitivity (%)	**Specificity** (%)	**Threshold** (mm^3)	**Area under curve** (%)
EKV (mm^3)	79	68	251.60	75
VEV (mm^3)	81	82	176.14	87
FEV (mm^3)	78	67	84.3	77
V:F	85	90	1.99	92

EKD: Entire kernel density

VED: Vitreous endosperm density

FED: Floury endosperm density

V:F: Vitreous-to-floury endosperm ratio

The importance of the X-ray µCT derived variables, as interpreted by principal component analysis and correlation coefficients

The interaction of all the variables (densities and volumes) of the entire sample set was illustrated in the PCA bi-plot (Fig. 5.9). All these measurements were done on individual kernels (n = 297). The first two principal components (PCs) described 76% of the variation within the model, with PC 1 describing the most (56%). Milling quality was described in the direction of PC 1. This was in accordance with the hardness (hard and soft kernels) study of Guelpa *et al.* (2014b).

The loadings indicated the relationship between the variables, and in particular, it could be observed that a stronger correlation existed between V:F, EKD, VEV, VED, FED and EKV. FEV showed no correlation. Considering the Spearman's rank correlation coefficients, as listed in Table 5.6, it was apparent that FEV was indeed poorly correlated with the other variables, except with V:F ($r = -0.70$, $P < 0.01$). Although FEV showed a poor relationship with the other variables in the PCA bi-plot, a good classification accuracy of 77% was obtained when classifying good and poor milling kernels based on this measurement. The PCA bi-plot, consequently illustrated that FEV described another milling quality feature that the other measurements did not describe.

The strongest correlations were indicated to be that of VEV and EKV. ($r = 0.89$, $P < 0.01$) and VEV and V:F ($r = 0.85$, $P < 0.01$). When considering the ROC curve classification results, V:F and EKD had the best classification accuracies (92% and 93%, respectively) when predicting milling quality. From the PCA bi-plot it was also evident that V:F and EKD, as well as VEV, were more strongly correlated with the good milling hybrids (good milling kernels lying closer to the respective variables on the plot).

It was also important to note that there were significant differences ($P < 0.05$) between all the variables, except between FED and FEV ($P > 0.1$) and that the variables (except FEV) thus contributed towards describing the milling quality of the individual maize kernels.

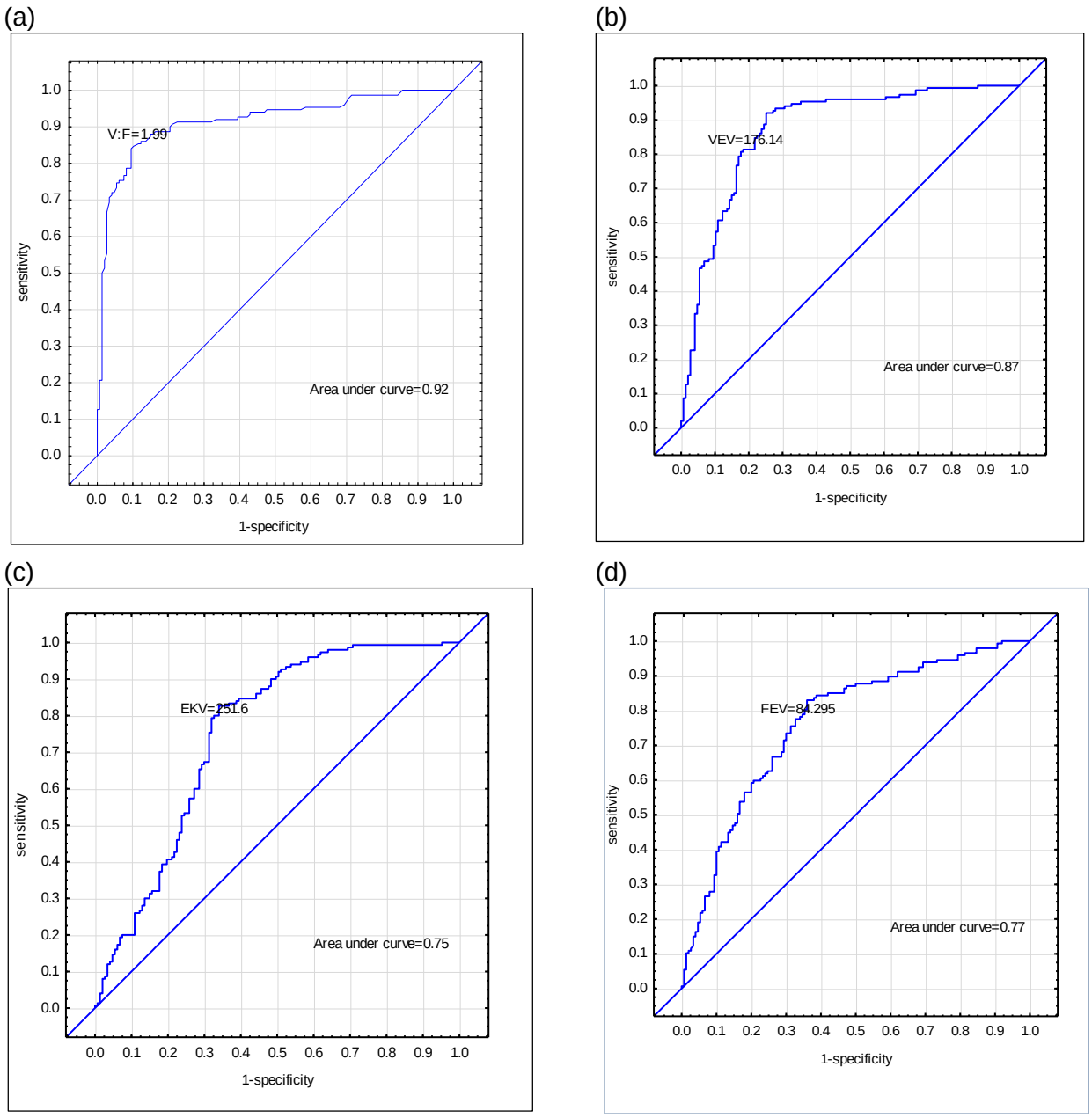

Figure 5.8. ROC curves indicating milling quality classification, using (a) V:F, (b) VEV, (c) EKV and (d) FEV.

The importance of the X-ray µCT derived variables, in relation to conventional hardness methods, as interpreted by principal component analysis and correlation coefficients

Six conventional hardness methods were compared to the X-ray µCT method, in order to determine and interpret the functionality of X-ray µCT as hardness descriptor. The first conventional method was particle size index (PSI), which involved milling and sieving and contributed breaking

susceptibility properties of maize kernels. Secondly, a hardness index (HI) was used where NIR absorption values at 2230 nm were used to calculate the HI. These measurements also conveyed particle size information, similar to PSI. Then, physical properties, such as volume and soundness, were expressed by hectoliter mass (HLM) and hundred kernel mass (HKM) measurements which were the fourth and fifth conventional methods. And lastly, protein content was determined as a descriptive quality parameter, along with NIR HSI that was used to quantify the proportion of vitreous endosperm. In order to perform these correlations, the X-ray µCT variables were taken as the averages of the 15 kernels per samples, as summarised in Table 5.7.

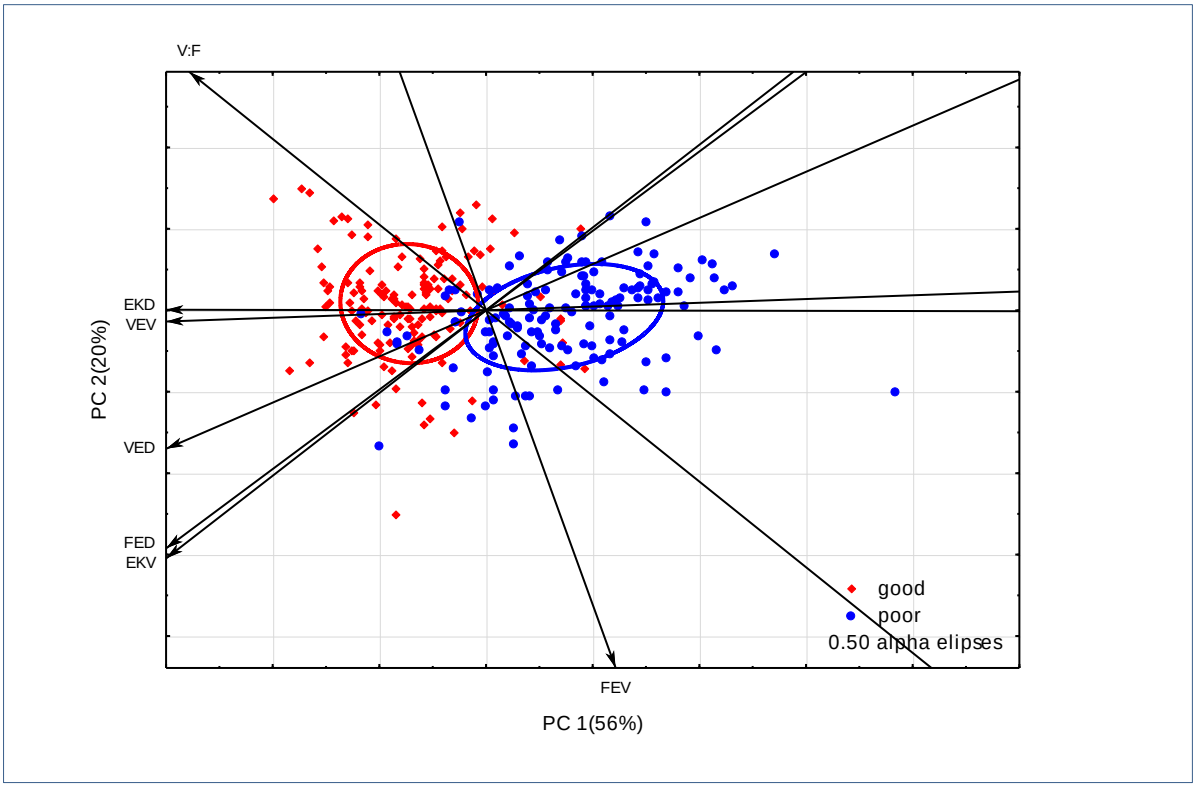

Figure 5.9. A PCA bi-plot, illustrating the interaction between the X-ray µCT derived variables on 297 maize kernels.

The interaction of the X-ray µCT derived variables, as well as variables derived from 6 conventional hardness methods, was illustrated in another PCA bi-plot (Fig. 5.10). The first two PCs describe 80% of the variation within the model, with PC 1 describing the major percentage (64%). Again, milling quality was described in the direction of the first PC. As indicated by the loadings, V:F, VEV and EKV were the X-ray µCT derived variables that showed strong correlations, along with PSI, HLM, NIR, protein, HKM and HSI (all the conventional methods). EKD, FED and VED did not correlate with the other variables, and FEV was not describe in either PC 1, nor in PC 2, therefore not indicated on the PCA bi-plot.

As PCA does not consider the variability (range) within the measurements, Spearman's rank correlation coefficients had to be interpreted along with the PCA bi-plot to better understand the relationship between the variables. The poor milling samples included 2 obvious outliers, one very

high in density (1.36 g.cm^{-3}), and the other with a very low density (1.11 g.cm^{-3}). For the X-ray µCT derived variables, the strongest correlations were that of V:F and VEV (r = 0.92, *P* < 0.01) and VED and FED (r = 0.90, *P* < 0.01). EKD, VED and FED were also strongly correlated, and was in agreement with the PCA bi-plot.

Table 5.6. Spearman's rank correlation coefficient matrix for the X-ray µCT variables done on individual maize kernels (n = 297)

	EKD	**VED**	**FED**	**EKV**	**VEV**	**FEV**	**V:F**
EKD	1.00						
VED	0.80*	1.00					
FED	0.76*	0.64*	1.00				
EKV	0.27*	0.31*	0.17**	1.00			
VEV	0.76*	0.39*	0.39*	0.89*	1.00		
FEV	-0.45*	-0.16*	-0.04****	0.20*	-0.26*	1.00	
V:F	0.77*	0.36*	0.30*	0.53*	0.85*	-0.70*	1.00

EKD: Entire kernel density (g.cm^{-3})
VED: Vitreous endosperm density (g.cm^{-3})
FED: Floury endosperm density (g.cm^{-3})
EKV: Entire kernel volume (mm^3)
VEV: Vitreous endosperm volume (mm^3)
FEV: Floury endosperm volume (mm^3)
V:F: Vitreous-to-floury endosperm ratio
*: P < 0.01
**: P < 0.05
***: P < 0.1
****: non-significant

When interpreting the relationship of the conventional methods with the X-ray µCT variables, it was evident that the density variables correlated poorly with the conventional methods. The conventional methods did not convey density information and it was thus expected that none of the conventional methods would correlate with the density variables. When considering the good classification accuracies that were obtained from the density measurements, using the ROC curves, densities were still seen as milling quality descriptors, despite of not being presented as contributing variables in the PCA bi-plot. Compared to all the other measurements, density measurements were also narrow in range, a factor that is not interpreted by a PCA bi-plot.

The volume variables, on the other hand, were strongly correlated with all the conventional methods, except protein. It was interesting to observe that PSI, HKM, HLM, NIR and HSI were so

similar in their descriptive properties. The strongest correlations were those between HSI and VEV (r = 0.95, *P* < 0.01), HKM and EKV (r = 0.90, *P* < 0.01), NIR and VEV (r = 0.88, *P* < 0.01), as well as NIR and V:F (r = 0.88, *P* < 0.01). The very strong correlation between HSI and VEV was expected, as the NIR HSI method also determined the percentage vitreous endosperm within individual maize kernels. Due to the available spatial information, pixels belonging to vitreous endosperm could be quantified. These results confirmed the usability of NIR HSI to quantify maize endosperm types.

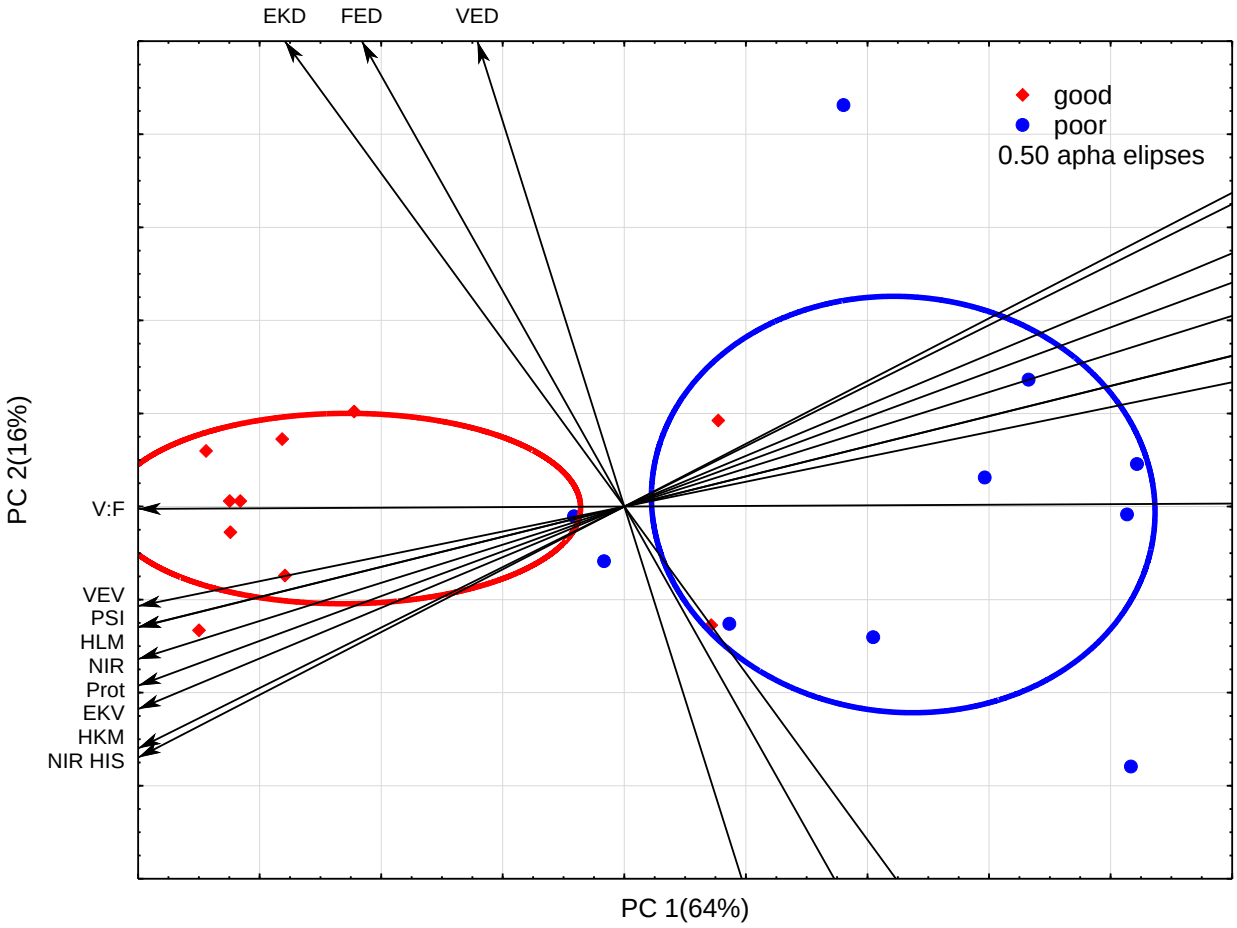

Figure 5.10. A PCA bi-plot, illustrating the interaction between the X-ray µCT derived variables, as well as the variables from 6 conventional hardness methods, of 20 maize samples.

Although PSI, HLM, HKM, NIR, NIR HSI and protein content had been shown to describe maize hardness, the PCA bi-plot indicated that density variables were lacking for the description of milling quality. It was evident that dedicated density methods were needed to describe milling quality, and as conventional density methods overlook the influence of cavities, X-ray µCT measured densities were very useful.

Table 5.7. Descriptive statistics of the averaged X-ray µCT variables, as well as the variables from the 6 conventional hardness methods, for each of the milling groups

	Good milling	**Poor milling**	***P*-value**
	Mean±SD	Mean±SD	
EKD ($g.cm^{-3}$)	1.30±0.03	1.22±0.07	< 0.01
VED ($g.cm^{-3}$)	1.37±0.04	1.35±0.06	< 0.05
FED ($g.cm^{-3}$)	1.14±0.04	1.10±0.06	N.S.
EKV (mm^3)	277.87±21.42	225.22±53.08	< 0.05
VEV (mm^3)	199.69±22.49	123.59±40.70	< 0.01
FEV (mm^3)	78.88±8.32	101.90±14.05	< 0.01
V:F	2.76±0.48	1.27±0.29	< 0.01
PSI (c/f)	2.74±0.97	1.57±0.62	< 0.05
HKM (g)	40.72±5.45	31.45±9.64	N.S.
HLM ($kg.hL^{-1}$)	79.56±1.20	75.03±1.67	< 0.01
Protein (%)	8.94±0.73	7.79±0.73	< 0.01
NIR @ 2230 nm	10.89±3.03	3.10±3.15	< 0.01
%VE	33.60±8.44	16.11±7.70	< 0.01

SD: Standard deviation

EKD: Entire kernel density

VED: Vitreous endosperm density

FED: Floury endosperm density

EKV: Entire kernel volume

VEV: Vitreous endosperm volume

FEV: Floury endosperm volume

V:F: Vitreous-to-floury endosperm ratio

PSI (c/f): Particle size index (coarse over fine ratio)

HKM: Hundred kernel mass

HLM: Hectoliter mass

Protein: Protein content (Dumas method)

NIR @ 2230 nm: Near infrared spectroscopy (hardness index)

%VE: % vitreous endosperm as determined using NIR HSI

N.S.: Non-significant ($P > 0.05$)

Table 5.8. Spearman's rank correlation coefficient matrix for the X-ray µCT derived variables (averaged per sample), as well as for the variables from the 6 conventional methods

	EKD	VED	FED	EKV	VEV	FEV	V:F	PSI	HKM	HLM	Prot.	NIR
EKD	1.00											
VED	0.77*	1.00										
FED	0.81*	0.90*	1.00									
EKV	0.36***	0.27***	0.36***	1.00								
VEV	0.60*	0.38***	0.53**	0.88*	1.00							
FEV	-0.51***	-0.26***	-0.39***	-0.07***	-0.48**	1.00						
V:F	0.68*	0.45***	0.62*	0.69*	0.92*	-0.65*	1.00					
PSI	0.40***	0.32***	0.48**	0.65*	0.78*	-0.55**	0.76*	1.00				
HKM	0.34***	0.35***	0.40***	0.90*	0.80*	-0.06***	0.68*	0.72*	1.00			
HLM	0.59*	0.29***	0.47**	0.71*	0.88*	-0.53**	0.87*	0.62*	0.57*	1.00		
Prot.	0.35***	0.27***	0.43***	0.48**	0.67*	-0.65*	0.71*	0.76*	0.57*	0.58*	1.00	
NIR	0.55*	0.40**	0.48**	0.74*	0.88*	-0.55**	0.88*	0.83*	0.75*	0.83*	0.65*	1.00
%VE	0.42**	0.40**	0.53**	0.85*	0.95*	-0.41***	0.89*	0.81*	0.85*	0.82*	0.71*	0.81*

EKD: Entire kernel density ($g.cm^{-3}$)
VED: Vitreous endosperm density ($g.cm^{-3}$)
FED: Floury endosperm density ($g.cm^{-3}$)
EKV: Entire kernel volume (mm^3)
VEV: Vitreous endosperm volume (mm^3)
FEV: Floury endosperm volume (mm^3)
V:F: Vitreous-to-floury endosperm ratio
PSI (c/f): Particle size index (coarse over fine ratio)
HKM: Hundred kernel mass
HLM: Hectoliter mass
Protein: Protein content (Dumas method) (%)
NIR @ 2230 nm: Near infrared spectroscopy (hardness index)
%VE: % vitreous endosperm as determined using NIR HSI
*: $P < 0.01$
**: $P < 0.05$
***: Non-significant ($P > 0.05$)

Conclusion

An attempt was made to classify maize hybrids, based on X-ray µCT determined densities and volumes. Density measurements, in particular EKD, obtained from low resolution (80 µm) scans, allowed for good classification accuracies (93%). The more easily obtained volume measurements ranged in classification accuracies of 77% to 92%, also indicating good classification, especially for V:F (sensitivity = 85% and selectivity = 90%). The loadings of a PCA bi-plot indicated a relationship

between all the density and volume variables, except that of FEV, which were confirmed with Spearman's rank correlation coefficients. But, when conventional hardness methods were added as supplementary properties to describe milling quality, the density measurements were not associating with the rest of the variables any more. Conventional hardness methods, i.e. PSI, HLM, HKM, NIR, NIR HSI and protein content contributed towards describing the same features that the volume measurements described. To discriminate between milling quality, it seemed that density properties had to be present.

References

Benson, G.O. & Pearce, R.B. (1987). Corn Perspective and Culture. In: *Corn: chemistry and technology.* (edited by S.A. Watson & P.E. Ramstad). St. Paul, Minnesota; USA: American Association of Cereal Chemists.

Cnudde, V. & Boone, M.N. (2013). High-resolution X-ray computed tomography in geosciences: A review of the current technology and applications. *Earth-Science Reviews*, **123**, 1-17.

De Carvalho, M.L.M., Van Aelst, A.C., Van Eck, J.W. & Hoekstra, F.A. (1999). Pre-harvest stress cracks in maize (*Zea mays* L.) kernels as characterized by visual, X-ray and low temperature scanning electron microscopical analysis: effect on kernel quality. *Seed Science Research*, **9**, 227-236.

Delcour, J. & Hoseney, R.C. (2010). *Principles of Cereal Science and Technology.* Pp. 1-22. Minnesota, USA: AACC International Press.

Erasmus, C. & Taylor, J.R.N. (2004). Optimising the determination of maize endosperm vitreousness by a rapid non-destructive image analysis technique. *Journal of the Science of Food and Agriculture*, **84**, 920-930.

Figueroa Cárdenas, J.D., Reyes Vega, M.L., Rincón Sánchez, F., Gaytán Martínez, M. & Morales Sánchez, E. (2006). Microstructure of starch granule related to kernel hardness in corn. *Revista Fitotecnia Mexicana*, **29**, 135-139.

Fox, G. & Manley, M. (2009). Hardness methods for testing maize kernels. *Journal of Agricultural and Food Chemistry*, **57**, 5647-5657.

Guelpa, A., Bevilacqua, M., Marini, F., O'Kennedy, K., Geladi, P. & Manley, M. (2014a). Application of Rapid Visco Analyser (RVA) viscograms and chemometrics for maize hardness characterisation. *Food Chemistry*, **173**, 1220-1227.

Guelpa, A., Du Plessis, A., Kidd, M. & Manley, M. (2014b). Non-destructive estimation of maize (Zea mays L.) kernel hardness by means of an X-ray micro-computed tomography (µCT) density calibration. *Food and Bioprocess Technology. Submitted.*

Gustin, J.L., Jackson, S., Williams, C., Patel, A., Armstrong, P.R., Peter, G.F. & Settles, A.M. (2013). Analysis of maize (*Zea mays*) kernel density and volume using micro-computed tomography and single-kernel near infrared spectroscopy. *Journal of Agricultural and Food Chemistry*, **61**, 10872-10880.

Hamilton, T., Hamilton, B.C., Johnson, B.C. & Mitchell, H. (1951). The dependence of the physical and chemical composition of the corn kernel on soil fertility and cropping system. *Cereal Chemistry*, **28**, 163-176.

Johnson, D.Q. & Russell, W.A. (1982). Genetic variability and relationships of physical grain-quality traits in the BSSS population of maize. *Crop Science*, **22**, 805-809.

Kalender, W.A. (2006). X-ray computed tomography. *Physics in medicine and biology*, **51**, R29.

Kotwaliwale, N., Singh, K., Kalne, A., Jha, S.N., Seth, N. & Kar, A. (2011). X-ray imaging methods for internal quality evaluation of agricultural produce. *Journal of Food Science and Technology*, **51**, 1-15.

Lee, K.M., Bean, S.R., Alavi, S., Herrman, T.J. & Waniska, R.D. (2006). Physical and biochemical properties of maize hardness and extrudates of selected hybrids. *Journal of Agricultural and Food Chemistry*, **54**, 4260-4269.

Maire, E. & Withers, P.J. (2014). Quantitative X-ray tomography. *International Materials Reviews*, **59**, 1-43.

McGoverin, C. & Manley, M. (2012). Classification of maize kernel hardness using near infrared hyperspectral imaging. *Journal of Near Infrared Spectroscopy*, **20**, 529-535.

Neethirajan, S., Karunakaran, C., Symons, S. & Jayas, D.S. (2006). Classification of vitreousness in durum wheat using soft X-rays and transmitted light images. *Computers and Electronics in Agriculture*, **53**, 71-78.

Paiva, E., Kriz, A.L., Peixoto, M.J.V.V.D., Wallace, J.C. & Larkins, A.B. (1991). Quantitation and distribution of ã–zein in the endosperm of maize kernels. *Cereal Chemistry*, **68**, 276-279.

Peplinski, A.J., Paulsen, M.R., Anderson, R.A. & Kwolek, W.F. (1989). Physical, chemical, and dry-milling characteristics of corn hybrids from various genotypes. *Cereal Chemisty*, **66**, 117-120.

Pomeranz, Y., Martin, C.R., Traylor, D.D. & Lai, F.S. (1984). Corn hardness determination. *Cereal Chemistry*, **61**, 147-150.

Robutti, J.L. (1995). Maize kernel hardness estimation in breeding by near-infrared transmission analysis. *Cereal Chemistry*, **72**, 632-636.

Robutti, J.L., Borras, F.S. & Eyherabide, G.H. (1997). Zein compositions of mechanically separated coarse and fine portions of maize kernels. *Cereal Chemistry*, **74**, 75-78.

Singhal, A., Grande, J.C. & Zhou, Z. (2013). Micro/Nano CT for visualization of internal structures. *Microscopy Today*, **21**, 16-22.

Siska, J. & Hurburgh, C.R. (1995). Corn density measurement by near-infrared transmittance. *Transactions of the ASAE*, **38**, 1821-1824.

Takhar, P.S., Maier, D.E., Campanella, O.H. & Chen, G. (2011). Hybrid mixture theory based moisture transport and stress development in corn kernels during drying: Validation and simulation results. *Journal of Food Engineering*, **106**, 275-282.

Watson, S.A. (1987). Structure and Composition. In: *Corn Chemistry and Technology* (edited by S.A. Watson & P.E. Ramstad). Pp. 53-82. St. Paul, Minnesota, USA: American Association of Cereal Chemists, Inc.

Weber, C., Dai Pra, A.L., Passoni, L.I., Rabal, H.J., Trivi, M. & Poggio Aguerre, G.J. (2014). Determination of maize hardness by biospeckle and fuzzy granularity. *Food Science & Nutrition*, **2**, 557-564.

Wolf, M.J., Buzan, C.L., MacMasters, M.M. & Rist, C.E. (1952). Structure of the mature corn kernel. I. Gross anatomy and structural relationships. *Cereal Chemistry*, **29**, 321-333.

Chapter 6

Prediction of kernel density of single maize (*Zea mays* L.) kernels using a miniature near infrared (NIR) spectrophotometer

Abstract

Single maize (*Zea mays* L.) kernels (n = 297) from a variety of breeding materials were scanned using a miniature near infrared (NIR) spectrophotometer, i.e. a microNIR. As maize kernel density affects milling performance, X-ray µCT determined entire kernel density (EKD) measurements were used as reference values for the NIR prediction model building. Spectra were acquired in the wavelength range from 908 - 1680 nm at a resolution of 30 x 250 µm / 50 µm. Maize kernels were positioned both germ facing towards the detector (germ-up) and facing away from the detector (germ-down). Mean centered and standard normal variate (SNV) pre-processed spectra were subjected to partial least squares (PLS) regression model building of EKD measurements. The use of microNIR spectroscopy as a possible non-destructive and fast single-kernel analysis method for predicting EKD, was investigated. Prediction statistics for the larger sample set (where each kernel was scanned both germ-up and germ-down) for EKD was: R^2_V = 0.60, RMSEP = 0.03 g.cm^{-3}, RPD = 1.67 and for the smaller sample set (where each kernel was scanned only germ-down) for EKD was: R^2_V = 0.32, RMSEP = 0.03 g.cm^{-3}, RPD = 1.67. There is a need to develop cost-effective technologies for fast sorting of small amounts of grain samples, such as those from breeding programmes. These results indicated that reasonable predictions can be made at the fast NIR scan rate that would be suitable for breeders as a rough screening method.

Introduction

The hardness of maize is a critical quality parameter that defines the suitability thereof for different processes and end-product quality (Armstrong & Tallada, 2012). Hard maize hybrids are favoured by the dry-milling industry for the production of high quality grits and optimal yields (Lee *et al.*, 2007). Near infrared (NIR) reflectance spectroscopy is prominent among major analytical technologies and used routinely in the grain industries to predict quality attributes, as it is a non-destructive, fast and a low-cost method (McClure, 2004; Manley, 2014). NIR absorption bands occur due to C-H,N-H, O-H and S-H functional groups that causes overtone and combination vibrations. Therefore, any organic molecule, which is abundant in biological material, is suitable for NIR analysis, including maize kernels. NIR analysis has been successfully used for bulk maize characterisation for a number of measurements, i.e. oil, protein, starch and moisture (Jiang *et al.*, 2007).

Grain quality, linked to processing quality, has been identified by researchers as an area for further single-kernel calibration development (Fox & Manley, 2014). However, the prediction of single-kernel traits poses obstacles as it is difficult to collect reliable and representative spectra from a heterogeneous sample (such as a maize kernel). To overcome the presented limitation, Armstrong (2006) developed a device where the kernels passed through a glass tube as the spectra were collected. Spielbauer *et al.* (2009) modified this approach by integrating kernel weight measurements along with the spectral acquisition. Janni *et al.* (2008) managed to obtain averaged reflectance spectra from individual kernels as they tumbled within an airstream during acquisition.

The microNIR is a new portable spectrophotometer designed for hand-held applications. This pocket-sized spectrophotometer makes use of linear variable filter (LVF) technology that is known for stable and reliable optics (Macleod, 2010). The LVF comprises of a thin film used as a dispersive element, and apart from reducing costs, the LVF technology results in a compact and rugged spectral engine with no moving parts (O'Brien *et al.*, 2012; Alcalà *et al.*, 2014). Successful applications of the microNIR spectrophotometer was for predicting authentic or counterfeit medical tables (Alcalà *et al.*, 2014) and for identifying similar species of fish fillets (Friedrich *et al.*, 2014).

As maize hardness is predominantly a genetic trait (Watson, 1987), plant breeding programmes have the opportunity to improve some of these quality characteristics (Fox & Manley, 2014). The evaluation of the success of respective breeding efforts, is best performed on a single-kernel basis as single cobs with the value added trait are sometimes produced, resulting in a limited amount of kernels (Janni *et al.*, 2008). There is thus still a need to develop cost-effective methods for fast sorting that can be used on limited samples, as those from breeding programmes (Fox & Manley, 2014).

Among the many methods that are available for hardness measurements, it had been established that milling quality requires density measurements to be adequately described (Chapter 5). As density measurements from conventional density methods are influenced by large cavities present in maize kernels, misleading results can be obtained. Therefore, using an X-ray micro-computed tomography (µCT) density calibration (Guelpa *et al.*, 2014) true kernel densities could be

calculated. The X-ray µCT method of determining kernel density is, however, not ideal for fast screening as an experienced technician is needed, along with tedious data analysis.

The aim of this study was to investigate the use of microNIR spectroscopy as a possible non-destructive and fast single-kernel analysis method for predicting EKD.

Material and methods

Samples used for model building

Maize hybrids, ranging in milling quality, were kindly supplied by PANNAR Seeds (Greytown, South Africa). The sample set consisted of 10 good milling hybrids and 10 poor milling hybrids, as described in Chapter 5 and listed in Table 5.1. For the single-kernel prediction model, 15 kernels from each of the 20 hybrids were scanned, both germ-up and germ-down, resulting in a sample set of 600 spectra. X-ray µCT density measurements were done on the same 300 kernels that were scanned with the microNIR spectrometer.

X-ray µCT derived measurements used for model building

Entire kernel density (EKD) was determined using a commercial micro-focus X-ray computed tomography system, i.e. Phoenix V|Tome|X L240 (General Electric Sensing and Inspection Technologies / Phoenix X-ray, Wunstorff, Germany). The acquisition of the images and the data analysis and processing is described in Chapter 5. In order to facilitate the calculation of the maize kernel densities, a density calibration had to be constructed from a range of polymers, using their averaged grey values, as obtained by X-ray µCT, and their respective known densities. Successful density calculations, using the density calibration, required simultaneous scanning of the polymers and maize kernels.

Data processing of 3 maize kernels were not possible due to artefacts, and the actual number of samples used for EKD measurements were 297.

Spectral acquisition

The absorbance of reflectance spectra was measured in the NIR region (908 - 1680 nm) of the electromagnetic spectrum at 6.2 nm intervals, resulting in 125 wavelength bands. The scans of 297 maize kernels were individually acquired, scanned germ-up as well as germ-down, using a microNIR 1700. The microNIR is a miniature NIR spectrometer (Fig. 6.1a) developed and manufactured by JDSU Corporation (Santa Rosa, CA, USA). A 128-pixel InGaAs detector was used to achieve a resolution of 30 x 250 µm / 50 µm. Each spectrum was the average of 64 scans. The microNIR was fitted with a LVF filter which can be compared to a scanning Fabry-Perot interferometer that scans with position instead of time (Macleod, 2010; O'Brien *et al.*, 2012). Two tungsten lamps allowed for illuminating a spot (3 mm in diameter) on the sample with the optimal focal distance being 3 mm from the sample.

The external white reference was a 99% diffuse reflectance standard (JDSU Corporation, Santa Rosa, CA, USA) measured once every 15 minutes during the sample acquisition period. The maize kernels were placed, one at a time, in a hollowed-out Teflon (PFTE) disk (Maizey's (Pty) Ltd, Kuils River, South Africa) (Fig. 6.1b) that completely covered the microNIR's connectable collar upon scanning. In order to keep the optimal focal distance of 3 mm constant, in spite of maize kernels differing in thickness, a range of hollowed-out disks were developed, varying in depth from 5 mm to 10 mm. MicroNIR software (JDSU Corporation, Santa Rosa, CA, USA) was used to perform the spectroscopic measurements and the data was saved in Microsoft Excel format for analysis in Evince 2.5.5 software (Umbio, Umeå, Sweden).

(a) (b)

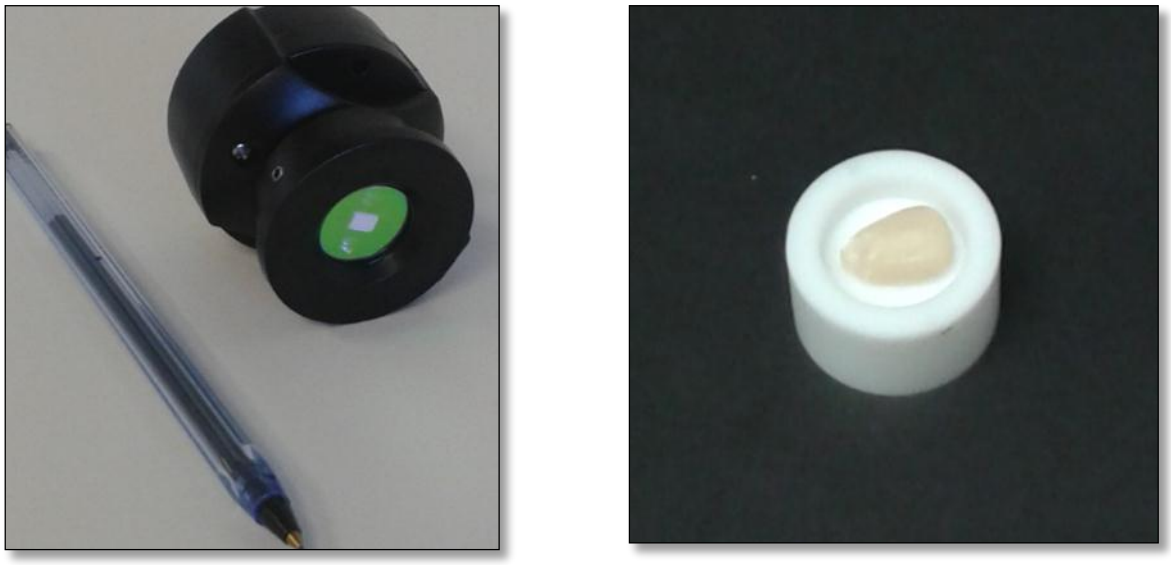

Figure 6.1. (a) A microNIR spectrometer imaged next to a pen to illustrate the small size of the device, and (b) a hollowed-out Teflon disk with a maize kernel inside as it was used when scanning individual maize kernels.

Principal component analysis and partial least squares regression models

Data was explored, using principal component analyses (PCA), whereas partial least squares (PLS) regression models were built to perform predictions on single-kernel spectra. EKD measurements were used as reference values. Spectra were mean-centered and standard normal variate (SNV) and multiplicative scatter correction (MSC) spectral pre-treatment were explored during model development. To test prediction ability, the samples were divided into a calibration set to build the regression models and a test set to independently validate the regression models. This was done by sorting the reference density values into ascending order and selecting every third sample for validation with the remaining used to develop the calibration model. This assured that both models had the same broad range of reference values. Full cross-validation (leave-one-out exclusion) regression modeling of the calibration set was used to establish a preliminary number of factors for the model. The calibration and validation models were evaluated individually, reporting the errors as

root mean square error of cross-validation (RMSECV) and root mean square error of prediction (RMSEP), as well as coefficients of determination for both the calibration and validation sets, R^2_C and R^2_V, respectively. RPD and standard error of laboratory (SEL) values were also reported.

Results and discussion

The performance of NIR prediction calibrations can be influenced by many factors, with the two most important ones being the representative nature of the samples and the accuracy of the measurements from the reference methods (Wang & Paliwal, 2007). In the current study, an attempt was made to optimise the presentation of the samples by making minor technical modifications. Custom designed Teflon sample holders were used to ensure that the kernels were maintained in the center of the sample area, when scanned. Furthermore, the sample holders differed in depth and could thereby ensure a constant optical focal distance, irrespective of kernel thickness. Additionally, the accuracy of the measurements of the reference method (entire kernel density as calculated using X-ray µCT) was validated by comparing estimated and measured masses (r = 0.99) and a very low standard error of measurement of 0.01 $g.cm^{-3}$ was obtained, confirming the measurements as very accurate (Guelpa *et al.*, 2014).

Reflectance measurements are surface-biased and the position of the germ, either showing towards or away from the detector, influences calibration accuracies (Jiang *et al.*, 2007). Therefore, the current study included both the orientations of the germ (germ-up and germ-down) into the prediction calibration, including more variation in the prediction model.

Only the wavelength range of 1000 - 1680 nm was considered for performing PCA and PLS regression modelling because of the low signal-to-noise ratio at the edge of the spectra. SNV was selected as a pre-treatment method as it resulted in the best calibration models. The mean-centered and SNV pre-treated spectral profile (n = 594) (Fig. 6.2) had the usual significant absorption peaks at 1450 nm for moisture and 1175 – 1225 nm for protein.

As the sample set consisted of both good milling and poor milling hybrids, a PCA model was calculated with the samples coloured according to their respective class. It was observed that milling quality properties were distinguishable when both the second and third PCs were interpreted. A degree of clustering was visible between the good milling samples (red dots) and the poor milling samples (blue dots) (Fig. 6.3). From the loading line plot of PC 2 (Fig. 6.4a) it was evident that this PC was important as it represented variation associated with protein (N-H stretch first overtone of $CONH_2$ as indicated by 1430 nm), as well as starch (C-H stretch second overtone of CH, indicted by 1225 nm). The three positively loaded peaks in PC 3 were associated with starch, as 1170 nm was associated with C-H stretch second overtone (HC=CH), 1395 nm with 2 x C-H stretch + C-H (CH_2) and 1660 nm was in turn associated with C-H stretch first overtone (*cis*-$RCH{+}CHR^1$) (Osborne *et al.*, 1993).

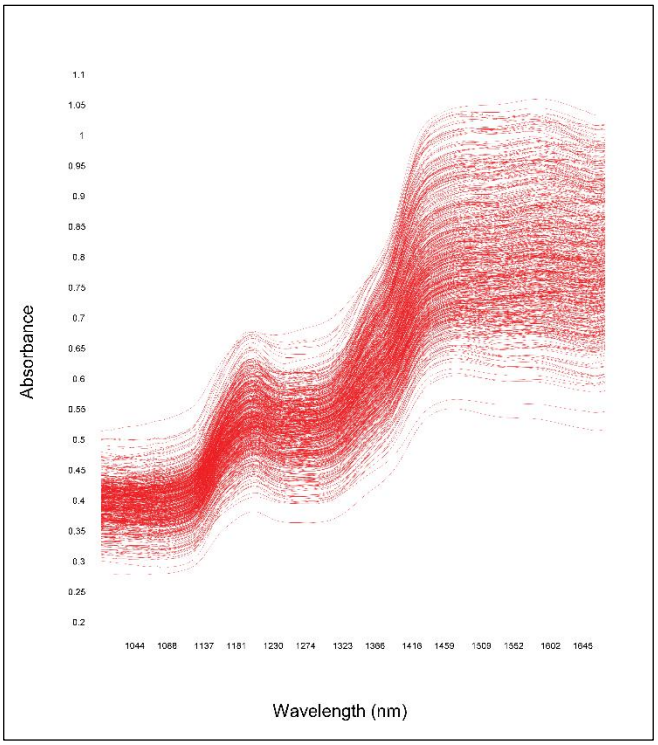

Figure 6.2. Mean-centered and SNV pre-treated NIR reflectance spectra, as acquired using a microNIR spectrophotometer, of the sample set, scanned both germ-up and germ-down.

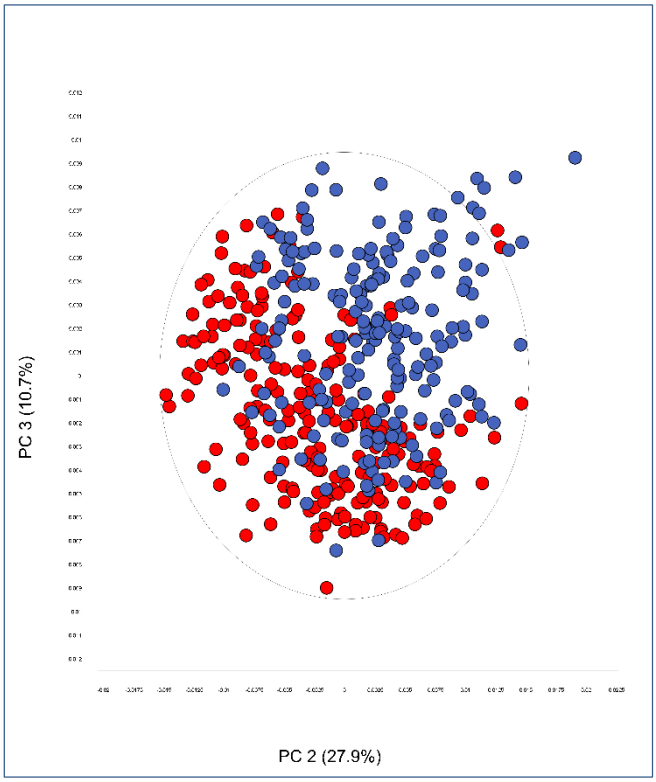

Figure 6.3. A principal component score plot of PC 2 vs. PC 3 (27.9% and 10.7%), illustrating both PCs to be important with respect to the variation found between the good milling (red dots) and poor milling (blue dots) kernels.

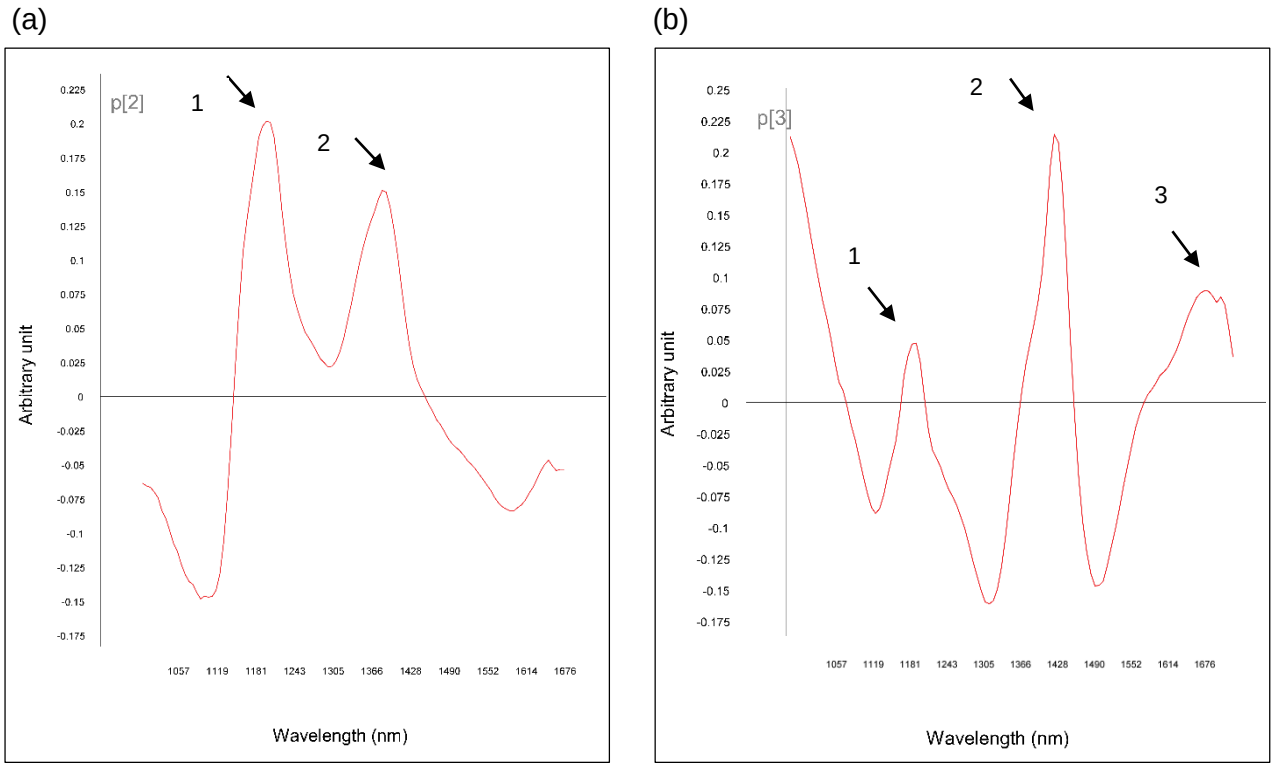

Figure 6.4. A loading line plot for (a) PC 2 showing 2 prominent positive peaks: (1) 1225 nm and (2) 1430 nm, associated with starch and protein, and (b) PC 3 showing 3 prominent positive peaks: (1) 1170 nm, (2) 1395 nm and (3) 1660 nm, all associated with starch.

Ten latent variables (LVs) were selected for optimal model building as they resulted in the lowest RMSECV, following full-cross validation of the calibration set of the mean-centered and SNV pre-processed germ-up and germ-down scanned spectra. The mean±SD for the calibration (130±0.05 g.cm^{-3}, n = 423) and external validation (1.27±0.05 g.cm^{-3}, n = 171) sets were very similar, which ensured accurate error estimation by external validation. An RMSECV of 0.02 g.cm^{-3} and RMSEP of 0.03 g.cm^{-3} was determined for EKD. Plotting predicted EKD versus actual EKD values for the external validation set, showed that the regression model predicted the variable reasonably good (R^2_V = 0.60) (Fig. 6.5). Although a SEL of 0.01 g.cm^{-3} was obtained with the X-ray µCT measurement method, it should, however, be stressed that large and expensive equipment was needed, and was also time-consuming.

Guidelines for interpretation of modeling results make use of RPD values, which is a ratio of the SD of the reference data to the SECV. RPD values can also be determined for the validation data. As suggested by Williams (1991), RPD values of 2.5 to 3 were suitable for rough screening; a value of 5 to 8 could be used for quality control.

In an earlier study, a RPD value of 2.53 was obtained for a regression model of total kernel density, determined using X-ray µCT, and single-kernel NIR Grain Analyser spectra (Gustin *et al.*, 2013). The latter study indicated the model as an effective screening tool, with a RMSEP of 0.03 g.cm^{-3} and R^2_V of 0.78. The prediction model of EKD for the current study obtained a RPD value of

only 1.67 (RMSEP = 0.03 g.cm^{-3} and R^2_V = 0.60) as a smaller SD (of 0.05 g.cm^{-3} compared to) was present. The current study included 20 hybrids, whereas the former study sampled from 64 hybrids, incorporating more variation in their sample set, therefore the larger SD of 0.07 g.cm^{-3} was found.

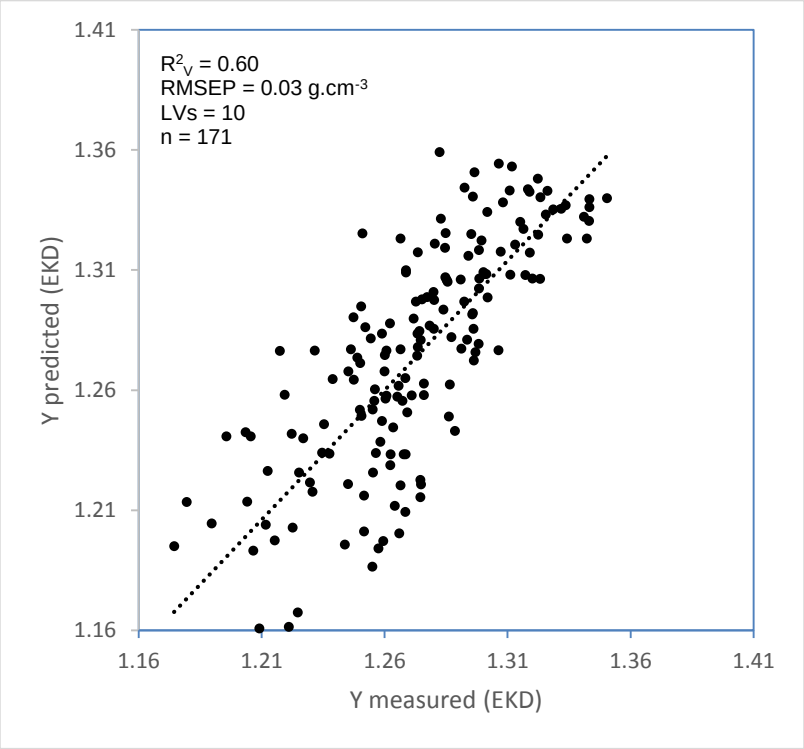

Figure 6.5. Validation set predictions for EKD (g.cm^{-3}) of the robust sample set (scanned germ-up and germ-down).

A second calibration was built, considering only kernels that was scanned germ-down. Milling quality properties were already distinguishable in the PCA score plot of PC1 vs. PC 2 (Fig. 6.6a), with the good milling kernels (red dots) separating from the poor milling kernels (blue dots) in the direction of PC 2. The loading line plot for PC 2 (Fig. 6.6b) revealed two positively loaded peaks, i.e. at 1195 nm and 1415 nm, both being associated with starch (CH_2) (Osborne *et al.*, 1993), which is the main constituent of endosperm. The spectra from the larger sample set (scanned both germ-up and germ-down) described variation in both protein and starch, with the germ contributing the protein constituents.

Three latent variables were selected, based on lowest RMSECV, after performing full-cross validation on the calibration set (n = 205), followed with mean-centering and SNV, for model building of spectra collected from germ-down kernels. EKD measurements were used as reference values. A better RMSECV, compared to that of the large sample set, was obtained (0.01 g.cm^{-3}), but the RMSEP stayed the same (0.03 g.cm^{-3}) and the R^2_c was 0.40. For the validation set (n = 91) a R^2_V of 0.32 was obtained for the predicted EKD versus actual EKD values (Fig. 6.7), with a RPD value of 1.67.

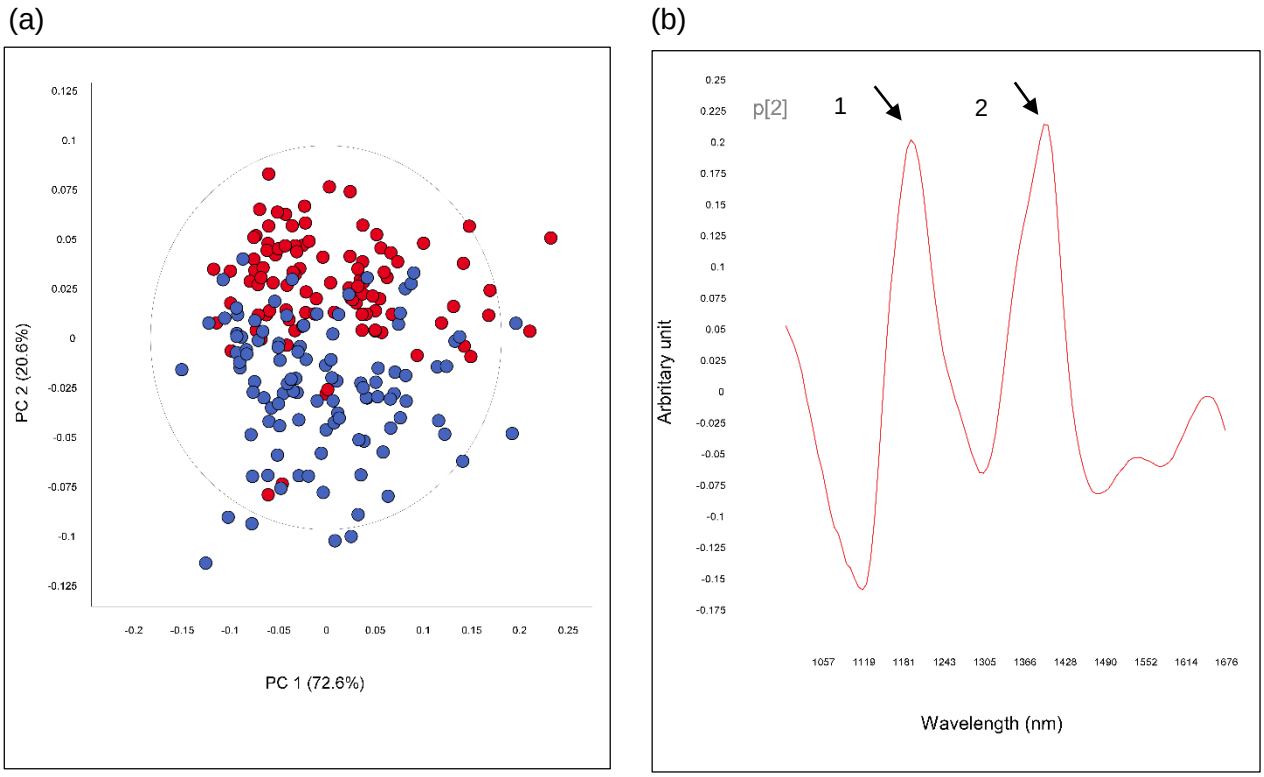

Figure 6.6. (a) Principal component score plot of PC 1 vs. PC 2 (72.6% and 20.6%) illustrating the good milling kernels (red dots) to cluster predominantly above PC 2 and the poor milling kernels (blue dots) to cluster below PC 2. (b) A loading line plot for PC 2 revealing 2 prominent positive peaks: (1) at 1195 nm and the other one at 1415 nm.

Four samples (encircled with red dotted line in Figure 6.7) were investigated as possible outliers. All four were poor milling samples, and although their measured densities were lower than the rest of the validation set, they were still presented as fitting into the corresponding PCA models, therefore they were not excluded as outliers.

The smaller model (using only spectra form germ-down scanned kernels) did not predict as well as the larger model (kernels were scanned both sides). Using NIR spectroscopy in industry, samples would be scanned from different orientations and a suitable prediction model would have to include this variability. Therefore, the better prediction model for the larger sample set indicated industrial application possibilities. It was, however, evident that a prediction model based on density measurements, derived from X-ray µCT, had to incorporate as much variability as possible to increase predictability.

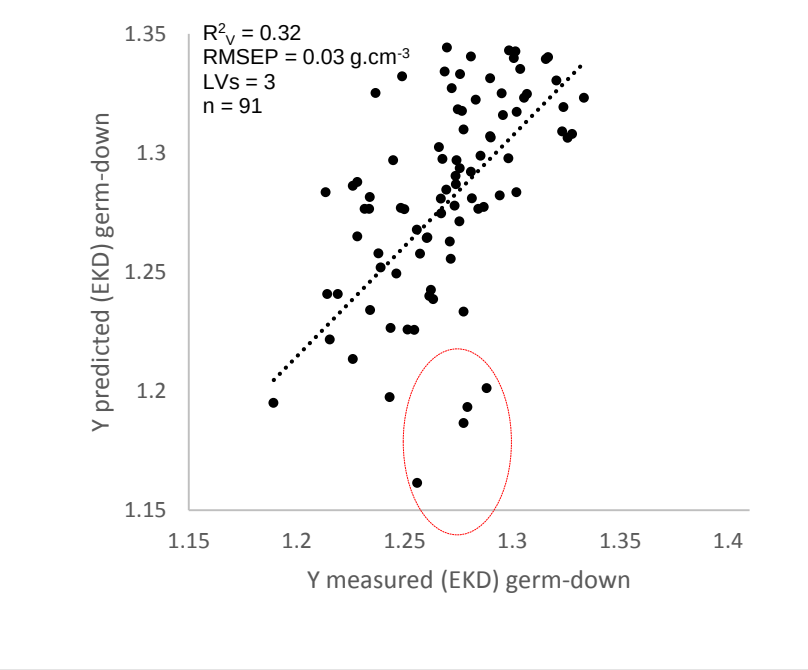

Figure 6.7. Validation set predictions for EKD (g.cm^{-3}) of the sample set scanned germ-down. Four samples encircled were investigate as possible outliers.

Conclusion

This study demonstrated that EKD, as derived from X-ray µCT, could be predicted to a fair extent, using the fast single-kernel microNIR spectrophotometer. As density measurements showed relatively small differences between kernels, the prediction models could be improved by extending the variability within the sample sets, thereby including the maximum number of hybrids and scanning the kernels positioned in different orientations. X-ray µCT measured densities of individual maize kernels, as used in the prediction models, were related to maize milling quality and consequently expanded the functionality of the models. The predictive performance demonstrated the ability to be a rough screening tool for breeding programmes.

References

Alcalà, M., Blanco, M., Moyano, D., Broad, N., O'Brien, N., Friedrich, D., Pfeifer, F. & Siesler, H. (2014). Qualitative and quantitative pharmaceutical analysis with a novel handheld miniature near-infrared spectrometer. *Journal of Near Infrared Spectroscopy*, **21**, 445-457.

Armstrong, P. (2006). Rapid single-kernel NIR measurement of grain and oil-seed attributes. *Applied Engineering in Agriculture*, **22**, 767.

Armstrong, P.R. & Tallada, J.G. (2012). Prediction of kernel density of corn using single-kernel near infrared spectroscopy. *Applied Engineering in Agriculture*, **28**, 569-574.

Fox, G. & Manley, M. (2014). Applications of single kernel conventional and hyperspectral imaging near infrared spectroscopy in cereals. *Journal of the Science of Food and Agriculture*, **94**, 174-179.

Friedrich, D.M., Hulse, C.A., von Gunten, M., Williamson, E.P., Pederson, C.G. & O'Brien, N.A. (2014). Miniature near-infrared spectrometer for point-of-use chemical analysis. In: *SPIE OPTO*. Pp. 899203-899211.

Guelpa, A., Du Plessis, A., Kidd, M. & Manley, M. (2014). Non-destructive estimation of maize (Zea mays L.) kernel hardness by means of an X-ray micro-computed tomography (µCT) density calibration. *Food and Bioprocess Technology. Submitted.*

Gustin, J.L., Jackson, S., Williams, C., Patel, A., Armstrong, P.R., Peter, G.F. & Settles, A.M. (2013). Analysis of maize (*Zea mays*) kernel density and volume using micro-computed tomography and single-kernel near infrared spectroscopy. *Journal of Agricultural and Food Chemistry*, **61**, 10872-10880.

Janni, J., Weinstock, B.A., Hagen, L. & Wright, S. (2008). Novel near-infrared sampling apparatus for single kernel analysis of oil content in maize. *Applied spectroscopy*, **62**, 423-426.

Jiang, H.Y., Zhu, Y.J., Wei, L.M., Dai, J.R., Song, T.M., Yan, Y.L. & Chen, S.J. (2007). Analysis of protein, starch and oil content of single intact kernels by near infrared reflectance spectroscopy (NIRS) in maize (Zea mays L.). *Plant breeding*, **126**, 492-497.

Lee, K.M., Herrman, T.J., Rooney, L.W., Jackson, D.S., Lingenfelser, J., Rausch, K.D., McKinney, J., Iiams, C., Byrum, L., Hurburgh, J.C.R., Johnson, L.A. & Fox, S.R. (2007). Corroborative study on maize quality, dry-milling and wet-milling properties of selected maize hybrids. *Journal of Agricultural and Food Chemistry*, **55**, 10751-10763.

Macleod, H.A. (2010). *Thin-film optical filters.* Baco Raton, Florida, USA: CRC Press.

Manley, M. (2014). Near-infrared spectroscopy and hyperspectral imaging: non-destructive analysis of biological materials. *Chemical Society Reviews*, **43**, 8200-8214.

McClure, W.F. (2004). Review: 204 years of near infrared technology: 1800–2003. *Journal of Near Infrared Spectroscopy*, **11**, 487-518.

O'Brien, N.A., Hulse, C.A., Friedrich, D.M., Van Milligen, F.J., von Gunten, M.K., Pfeifer, F. & Siesler, H.W. (2012). Miniature near-infrared (NIR) spectrometer engine for handheld applications. In: *Defense, Security, and Sensing SPIE*. Pp. 837404-837408.Baltimore, Maryland, USA.

Osborne, B.G., Fearn, T. & Hindle, P.H. (1993). *Practical NIR Spectroscopy with Applications in Food and Beverage Analysis.* Harlow, UK: Longman Scientific and Technical.

Spielbauer, G., Armstrong, P., Baier, J.W., Allen, W.B., Richardson, K., Shen, B. & Settles, A.M. (2009). High-throughput near-infrared reflectance spectroscopy for predicting quantitative and qualitative composition phenotypes of individual maize kernels. *Cereal Chemistry*, **86**, 556-564.

Wang, W. & Paliwal, J. (2007). Near-infrared spectroscopy and imaging in food quality and safety. *Sensing and Instrumentation for Food Quality and Safety*, **1**, 193-207.

Watson, S.A. (1987). Structure and Composition. In: *Corn Chemistry and Technology* (edited by S.A. Watson & P.E. Ramstad). Pp. 53-82. St. Paul, Minnesota, USA: American Association of Cereal Chemists, Inc.

Williams, P.C. (1991). Prediction of wheat kernel texture in whole grains by near-infrared transmittance. *Cereal Chemistry*, **68**, 112-114.

Chapter 7

General discussion and conclusion

Maize (*Zea mays* L.) is, amongst others, cultivated for human consumption and is a staple food in many countries. Dry-milling is used to process maize into maize meal and maize hardness methods are being used to measure maize milling quality, due to a lack of milling quality methods. This study intended to determine to what extent maize hardness and milling quality is related. For this purpose, a sample set of maize from different hybrids, localities and plantings, was ranked based on milling performance. An industrial guideline for assessing milling quality was used and was referred to as the estimation of the chop percentage. During an unsupervised inspection of seven conventional hardness methods by means of principal component analysis (PCA) score plots and loadings, as well as Spearman's rank correlation coefficients, it could be seen that all the hardness methods were important with respect to describing maize milling quality. The conventional methods that were used, were hectoliter mass (HLM), hundred kernel mass (HKM), protein content, particle size index (PSI c/f), percentage vitreous endosperm (%VE) as determined using near infrared (NIR) hyperspectral imaging (HSI) and NIR absorbance at 2230 nm (NIR @ 2230 nm).

As endosperm is the main constituent of a maize kernel (Watson, 1987), this study investigated the fundamental textural properties thereof. Digital images, scanning electron microscopy (SEM) micrographs and X-ray µCT images revealed that the morphology of the two endosperm types i.e. vitreous and floury, both present in a maize kernel, presented density and volume differences. The vitreous endosperm appeared much denser than the floury endosperm, due to a thicker protein network that compacts the starch granules, whereas the floury endosperm revealed loosely packed granules with intracellular air spaces present, as the protein network was mostly absent. It was also seen that the proportion in which the endosperm types was present, differed between individual kernels. Cavities or relatively large air spaces were also observed and considered as a possible influence on milling quality.

The choice of analytical methods, use for investigating maize endosperm texture, was based on the success of former studies to discriminate between hardness properties, and the availability of new technologies that seemed viable. The Rapid Visco Analyser (RVA) would not typically be used to describe hardness differences in maize, but as this grain consists of mainly starch, the functionality of the RVA to capture pasting properties seemed just as useful to capturing milling quality differences. In this study, the RVA viscograms were subjected to partial least squares (PLS) regression model building and showed to be able to predict hardness properties, without being influenced by different profiles.

Furthermore, it was apparent that X-ray µCT would be able to characterise the differences (density and volume) related to maize endosperm, due to the advanced technology associated

with this method. Micro-computed tomography detects density differences as it identifies attenuation changes with X-rays passing through a material (Chawanji *et al.*, 2012). Individual maize kernels could be segmented, non-destructively, into desired regions-of-interest (ROIs), i.e. vitreous endosperm, floury endosperm and cavities. Depending on the resolution of the images, textural properties such as porosity (intra-cellular air spaces) could also be detected. Using X-ray µCT, a density calibration was constructed that facilitated density calculations of the respective ROIs, as well as that of the entire kernels. Quantification of the ROIs and porosity (when imaged at high resolution) was also achieved. Formerly, quantification of the different endosperm types was only possible using hand-dissection (Erasmus, 2003), or more recently, using NIR HSI (McGoverin & Manley, 2012).

This study demonstrated the versatility of X-ray µCT as it was possible to acquire very high resolution images (3 µm) containing detailed information of single kernels or sub sections thereof, or imaging multiple kernels (150) simultaneously, achieving a lower resolution (80 µm), but still adequate for density and volume analysis. The usefulness of X-ray µCT was also illustrated by the ability to exclude ROIs that would ensure more accurate measurements. This was demonstrated with the removal of the cavities when calculating entire kernel density. Conventional hardness methods measuring density, such as the floating test, overlook the importance of this feature and misleading results are obtained.

Discrimination between hard and soft maize hybrids were achieved based on all three X-ray µCT derived entire kernel densities (EKD), vitreous endosperm densities (VED), floury endosperm densities (FED), as well as the percentage porosity quantified within each kernel. Receiver operator characteristic (ROC) curves contributed threshold values that were used to establish classification accuracies.

Milling quality classification of maize hybrids was also accomplished, using X-ray CT derived densities (EKD, VED, FED) and volumes (entire kernel volume (EKV), vitreous endosperm volume (VEV), floury endosperm volume (FEV) and the vitreous-to-floury endosperm ratio (V:F)). The best classifications were possible when using EKD and V:F.

In order to interpret the relationship of the X-ray µCT derived measurements with respect to conventional hardness methods (PSI, HLM, HKM, NIR HSI and protein content), PCA bi-plots and Spearman's rank correlation coefficients were examined. These statistical data analysis methods indicated that milling quality could not be described without including density measurements. This was a very important finding as it indicated that density properties were the discriminatory factor with respect to maize hardness and maize milling quality.

Lastly, an attempt was made to combine the X-ray µCT derived EKD measurements with fast and simple NIR spectroscopy by building a prediction model, from spectra acquired using a miniature hand-held microNIR instrument. Due to not enough variation in the sample set, the PLS model was only good enough to be used as a rough screening method in industry. It was, however, established that the prediction model was better when it included spectra from kernels

scanned both sides, i.e. germ-up and germ-down. This confirmed that a model with maximum variability would improve the prediction capability.

The findings from this study imply that milling quality can only be partially assessed using conventional hardness methods. For a true reflection of maize kernel milling quality, a kernel's density needs to be measured, after the exclusion of the cavities present. X-ray µCT is a technology capable of such manipulations due to the 3-D nature of the captured data. The applicability of the findings resolves around the ability to incorporate the milling quality measurements (as obtained by X-ray µCT) into functional NIR spectroscopy calibrations. The inclusion of maximum variability in the data sets, as well as using suitable chemometrical tools, will ensure optimal milling quality prediction models that can be purposefully applied in the industry.

References

Chawanji, A.S., Baldwin, A.J., Brisson, G. & Webster, E. (2012). Use of X-ray micro tomography to study the microstructure of loose-packed and compacted milk powders. *Journal of Microscopy*, **248**, 49-57.

Erasmus, C. (2003). Maize kernel translucency measurement by image analysis and its relationship to vitreousness and dry milling performance. PhD Thesis. University of Pretoria, Pretoria, South Africa.

McGoverin, C. & Manley, M. (2012). Classification of maize kernel hardness using near infrared hyperspectral imaging. *Journal of Near Infrared Spectroscopy*, **20**, 529-535.

Watson, S.A. (1987). Structure and Composition. In: *Corn Chemistry and Technology* (edited by S.A. Watson & P.E. Ramstad). Pp. 53-82. St. Paul, Minnesota, USA: American Association of Cereal Chemists, Inc.